![Universität Zürich UZH]
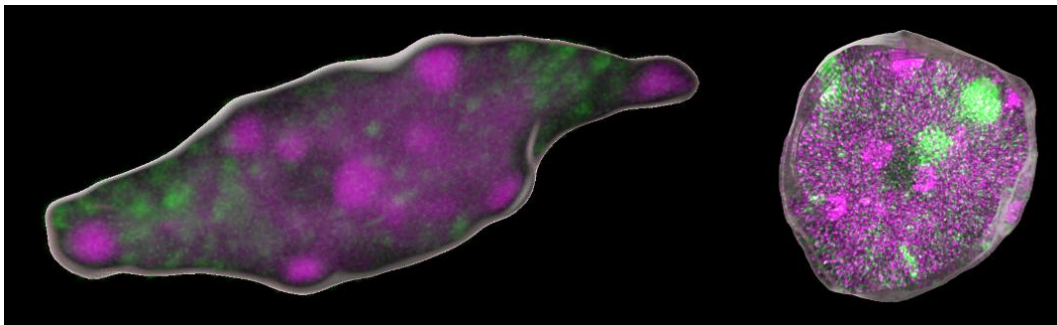
Master thesis in

Molecular and Cellular Biology

Investigating diurnal changes in the chromatin organization of *A. thaliana* and the involvement of linker histone H1.

Lena Perseus

(18-203-935)

February 2023

Supervised by

PD Dr. Célia Baroux

University of Zürich

Department of Plant and Microbial Biology

Table of content

Abstract

Light is not only a crucial source of energy for plants, but also delivers important information about the environment. It is perceived by a variety of photoreceptors that act to fine tune the plant cell metabolism and gene expression program. This enables adaptation to the environment. It remains unclear how light impacts gene expression, but it is thought to involve large-scale epigenetic and chromatin changes. During the diurnal rhythm genes are expressed in a coordinated manner and influence various physiological processes. This is thought to be controlled, at least partially, by changes in the 3D chromatin organization and by epigenetic modifications. A key regulator of genome packaging is the linker histone H1, which impacts molecular and spatial chromatin organization. Depletion of H1 in *A. thaliana* has been shown to cause aberrant root development in plants grown under different light regimes. However, it remains unclear how chromatin architecture is changing along the diurnal rhythm and what role H1 plays in this process. Our cytological analysis of chromatin features in *A. thaliana* revealed rhythmic abundance of H3K27me3, H3K4me3 and RNA Polymerase II S2P levels along the diurnal rhythm. Mutant analyses revealed that H1 contributes regulating the diurnal abundance of histone modifications and RNA Pol II activity, but only moderately influences Pol II S2P distributions. Major changes occur before light is turned on or off, suggesting a circadian entrainment to re-organize these chromatin features. Collectively, our results suggest a possible implication of H1 in regulating subtle, but significant chromatin dynamics at large scale, hence uncovering a novel function for linker histones in plants.

Abbreviations

WT   Wildtype

3h1   h1.1 h1.2 h1.3 triple homozygous mutant

LN   Liquid nitrogen

Dag   Days after germination

RT   Room temperature

CCs   Chromocenters

RHF   Relative heterochromatin fraction

AB   Antibody

Pol II S2P   RNA polymerase Serin 2 phosphorylation

PRC2   Polycomb repressive complex 2

PcG   Polycomb Group

LLPS   Liquid-liquid phase separation

TSS   Transcriptional start site

STED   Stimulated Emission Depletion

1 Introduction

Millions of years ago, plants started to expand on earth and today they colonize many different habitats. Unlike animals, plants are sessile and therefore it is critical for them to perceive environmental cues and react to these. They have developed complex adaptive strategies to ensure their survival and reproduction. Changes in the environment can lead changes in gene expression, which in turn results in changes of cellular functions. Multiple layers of regulation and feedback loops are involved to allow organisms fine-tuning their responses to changing environmental conditions. At a molecular level changes of gene expression take place in the nucleus, which contains the entire genome in eukaryotic organisms. A dynamic and controllable packaging of the DNA is essential to differentially express genes depending on demands of adaptation, but also to ensure DNA repair and replication function efficiently [Reviewed in (Rosa and Shaw, 2013)]. The spatial organization and chromatin regulation is impacted by different biotic factors such as pathogens or symbionts, and abiotic factors such as nutrients, light or temperature. Understanding the underlying mechanisms of how plants respond to a changing environment is important to face future challenges connected to climate change and could contribute to more sustainable agricultural approaches.

1.1 General principles of chromatin organisation

Chromatin is the nucleic DNA associated with chromatin proteins, so called histones. Around 147bp of DNA is wrapped around an octamer of 4 core histones, H2A, H2B, H3 and H4 to form a nucleosome. This level of organization resembles a "bead-on-string" structure, which can further fold into higher order chromatin structures (Figure 1A) (Alberts, 2015). Originally, two chromatin domains have been defined based on their density in DNA staining: dense and bright regions called heterochromatin and more loosely stained regions called euchromatin. Chromatin in cytological analysis of interphase nuclei was first described by Emil Heitz in 1928 (Berger, 2019). Later these two domains were associated with their transcriptional state, where heterochromatin contains compact, and gene-poor regions and euchromatin loose, gene-rich regions. These chromatin states influence how transcription machineries can access genes and therefore if they remain silent or can be actively transcribed [Reviewed in (Olins and Olins, 2003)].

Heterochromatin is subdivided into constitutive and facultative heterochromatin, depending on its behaviour in the cell cycle [(Brown, 1966) and reviewed in (Vanrobays, Thomas and Tatout, 2017)]. Constitutive heterochromatin generally remains condensed and contains predominantly highly repetitive sequences which are not expressed. In contrast, genes of facultative heterochromatin are only temporarily silenced and can be re-expressed by corresponding modifications if necessary. Genes in an euchromatic state are usually less condensed and can therefore be more easily accessed by the transcriptional machinery. Meanwhile even more chromatin states (CS) have been distinguished and a nomenclature with nine CS, based on predominant combinations of chromatin features and positions, has been widely agreed on in *A. thaliana*. Four of these CS resemble different euchromatin states (CS 1, 3, 6, 7) two resemble heterochromatin states (CS 8, 9) and three CS are enriched in the distinct Polycomb mark H3K27me3 (CS 2, 4, 5) (Sequeira-Mendes *et al.*, 2014).
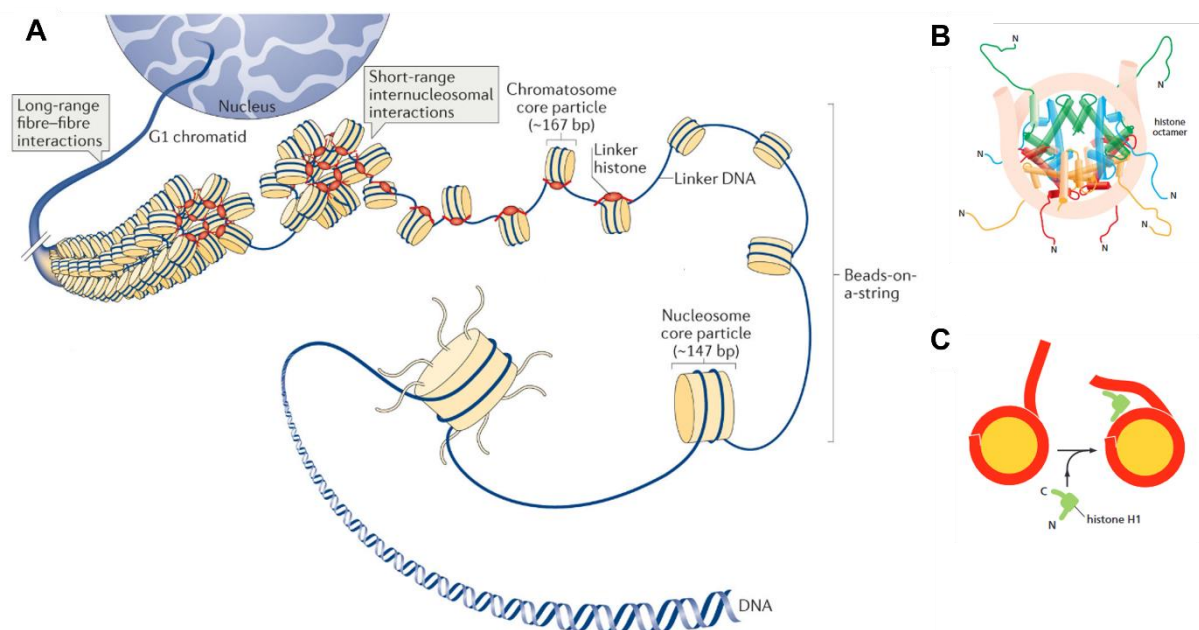
Figure 1 Overview of nuclear chromatin organization including histones. **(A)** DNA gets wrapped around an octamer of core histones to form a nucleosome. Nucleosomes are connected by linker DNA, which can be bound by the linker histone H1 to form a chromatosome. H1 regulates the internucleosomal space and influences the folding of higher chromatin structures. Adapted from Vanrobays, Thomas and Tatout, 2017 **(B)** Four dimer of core histones H2A, H2B, H3 and H4 aggregate to an octamer and get wrapped by DNA. N-terminal tails extend from the core body, which can serve as binding sites for post-translational modifications (PTMs). Alberts, 2015. **(C)** Arrangement of H1 that binds to the nucleosome and the linker DNA to change DNA compaction. Alberts, 2015.

Histones are found in all eukaryotic organisms and their structure is highly conserved, which speaks to their importance. The N-terminal domains of core histones extend

from the nucleosome (Figure 1B) and can carry various post-translational modifications (PTMs), which influence the structure and accessibility of chromatin [Reviewed in (Millán-Zambrano *et al.*, 2022)]. The linker histone H1 is an important protein for regulating the distance between nucleosomes and the formation of heterochromatin. In contrast to the core histones, H1 is less conserved and shows high variability in length and composition of its tails [Reviewed in (Kasinsky *et al.*, 2001)]. It consists of a short N-terminal tail, a globular domain (GH1) and a carboxyl-terminal tail, which is enriched in lysine (K) [Reviewed in (Jerzmanowski, 2004)]. The basic character of this tail leads to the binding of linker DNA at the entry and exit of the nucleosome, which is located between two nucleosomes. The GH1 has a high affinity to compounds of the nucleosome. With these contacts H1 can regulate the distance between adjacent nucleosomes and condenses the chromatin into higher organizational structure (Figure 1C). If H1 is bound to a nucleosome and linker DNA it is called chromatosome [Reviewed in (Jerzmanowski, 2004; Vanrobays, Thomas and Tatout, 2017)]. To dynamically change between different CS a highly complex system is needed which is controlled by epigenetic modifications.

1.2 The mechanisms shaping the epigenetic landscape

Chromatin can be biochemically and physically modified in several different ways. DNA can be directly methylated at cytosine residues in different contexts, such as CG, CHG and CHH (H stands for A, C or T). They are modified by specific DNA methylases, methyltransferases or demethylases [Reviewed in (Rosa and Shaw, 2013)]. Different core histone variants exist and can be incorporated in nucleosomes. These canonical histone variants have specific or redundant functions and are sometimes ubiquitously expressed or in other cases tissue specific. One example of a highly specific variant is CENH3, which only occurs in nucleosomes of centromeric regions. This H3 variant is needed for genome stability and differs from other H3 variants in its N-terminal tail. Also the linker histone H1 has several canonical variants which have redundant or specific functions (Reviewed in (Jerzmanowski, 2004)). Already small differences in the amino acid sequence of histones can largely influence the incorporation into chromatin [Reviewed in (Martire and Banaszynski, 2020)]. Histone tails can carry a various number of post-translational modifications (PTMs) such as acetylation, methylation, phosphorylation, SUMOylation, crotonylation and ubiquitination at different binding sites of their N-terminal tails (Figure 1B). To organize histone

modifications many different enzymes are needed which are "writers" to catalyse, "readers" to recognize and "erasers" to remove PTMs. One histone, or even the same histone tail, can hold several different PTMs which leads to an incredible number of regulatory possibilities and creates a high level of complexity [Reviewed in (Millán-Zambrano *et al.*, 2022)]. Different modifications lead to alterations in chromatin structure, which influence the state of this chromatin section. Certain chromatin states are enriched with specific PTMs pattern that show distinct histone modification profiles (Millán-Zambrano *et al.*, 2022). Generally, histone modifications can be split in repressive-related and activating-related marks correlating to their transcriptional activity. Acetylation and phosphorylation are usually associated with active genes in euchromatic regions [Reviewed in (Rosa and Shaw, 2013; Vanrobays, Thomas and Tatout, 2017)]. It was shown that acetylation directly rises transcription levels (Protacio *et al.*, 2000). Methylation and ubiquitination marks can occur in both hetero- and euchromatin. Methylation PTMs mostly occur at lysine (K) residues of histone tails and can be mono-, di-, or trimethylated [Reviewed in (Rosa and Shaw, 2013; Vanrobays, Thomas and Tatout, 2017)]. Histone 3 lysine 4 trimethylation (H3K4me3) is one of the best known PTMs for transcription and is placed at most active promotors. It facilitates transcription by positively influencing recruitment of transcriptional machineries to transcriptional starting sites (TSS) [Reviewed in (Millán-Zambrano *et al.*, 2022)]. A well-known repressive histone modification is histone 3 lysine 27 trimethylation (H3K27me3) which marks facultative heterochromatin. This mark is placed by the Polycomb repressive complex 1 and 2 (PRC1, PRC2) which belong to Polycomb Group proteins (PcG) that target genes to be silenced [Reviewed in (Kim *et al.*, 2017; Millán-Zambrano *et al.*, 2022)]. However, PTMs do not only define CS and transcriptional activity, but are also involved in other cellular processes such as DNA repair, replication and defining 3D genome topology [Reviewed in (Millán-Zambrano *et al.*, 2022)]. Many different factors such as DNA methylation, PTMs and histone variants act together in a complex network to help shaping the epigenetic landscape [Reviewed in (Lloyd and Lister, 2022)].

1.3 Cytological observations of dynamic heterochromatin in plants

Chromocenters (CCs) are brightly stained regions in interphase nuclei (Figure 2A, B). The CCs contain centromeric repeats, pericentromeric repeats (5S rDNA) and telomeric nucleolus organizer regions (NOR, 45S rRNA genes), including transposable elements (TEs) (Fransz *et al.*, 2002; Tessadori, Chupeau, *et al.*, 2007). In the current model in *A. thaliana* they are structured as "Rosette-loop" (Fransz *et al.*, 2002), where euchromatic loops emanate from CCs (Figure 2C). This is how the formation of chromosome territories is established (Figure 2D) [Reviewed in (Vanrobays, Thomas and Tatout, 2017)]. In *A. thaliana* 6-10 CCs can be observed and most of them are distributed in the nuclear periphery forming distinct areas. Except for two CCs that remain close to the nucleolus, which are especially enriched in NOR and can be explained that 45S rDNA need to be actively transcribed 67 within the nucleolus. [Reviewed in (Vanrobays, Thomas and Tatout, 2017)].
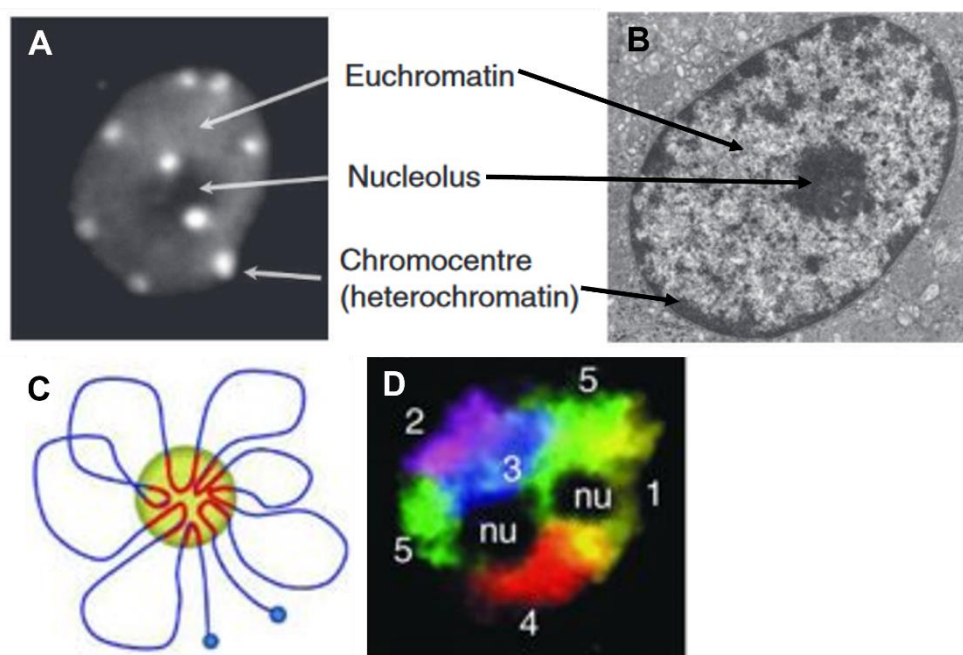
Figure 2 Chromatin organization in the nucleus viewed on cytological level **(A)** *A. thaliana* nucleus stained with DAPI. Heterochromatin is heavily stained and visible as bright spots (chromocenters, CC). Euchromatin is less densely stained. The nucleolus is almost not stained and thus visible as black hole. Two CCs are usually located close to the nucleolus (containing NOR), whereas the rest of the CCS are usually towards the nuclear periphery. **(B)** Electron microscopy image of a nucleus, showing light euchromatin, dark heterochromatin and a dark nucleolus. **(C)** Model of the rosette-loop conformation of chromosomes. In the middle the chromocenter (CC, yellow) is formed containing heterochromatin to form dense foci. Euchromatic loops extend from the CC. Telomers are shown in blue. **(D)** With a FISH experiment five chromosome territories were identified and painted. Images adapted from Vanrobays, Thomas and Tatout, 2017.

With new technologies, such as immunolabelling or fluorescent *in Situ* hybridization (FISH) it became easier to visualize chromatin changes on the cytological level. When differentiated mesophyll cells de-differentiate into protoplasts a massive rearrangement can be observed. Chromocenters begin to disrupt and heterochromatin decondenses, including centromeric repeats (Figure 3A). Only the 45S rDNA remains compact (Tessadori, Chupeau, *et al.*, 2007). Similar reorganizational events happen at the floral transition. A huge relaxation of heterochromatin occurs ~4 days prior bolting, which is also visible in a reduction of the relative heterochromatin fraction (RHF) levels (Figure 3B). This change is only temporary and recovers again after the development of the floral stem and flower buds. As for dedifferentiation, the 45S rDNA region is less affected than other heterochromatin regions and remains mostly unaffected (Tessadori, Schulkes, *et al.*, 2007). These examples indicate that large-scale chromatin reorganizations happen in response to developmental or environmental cues and heterochromatin dynamics can serve as markers for large-scale chromatin restructuring.
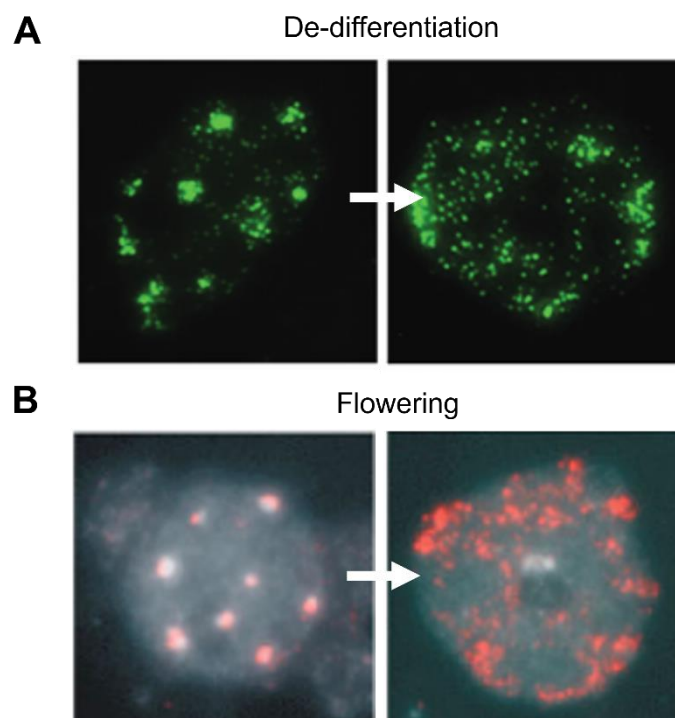
Figure 3 Heterochromatin is dynamic upon developmental transitions. **(A)** Before flower development nuclei are clustered in chromocenters. During flower development this organization is dispersed, and CCs are relaxed. Immunolocalization of 5-methylcytosine (5-mC, green) counterstained with DAPI (grey). Tessadori, Chupeau, et al., 2007. **(B)** Leaf nuclei shows centromeres (CCs) first, which are dispersed in protoplast nuclei. In grey DAPI staining is shown, in red FISH localization of repetitive sequences is shown. Tessadori, Schulkes, et al., 2007.

1.4 Light impact on chromatin organisation and composition

Besides being the most important energy source, sunlight is an important environmental cue to direct physiological adaptations in plants [Reviewed in (Patitaki *et al.*, 2022)]. Various sensory mechanisms have evolved to perceive information about the diurnal and seasonal photoperiod. These mechanisms allow to control the right timing of different developmental processes such as seed germination, photomorphogenesis and initiation of flowering rely on the right timing to be successful. The reaction to changes is as important, for example to sense shadow-casting competitors, to adapt chloroplast movement, or to regulate stomata aperture [Reviewed in (Paik and Huq, 2019; Bourbousse, Barneche and Laloi, 2020)]. Plants have at least five classes of photoreceptors, that have different wavelength absorption spectra: Phytochromes (PHYA-E) detect red/far red light, cryptochromes (CRY1-3), phototropins (PHOT1,2) and F-box containing flavin binding proteins (ZEITLUPE, FKF1) detect blue light (UV-A) and UVR8 detects UV-B light (Figure 4). Some of these are even thought to function in a multi-functional way, not only integrating cues of light
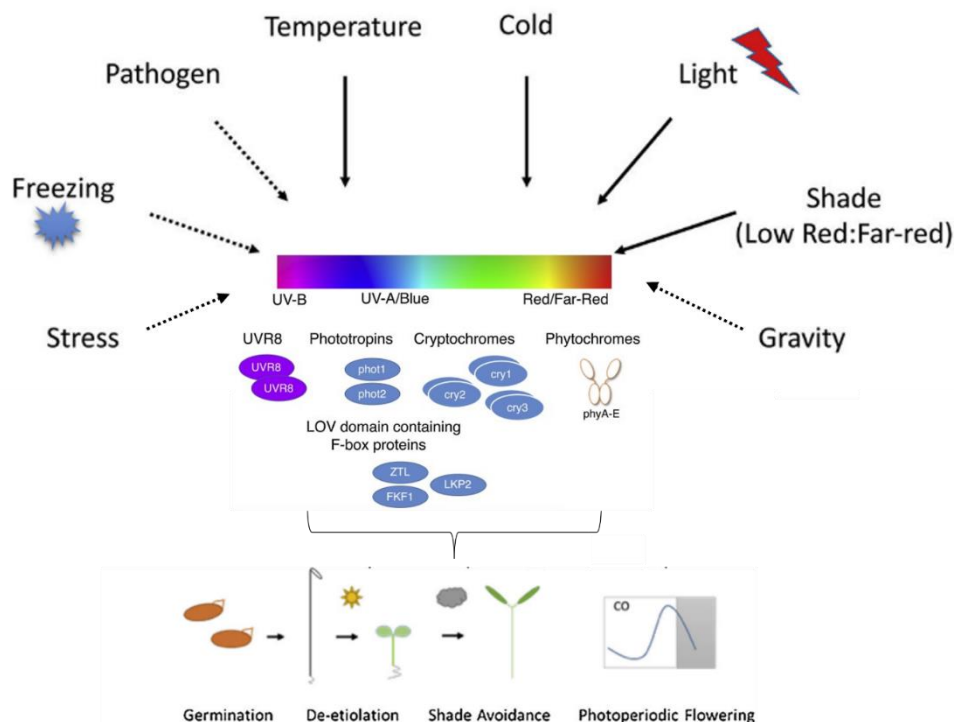
Figure 4 Plant photoreceptors are specific to wavelengths and integrate incoming signals to regulate many different physiological pathways. In *A. thaliana* five phytochromes (phyA-E) perceive red (650–670 nm) and far-red (705–740 nm) lights. Three cryptochromes (cry1, cry2, and cry3), two phototropins (phot1, phot2), and three LOV domain F-box proteins (ZTL, FKF1 and LKP2) perceive blue light. UVR8 perceives UV-B light. Certain receptors are also able to perceive stimuli other than light. Adapted from Paik and Huq, 2019

but also other biotic and abiotic cues [Reviewed in (Paik and Huq, 2019)]. Although sunlight is essential for photosynthesis and forms the basis of plant life, it can also be harmful in high doses. UV radiation can trigger mutations in the DNA or lead to accumulation of reactive oxygen species (ROS), which can have devastating consequences. As sessile organisms, the right balance between self-protection and fulfilling needs for survival, such as photosynthesising, is essential for plants [Reviewed in (Patitaki *et al.*, 2022) and (Bourbousse, Barneche and Laloi, 2020)].

1.4.1 Heterochromatin dynamics upon light perception

Light has been shown to have a dramatic impact on chromatin organisation at photomorphogenesis. In *A. thaliana*, a big re-organization happens when seeds start to germinate and sense light for the first time in their life. Nuclei of dry seeds have 2-4 subnuclear foci of highly compacted heterochromatin, which starts to de-condensation upon germination (Figure 5, phase 1). A few days after seeds showed a major increase in nuclear size and heterochromatin was settled in 8-10 CCs in presence of light. This change was dependent on blue-light receptors (Figure 5, phase 2), as CCs were not developed in absence of light (Figure 5, phase 3). The explanation for this was that
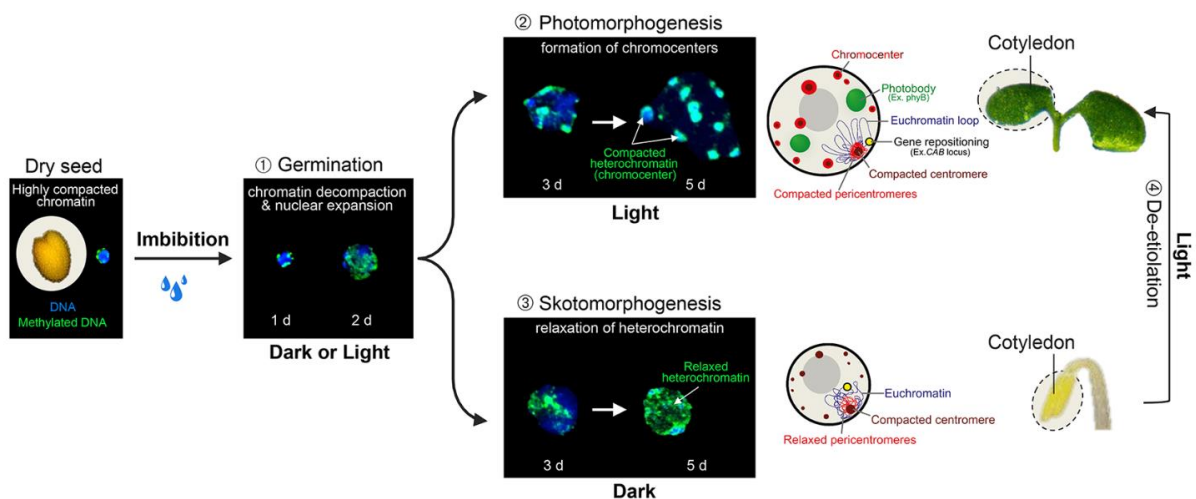
Figure 5 Light impacts the organization of chromatin in the nucleus in cotyledons. Phase 1: Seed imbibition leads to a heterochromatin de-condensation (methylated DNA in green disperses), and the nucleus expands in dark and light conditions. Phase 2: In presence of light the nucleus starts to further expand and there is a re-condensation of pericentromeric domains (visible as chromocenters). Phase 3: If the cotyledons grow in absence of light heterochromatin is further decondensed. As soon as etiolated cotyledons are exposed to light their chromatin restructures to be like phase 3 nuclei. Interestingly, there is also a relocation of light-inducible genes that are moved to the nuclear periphery and photoreceptor proteins (e.g. phyB, COP1, PIFs) aggregate in photobodies (Phase 4). d; days after imbibition. Bourbousse, Barneche and Laloi, 2020.

DE-ETIOLATED 1 (DET1) and CONSTITUTIVE PHOTOMORPHOGENESIS 1 (COP1) were supressing the formation of CCs when light was absent (Bourbousse *et al.*, 2015). Similar light dependent re-arrangements of chromatin were observed in changes of developmental stages. When apical shoot meristem changes to flowering meristems there is a transition from vegetative to reproductive tissues and heterochromatin undergoes a relaxation (Tessadori, Schulkes, *et al.*, 2007). Interestingly this change was found to be dependent as well on blue light receptors, but compared to seed germination had opposite effects on heterochromatin (Reviewed in (Bourbousse, Barneche and Laloi, 2020)).

1.4.2 Photobodies are nuclear domains responding to light

Besides major heterochromatic changes upon light stimuli also light-dependent gene repositioning have been unravelled in mono- and dicotyledon plants. When nuclear photoreceptors such as phyA-E or cry2 are excited, they are tethered in so called "photobodies" (Van Buskirk, Decker and Chen, 2012; Perrella and Kaiserli, 2016). The function of these nuclear bodies is not yet fully understood, but may enable rapid transcription of similarly regulated genes not located close to each other (Reviewed in (Bourbousse, Barneche and Laloi, 2020). Another relocation event happens when *A. thaliana* cotyledons undergo de-etiolation, where different light-sensitive genes are moved from the centre to the periphery of the nucleus (Figure 5, phase 4). A hypothesis is that the transcription process is even more accelerated through a fast mRNA export when transcription and processing happen close to nuclear pore complexes (Reviewed in (Bourbousse, Barneche and Laloi, 2020). De-etiolation in cotyledons causes an increase in DNA ploidy levels (López-Juez *et al.*, 2008) in contrast to hypocotyls where the same result is visible but upon etiolation (Gendreau *et al.*, 1997). This indicates a high specificity of the different organ tissues responding variably to light. Furthermore, light intensity seems influence endoreduplication, which occurs when chromosomes get duplicated, but cells are not divided afterwards. It is thought that this mechanism leads to an increase in gene expression and provides a sort of protection from DNA mutations (Larkins *et al.*, 2001). Higher ploidy levels come together with an increase in cell size (Jovtchev *et al.*, 2006). Low light conditions maintain low ploidy levels in *A. thaliana* and therefore reduce endoreduplication (Cookson, Radziejwoski and Granier, 2006). In contrast, in epidermal pavement cells endoreduplication was promoted when exposed to high light intensities (Kinoshita, Sanbe and Yokomura, 2008) and showed

reductions in heterochromatin density. Furthermore, a shift of CCs towards the centre of the nucleus was observed. So it is likely that ploidy level has an impact on the chromatin organization in plants [Reviewed in (Bourbousse, Barneche and Laloi, 2020)].

1.4.3 Light dynamically changes epigenetic landscape

Looking at the influences of light on the epigenetic landscape, interesting findings have been made in the past years. Different phenotypes related to photomorphogenesis were identified when PTMs of histones were removed. One example is the *det1* mutant which shows a genome wide destabilization of acetylation levels (Nassrallah *et al.*, 2018) suggesting that some histone transferases and deacetylases are connected to light-regulated adaptations [Reviewed in (Bourbousse, Barneche and Laloi, 2020)]. Besides this, also several chromatin remodelers were discovered to be involved in adaptation processes following light stimuli. The chromatin remodeler PICKLE, which interacts with transcription factors such as HY5 or PIF3, was found to accumulate at promotors of genes responsible for hypocotyl elongation in the dark. HY5 and PIF3 are known to be involved in light-signalling cascades and are negatively regulated by PICKLE through H3K27me3 repression on target loci (Jing *et al.*, 2013; Zhang *et al.*, 2014). Light seems to influence the homeostasis of histone marks and variants through orchestrating availability of chromatin modifiers. The monoubiquinated H2B (H2Bub) is regulated by the C3D complex, consisting of COP10, DET1, DDB1, and DDA1 [Reviewed in (Bourbousse, Barneche and Laloi, 2020)]. This complex is believed to facilitate RNAPII progression across nucleosomes by regulating histone H2Bub marks during transcription and is associated with most *A. thaliana* genes (Henry *et al.*, 2003). Low H2Bub levels during skotomorphogenesis could be connected to low RNA polymerase II (RNAPII) activity (Bourbousse *et al.*, 2015). This study shows that light not only affects gene-specific targeting mechanisms and chromatin domains, but also modifies the chromatin composition and its regulators to enable adaptions in the chromatin landscape to transcriptional processes [Reviewed in (Bourbousse, Barneche and Laloi, 2020)]

1.4.4 The photoperiod is associated with diurnal regulations of transcription and epigenetic states

The diurnal changes in chromatin architecture are tightly linked to transcriptional output. Genome-wide rhythmic binding of RNAPII occurs approximately 2-3 hours before mRNA accumulates (Le Martelot *et al.*, 2012; Deng *et al.*, 2022). To ensure coordinated transcription, genes expressed in the same phase are tethered into close proximity, eventually forming spatial clusters (Deng *et al.*, 2022). Another study showed that rhythmic differentially expressed genes (RGDs) during the day were mainly involved in photosynthesis and during the night in stress-response. It was found that next to light-dependent pathways, circadian-related RGDs are also important for hormone signalling and starch synthesis (Li *et al.*, 2021). Not only plants show these kinds of rhythmic gene expression mechanisms, in fact RNAPII gets recruited to euchromatic loci in mouse liver in a diurnal way. Thus, similar mechanisms could be conserved among animal and plant species (Le Martelot *et al.*, 2012). These kind of transcriptional rhythms underly the circadian clock and clock regulators, which provide an oscillating 24h rhythm to adapt metabolism, physiology, and development to diurnal rhythms. In the morning transcription factors such as CIRCADIAN CLOCK ASSOCIATED1 (CCA1) and LATE ELONGATED HYPOCOTYL (LHY) are responsible to repress evening-clock genes during the day, whereas in the evening transcription factors as TIMING OF CAB2 EXPRESSION1/PSEUDO RESPONSE REGULATOR1 (TOC1/PRR1) repress morning genes during the night [Reviewed in (Chen and Mas, 2019)]. Transcriptomic analysis revealed a reciprocal relationship between circadian clock genes and histone. CCA1 and LHY regulate expression of the eraser (*JMJ14*) and writer (*SDG2*), which help to modify H3K4me3. H3K4me3 was found to peak in morning phases to express morning-phased genes and therefore expressing them in a diurnal manner (Song *et al.*, 2019). Also, other histone modification as H3K9ac, H3K27ac and H3S28p were found to change in a diurnal way. Genes with these modifications mostly encode for proteins involved in circadian clock and starch metabolism (Baerenfaller *et al.*, 2016). This implies that histone modifications have specific roles in the regulation of diurnal gene expression.

1.5 H1 depletion in *A. thaliana* leads to major chromatin re-organization

In *A. thaliana* H1 is widely distributed along the genome in eu- and heterochromatic domains (Rutowicz *et al.*, 2015). Three canonical variants exist: H1.1, H.2 and H1.3. H1.1 and H1.2 show a high homology and are ubiquitously expressed in vegetative tissues and evicted upon reproductive tissue development. Whether they have redundant or specific functions is not known yet [Reviewed in (Izzo and Schneider, 2016)]. In contrast the variant H1.3 is only expressed under stress conditions and might influence transcriptional reprogramming in order to react to environmental cues (Rutowicz *et al.*, 2015). As all 3 variants can be knocked out in *A. thaliana*, it serves as an ideal model organism to study the role of H1, and several phenotypes have been described. Knock-out mutants of all three variants (*3h1*) show various phenotypes for example delayed seed dormancy, early flowering, increased number of lateral roots, increased hair-density of lateral roots and disordered stomatal complexes (Rutowicz *et al.*, 2019). Additional to physiological phenotypes, also changes on cytological scale have been observed upon H1 depletion. Chromocenters are reduced and heterochromatin is relaxed (Figure 6A). Only the two CCs associated to the nucleolus remain in most cases, as seen before in developmental transitions like flowering. Accordingly, *3h1* plants show a reduced relative heterochromatin fraction (RHF) and
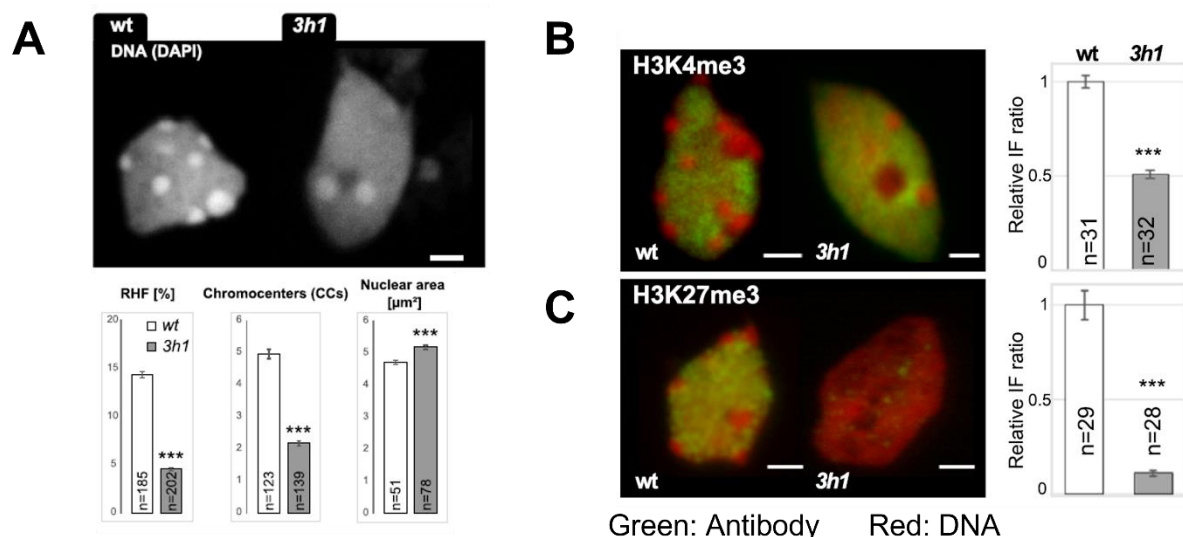
Figure 6 Cytological analysis reveals impact of H1 depletion on chromatin organization. **(A)** WT leaf nuclei compared to *3h1* mutant, stained with DAPI. Quantification of relative heterochromatin factor (RHF), number of CCs and the nuclear area in µm^2. **(B, C)** WT leaf nuclei compared to *3h1* mutant, that shows a decreased abundance of H3K4me3 **(B)** or H3K27me3 **(C)**. Antibody signal in green, DNA (PI) signal in red. Quantification shows ratio of AB intensity/DNA intensity relative to wt. Scalebar = 2 µm. (Rutowicz et al., 2019)

CC number concomitantly to an increase in nuclear size (Figure 6A). H1 seems to be needed for preserving heterochromatic structures but not necessarily for the compaction of rDNA repeat sites. Furthermore, changes in the abundance of histone modifications were observed. Upon H1 depletion H3K4me3 (Figure 6B) and H3K27me3 (Figure 6C) levels are significantly reduced, which suggests that H1 is required for maintaining these PTMs (Rutowicz *et al.*, 2019).

Strikingly, the lateral root phenotype depends on the light regime. Lateral root number is higher under continuous light but not when plants are grown under a diurnal regime (Figure 7A, B). In both cases this phenotype could be rescued when complemented with H1 (Baroux, Rutowicz, unpublished). This observation suggests that H1 is connected to light-dependent re-organization in some way, however how and when remains to be investigated. As a first step a transcriptomics experiment (RNAseq) was conducted on six different timepoints of WT and *3h1* plants. Interesting findings were made, indicating that a numerous number of genes gets desynchronized, meaning that
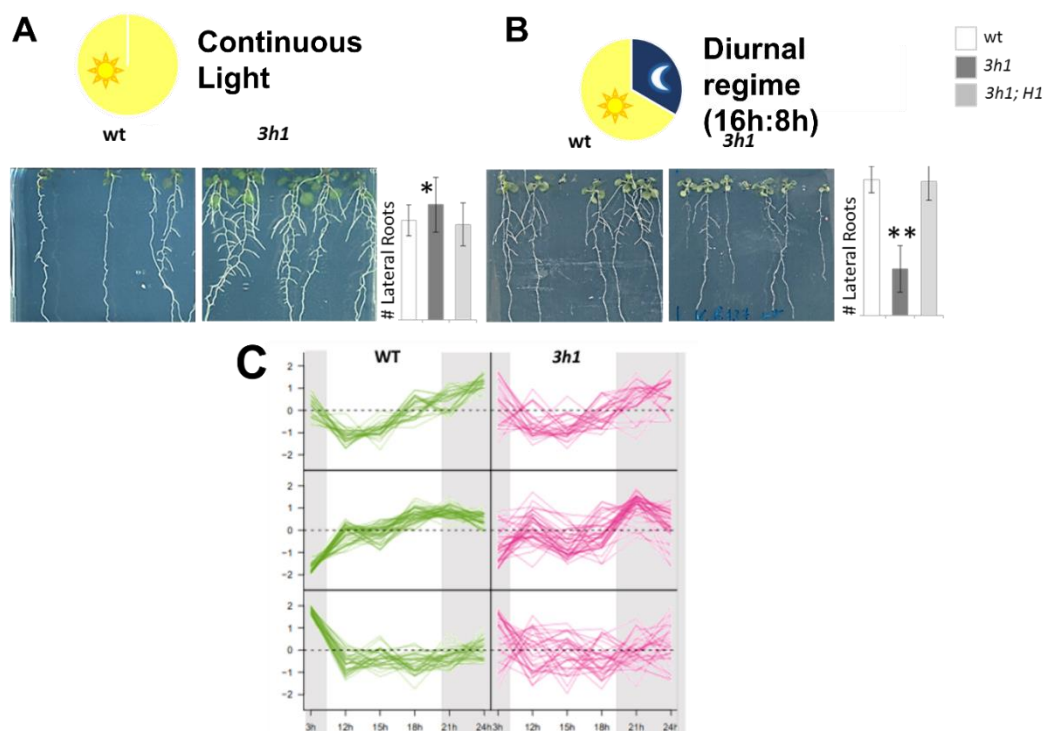
Figure 7 H1 seems to react to a change in light regime which results in lateral root phenotype. **(A)** *A. thaliana* seedlings grown under continuous light condition of WT and *3h1* genotype. *3h1* show stronger lateral root growth compared to WT plants. This phenotype can be rescued upon complementation. **(B)** *A. thaliana* seedlings grown under diurnal light regime. WT and *3h1* genotype. *3h1* show weaker lateral root growth compared to WT. This phenotype can be resuced upton complementation **(C)** Gene clusters regulated by the photoperiod in WT plants (green) and *3h1* plants (pink). Only 3/6 clusters are shown. Each line represents a gene. Time points in X axis (3h, 12h, 15h, 18h, 21h 24h). Data and results: Rutowicz, Schmidt, Baroux, unpublished

they are differentially expressed upon *3h1* compared to WT plants and showing changes from one timepoint to the next. Most genes found to be desynchronized were connected to the plant defence system (Figure 7C) (Rutowicz, Schmidt, Baroux, unpublished).

1.6 Objectives of my research project

Following the observation that H1, an important chromatin organizer, has an impact on diurnal gene expression, we asked whether the photoperiod is associated with subtle or large changes in chromatin organisation, and whether those would be possibly influenced by the presence of H1.

For this, a cytological approach was chosen to characterise chromatin organisation and composition along six time points during the day and night in WT and *3h1* plants. To characterize heterochromatic changes nuclei were analysed for the relative heterochromatin fraction (RHF) and number of chromocenters (CCs). Two canonical histone marks, H3K27me3 and H3K4me3, were chosen to visualize changes in facultative heterochromatin and euchromatin, respectively. For analysing transcriptional sites in the nucleus, the active RNA polymerase S2P was chosen. These central tasks were followed by a pilot project aiming at analysing the spatial distribution of two chromatin features at super resolution during two key time points.

The aim of this project was to investigate abundances of chromatin features along the diurnal rhythm and contribute to test the current model in our group suggesting that H1 acts as fine-tuning regulator to enable a smooth transcriptional reprogramming and secure robust epigenetic landscapes (Figure 8).
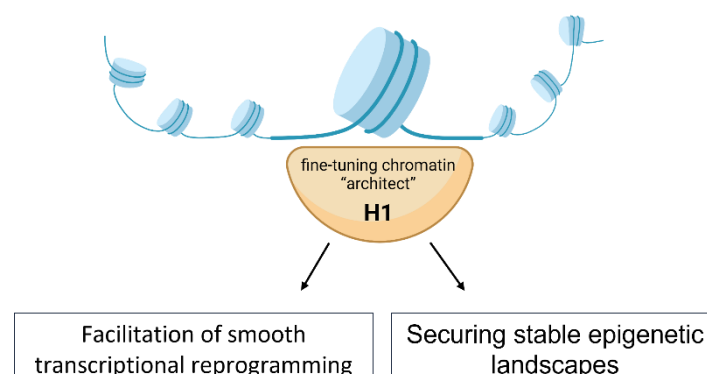

Figure 8 The current working model of H1, that is thought to be needed for facilitating transcriptional reprogramming as response to different cues (in our case light-related stimuli) and therefore stabilizing the epigenetic landscapes.

2 Material and Methods

2.1 Plant material preparation

Different genotypes of the *Arabidopsis thaliana* plants were used during the study. All plants were of the Col-0 ecotype background. The *h1.1 h1.2 h1.3*, triple homozygous mutant based on CRISPR-Cas9 editing was obtained and kindly shared by Maciej Kotlinski (University of Warsaw, Poland), Tomasz Bieluszewski (Adam Mickiewicz University, Poznan, Poland) and Kinga Rutowicz (University of Zürich) and will be from now on referred to as *3h1*. Additionally, this study uses the RNA Pol II Ser2P live reporter line *RPS5aSer2P-Mintbody-H2bmRuby* (Shibuta *et al.*, 2021).

2.1.1 Seed sterilization

Plant seeds were sterilized in a sterile hood with 70% ethanol, followed by three washes using sterile ddH2O. Seeds were spread on a filter paper to dry and then transferred onto MS agar plates. Per plate around 16-20 seeds were evenly distributed. The MS agar plates consisted of 0.5x Murashige and Skoog salt (MS, Caroline) and 1% of plant agar (Duchefa Biochemie) adjusted to a pH of 5.7. The full protocol can be found in the Appendix (8.1.1 and 8.1.2).

2.1.2 Growth conditions

Plates were stored in the dark at 4°C for 3 days for stratification. Then, the plants were transferred to a plant growth incubator (Percival, Germany) with long day photoperiod consisting of 16h light and 8h darkness. Two different settings of incubators were used for different experiments. For the experiment 1 and 2 (Figure 9) the time of the incubator was shifted by 12 hours to enable an inverted sample collection. Temperatures were set to 22°C during the day and 18°C during the night, except in the second extraction round, where day temperature was reduced to 20°C. The humidity and illumination were kept constant in all experiments and amounted 50% and 110-120 µmol m^{-2} s^{-1}. Light-time seedlings were harvested with lights on for transport and extraction in the fume hood, and dark-time seedlings were kept in a dark box for transportation until right before tissue collection in the fume hood, where light was on. The time necessary to take seedlings out of the box until fixing of the tissue didn't exceed 2min.

2.2 Slide preparation

2.2.1 Nuclei extraction

The detailed protocol can be found in the Appendix (8.1.3). Around 18 leaves from 19dag (days after germination) old seedlings were collected and directly added to a fixative formaldehyde solution. Seedlings were vacuumed twice followed by three washing steps with 1xPBS (Appendix 8.1.3). Next, leaves were chopped with a razor blade in a drop of nuclei isolation buffer (NIB, Appendix 8.1.3) until homogenization. The solution was filtered through a 30μm Partec Filter and centrifuged to separate the nuclei from other debris. The supernatant was resuspended in NIB and then sonicated for 6 cycles in ice cold water. Last, 5 μl of the nuclei extract was spread on Superfrost microscopy slides and air dried. The extraction was done at certain timepoints during the day and night, based on work published by (Song *et al.*, 2019) and a transcriptomic experiment conducted previously in our group (Rutowicz, unpublished). During the day at 10:00, 19:00 and 22:00 plant tissue was collected when light still was on. In the night plant tissue was collected at 02:00, 04:00 and 06:00 when the light in the incubator was still off. In experiments 1 and 2, two extractions were made as biological replicates (A and B, C and D) for every timepoint and genotype. Each extract gave 20 technical replicates. For experiment 3 only one extraction was done for every timepoint ending in 10 normal slides and 10 slides with acrylamide embedded pads. The experimental
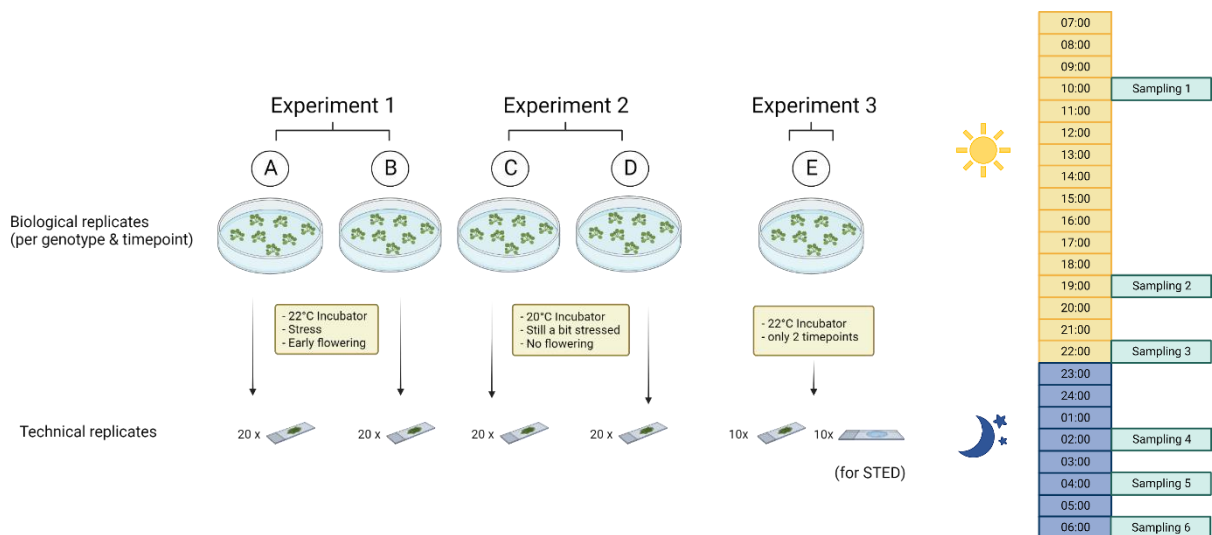
Figure 9 Overview of the experimental setup including different temperatures of incubator, observed phenotypes, and timepoints of tissue collection which were at 10:00, 19:00, 22:00, 02:00, 04:00 and 06:00. For experiment 1 and 2 always 2 biological replicates (A/B and C/D) were extracted. From those always 20 slides were made as technical replicates. This was done for two genotypes (WT and *3h1*) and 6 different timepoints. For experiment 3 only one biological replicate was made, and 10 normal extraction slides plus 10 acrylamide pad embedded slides for STED imaging were made.

setup can be found in Figure 9. Most slides used for producing results in this master thesis came from experiment 1 and 3.

2.2.2 Acrylamide Pad Embedding

The detailed protocol can be found in the Appendix (8.1.4). Nuclei extract got mixed with the polymerisation buffer (a mix of 20% NaS and 20% APS). Then, 15 µl of that mixture was added to Superfrost slides and covered with a regular 22x22mm coverslip until the acrylamide pad is polymerized. To avoid early aggregation fast work was required.

2.2.3 Clearing steps

This step was included before the immunostaining protocol to clear nuclei extracts with a lot of debris and helped to wash off unwanted particles on the slides. It was not used on acrylamide pad embedded extractions. The following steps were performed under the fume hood and washing didn't include shaking. Coplin jars were covered in Alu foil during the washing. First, slides were washed in coplin jars for 5min in ethanol - xylene solution (100% Ethanol, mixed 1:1). Then slides were transferred to coplin jars containing 100% Methanol and washed again for 5min. A wash of 5min in Methanol - 1xPBS (100% Methanol, mixed 1:1) followed and a last wash of 10min in only 1xPBS finished the procedure. Slides were then carefully dried with dust free paper around the drop of extract. It was important that the drop on the nuclei extract never fully dried out. The full protocol can be found in the Appendix (8.1.5).

2.3 Immunostainings

The detailed protocol can be found in the Appendix (8.1.6). First, blocking buffer was added to the slide containing the nuclei extract. This was covered by a coverslip and incubated for 45min. The humid chamber was wrapped in Alu foil for all following incubation steps. Slides were washed for 10min in 1xPBS in coplin jars which were also wrapped in Alu foil or were placed in a light shut box. Then, the primary antibody was added (Table 1). Again, the slides were covered by a coverslip and incubated for 30min at 37°C. The same washing and incubation step were repeated for the secondary antibody (Table 1). A final washing step was repeated, and slides were then incubated with RNAse A for 30min at 37°C. For acrylamide embedded nuclei extracts the incubation time was increased to 1hour at 37°C for primary and antibody

incubation. Slides were washed in 1xPBS for 10min, and counterstain was added. Then, slides were mounted with Vectashield, covered with a confocal coverslip (Hecht-Assistant) and sealed with Twinseal. Slides can be stored in the dark at 4°C for several months. The primary and secondary antibodies and counterstains used in the experiments can be found in Table 1 Antibodies and DNA stains used in experiments. The #reference number refers to the database of the Grossniklaus group. In blue all primary antibodies, in green the secondary antibodies and in orange the DNA counterstains are listed..

Target	Name	Company	Stock
H3K27me3	**Rabbit-anti-H3K27me3**, IgG, polyclonal (#10/12)	Active motif/ Upstate	1µg/µl
H3K4me3	**Rabbit-anti-H3K4me3**, IgG, polyclonal (#16)	Abcam	1mg/ml
Pol II S2P	**Rabbit-anti-R-α-RNAPolII-Ser2P**, IgG, polyclonal (#163)	Abcam	0.5mg/ml
Pol II S5P	**Rabbit-anti-PolymeraseII CTD Phospho S5**, IgG, polyclonal (#76)	Abcam	0.8mg/ml
For DM6000:	**Goat-anti-Rabbit**, IgG (H+L), **Alexa 488** conjugate (#78)	ThermoFisher Scientific	2mg/ml
For STED:	**Goat-anti-Rabbit STAR 635P**, polyclonal (#167)	Abberior	1mg/ml
DAPI	VECTASHIELD® Antifade Mounting Medium with DAPI H-1100 (#174)	Vector Laboratories	
Propidium iodide	VECTASHIELD® Antifade Mounting Medium with Propidium Iodide (PI) H-1300 (#47)	Vector Laboratories	
Live560	Abberior LIVE 560	Abberior	0.1mM in DmSO

Table 1 Antibodies and DNA stains used in experiments. The #reference number refers to the database of the Grossniklaus group. In blue all primary antibodies, in green the secondary antibodies and in orange the DNA counterstains are listed.

2.4 Microscopy and image analysis

2.4.1 Image acquisition

To reduce bias in selecting nuclei, they were always chosen based on their DNA staining and not the AB staining. Nuclei that looked clearly damaged were excluded from imaging.

If not stated differently, images were acquired with the Leica DM 6000B microscope and the Andor Neo 5.5 camera. 16-bit images were taken with the 63x1.4 oil immersion objective and the option low-noise gain was chosen. For immunostaining experiments

single plane images were captured, whereas for relative heterochromatin fraction (RHF) and chromocenters (CC) experiments z-stacks were acquired. Acquisition settings were different for every marker and were further changed because of the fluorescent lamp exchange about halfway of the experiments. But for quantification only images with identical acquisition settings were used. The H3K27me3 immunostaining slides were imaged under 200ms exposure time and 100% laser intensity for the Alexa488 channel and under 20ms exposure and 55% FIM for the PI channel. The settings for the H3K4me3 immunostaining slides were 27ms exposure and 55% FIM for the Alexa488 channel and 13ms exposure and 55% for the PI channel. For Polymerase II S2P, the settings were 33ms exposure time and 55% FIM for the Alexa488 channel and 15ms and 30% laser intensity for the PI channel. For Pol II S5P, the settings were 15ms exposure and 100% FIM for both channels. For RHF and CC experiments only one channel for DAPI was used, with 15ms exposure time and 30% laser intensity.

For acquiring live cell images of the *RPS5aSer2P-Mintbody-H2bmRuby* line the Confocal SP8 was used with the 63x water objective and immersol (Zeiss) as mounting medium. The excitation wavelengths were 488nm and 560nm for GFP and mRuby respectively, while the white light laser intensity was set at 30% for both.

For investigating chromatin at nanoscale levels, the SP8 STED microscope was used with a 93x1.3 Glycerol STED objective. Pixel size was set to 20x20nm with z-step size of 0.07nm and 512x512 image format. The delay time was 1000ps and the MOTCOR was adapted individually for every slide. The scanning speed was 700Hz and gating windows were set to 0.3-8. For H3K27me3, the settings of the 561nm channel were 20% excitation laser, 60% depletion laser (775nm) and 30% STED 3D laser. The 633nm channel (STAR635P) was set to 40% excitation, 50% depletion and 20% STED 3D laser. For Pol II S2P, the settings of the 561nm channel (Live 560) were 20% excitation, 60% depletion (775nm) and 30% STED 3D laser. The 633nm channel (STAR635P) was set to 40%, the other two lasers remained the same.

2.4.2 Image analysis and segmentation

For analysing immunostaining images, the free software Fiji (Schindelin *et al.*, 2012) was used to manually draw region of interests (ROIs) around nuclei. To simplify and speed up the process different macros were written to split channels and create a

montage of a set of nuclei (Appendix 8.2.3) that could be measured all together. Different features of both channels such as mean intensity (=sum intensity/number of pixels), standard deviation (of the mean intensity), area (in square pixels), circularity (=4π*area/perimeter^2), aspect ratio (AR, =major axis/ minor axis), solidity (=area/convex area) and roundness (=4*area/[π*major_axis^2 or inverse of AR]) were collected. The mean intensity of antibody signal was normalized against the DNA staining intensity.

For RHF a newly developed segmentation tool called *Nucl.Eye.D* was used (Johann to Berens *et al.*, 2022). The programme is based on deep learning, allowing the detection of nuclei and chromocenters (CCs) in an-semi-automated way. By loading the image dataset on Google drive and then running a script stored on Google Collab, the nuclei and CCs get segmented and can be used for further analysis with Fiji. For this, several macros can be found in (Johann to Berens *et al.*, 2022). Analysis of the experiment results already started before the public release of the final *Nucl.eye.D* version and a part of the results section (results 3.1.7) was dedicated to the troubleshooting and optimization of the usability of this software. The RHF was obtained by dividing the sum of CC signal intensities by the mean nucleus signal intensity.

For STED images, the program called Huygens Professional version 22.10.0p3 (Scientific Volume Imaging, The Netherlands, http://svi.nl) was used for deconvolution using all default parameters. Afterwards, the software Imaris 9.9.1 was used to segment the nuclei and calculate intensity ratios (=Antibody staining signal /DNA staining signal) of every voxel.

2.4.3 Image quantification and statistical methods

Graphs were plotted with RStudio (RStudio [2022.12.0+353] http://www.rstudio.com/) and data were statistically evaluated using ANOVA with Tukey HSD test to compare WT and *3h1* samples at different timepoints. The PCA analysis was conducted with the online tool ClustVis (Metsalu and Vilo, 2015). All results from the statistical tests can be found in the Appendix (8.3.3). All timepoints were tested pairwise with all timepoints, but not all results are shown in the graphs.

3 Results

3.1 Optimizing the workflows

3.1.1 Different phenotypes in experiment 1 and 2 observed

To have a solid setup for the different experiments we started by adapting plant growing conditions and by optimizing steps in the protocols. The experimental setup of replicates can be found in (Figure 9). After first plant growth trials, it seemed that the mutant plant did not grow as healthily as the wildtype segregant (WT). Wildtype seedlings after 19 days after germination (dag) had developed 5-7 green leaves (Figure 10A), whereas *3h1* leaves were smaller and showed a range of colour, from darker green and to more yellowish (Figure 10B). Not all seeds germinated on the WT or *3h1* plates. Seedlings grown for the experiment 1 (replicates A and B, Figure 9) showed an early flowering phenotype (Figure 10C), which can be induced by stress situations. The development of flowers leads to a large-scale reorganization of chromatin (Tessadori, Schulkes, *et al.*, 2007) therefore we discarded early flowering seedlings, and used only non-flowering plants to avoid re-organization due to flowering. Another undesired phenotype that could be observed was anthocyanin stress reactions visible as tiny purple leaves (Figure 10D). This occurred both in young WT and *3h1* plants (10dag), but after some days the plants started to develop normal green leaves. To reduce stress phenotypes in experiment 2 and 3 (replicates C, D and E, Figure 9) the incubator temperature was reduced to 20°C, which decreased both stress phenotypes.
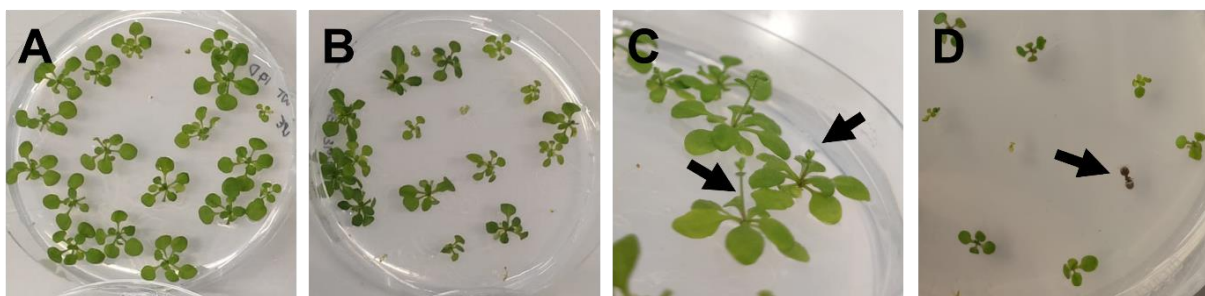

Figure 10 Phenotypes in our WT and *3h1* plants **(A)** WT seedling after 19dag **(B)** *3h1* seedling after 19dag (days after germination). **(C)** Early flowering phenotype (visible in WT (shown here) and *3h1* plants, 19dag, in A and B replicates) **(D)** Anthocyanin stress reaction (10dag, WT and *3h1* (shown here) plants, in all replicates).

3.1.2 Evaluation of deep-freezing tissue samples on nuclei quality

To optimize the workload during an experiment of extracting six timepoints throughout 24hrs, I evaluated the possibility to freeze leaf tissue in liquid nitrogen (LN). This could potentially preserve the state of the nuclei until a later extraction. Therefore, I collected leaves (19dag, WT), froze them in LN and let them thaw at room temperature (RT). As a control, I also collected fresh leaves from the same plate. I carried out nuclei extractions on both fresh and frozen samples and immunostained them for H3K27me3 or H3K4me3 and counterstained with PI. In Figure 11A a nucleus from the fresh extract showed an evenly distributed speckled pattern for the antibody (H3K27me3, green) with clear chromocenters (DNA, magenta). When looking at nuclei that were frozen in LN (Figure 11B), the boundaries were altered, and the immunostaining was not even suggesting chromatin damages by the procedure. Only some parts of the nuclei were stained with the antibody and no clear chromocenters (CCs) were visible. Similar results could be observed in *3h1* tissue and immunostaining of H3K4me3. The freshly extracted sample (Figure 11C) showed more intact nuclei and only some debris on the slides. The LN frozen extracted samples (Figure 11D) had lots of round organelles that were either stained with PI or possibly auto fluorescent. Only those organelles with a clear antibody staining (H3K4me3, green) were in fact true nuclei, and even those seemed to be damaged. To avoid the risk of a change in the chromatin organization and morphology of nuclei, I decided not to store the leaves in LN and to directly extract nuclei after tissue collection instead.
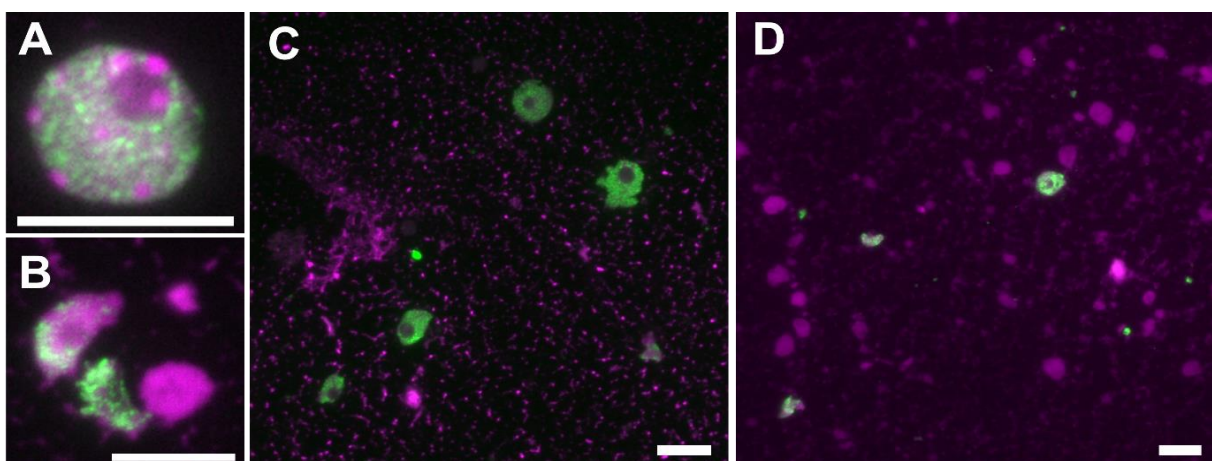
Figure 11 Impact of liquid nitrogen on nuclei morphology and immunostaining pattern. **(A)** WT nucleus, freshly extracted and stained with H3K27me3 (green) and PI (DNA, magenta). **(B)** WT nucleus, frozen in liquid nitrogen before extraction, stained with H3K27me3 (green) and PI (magenta). **(C)** *3h1* nuclei, freshly extracted, stained with H3K4me3 (green) and PI (magenta). **(D)** *3h1* nuclei frozen in liquid nitrogen before extraction, stained with H3K4me3 (green) and PI (magenta). Images were acquired with the DM6000, scalebar = 10µm.

3.1.3 An additional clearing step improves nuclei preparations

After several extractions, we noticed that the quality of the extraction was consistently poor, since the slides were crowded with small particles that interfere when imaging single nuclei. To assess this problem, I counterstained DNA of WT nuclei of several slides with DAPI, PI or using water (ddH$_2$O) as a control (Figure 11A, B, C). The staining quality looked similar in both DAPI and PI staining and the water control also showed a high background staining. Because of all the debris, the true nuclei were difficult to identify. Also, between WT and *3h1* extracts images looked similar (Figure 12C, F). Possibly, a wrong pH of the nuclei isolation buffer or changes in the molarity lead to bursting of certain cell organelles or there was a contamination by adding external solutions during the nuclei isolation. As particles were also excited in the light microscope with only adding water, some parts must have been auto fluorescent, which would speak for chloroplast particles. To solve this problem, we added a clearing step (Material and Methods 2.2.3) before starting the immunostaining protocol with xylene, which gives translucency to tissue (Rajan, 2014). This additional clearing removed the undesired debris, so nuclei became clearly distinguishable from the background (Figure 12D, E), which allowed me to use already made extractions for further experiments.

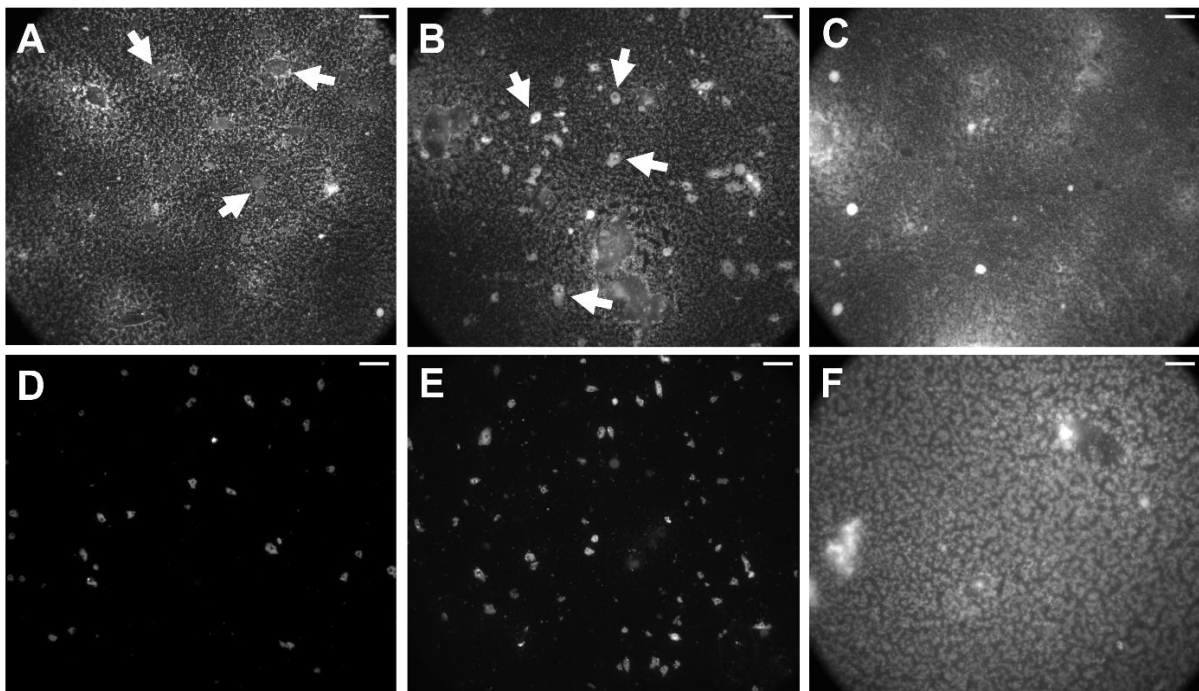**Figure 12** Additional clearing step helps to clean slides from debris. Arrows point to nuclei, which were difficult to spot. **(A)** WT slide counterstained with DAPI **(B)** WT slide counterstained with PI **(B)** WT slide with ddH$_2$O **(D)** WT slide counterstained with DAPI and additional clearing step **(E)** WT slide counterstained with PI and additional clearing step **(F)** *3h1* slide with ddH$_2$O. Scalebar = 20µm.

3.1.4 Identifying the best dilutions of secondary antibodies

The binding of antibody (AB) to cognate epitopes is influenced by temperature, incubation time and concentration. It is important to establish the right conditions for an antibody to exploit best results, which means that the detection should be on in a range to give high enough variation in immunodetection results, but not exceed levels close to saturation. We set incubation time, temperature and primary antibody concentration as constants and test different secondary antibody dilutions, here 1/500, 1/1000 and 1/2000. In H3K27me3 and H3K4me3 slides the PI didn't work well and hardly any CCs were stained. Therefore, only for Pol II S2P slides the antibody signal intensity was normalized (divided by) with the PI staining signal intensity. In this way the marker signals were relative to the DNA content of the nuclei. For H3K27me3 and H3K4me3 this was not possible and therefore the slides were analysed without normalization. In H3K27me3 (Figure 13A) and Pol II S2P (Figure 13C) slides the highest significant difference between WT and *3h1* plants as found in 1/1000 dilution. In H3K4me3 (Figure 13B) the results were not very conclusive, and against our expectations based on previous findings (Rutowicz *et al.*, 2019) for 1/500 the *3h1* showed higher AB intensity than WT. Most likely technical issues, like a mislabelling of slides was the reason for this. Based on previous experience (of other group members) the 1/1000 dilution was also chosen for later experiments.

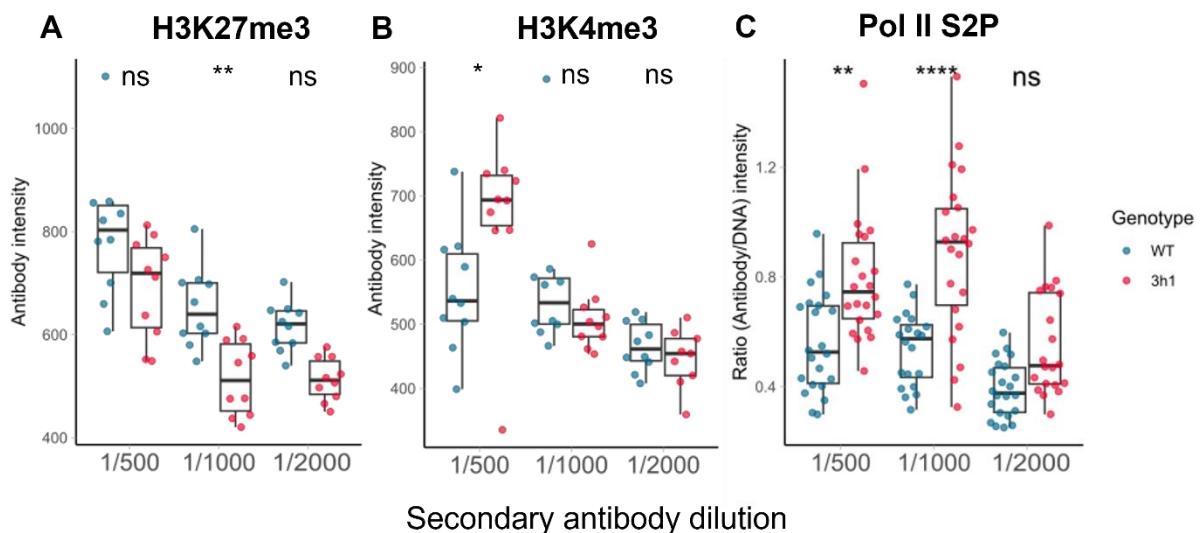
Figure 13 Establishing secondary antibody dilutions. **(A)** H3K27me3 intensity on slides with three different dilutions of secondary AB **(B)** H3K4me3 intensity on slides with three different dilutions of secondary **(C)** Ratio of mean Pol II S2P/PI (DNA) intensity. n (H3K27me3 and H3K4me3) = 10 nuclei, n (Pol II S2P) = 20 nuclei. * = P<0.05, ** = P<0.01, *** = P<0.001, **** = P<0.0001.

3.1.5 No significant difference found between biological replicates A and B

As previously explained in the methods (Figure 9) for every timepoint and genotype two nuclei extracts were made in parallel, where each contained leaves from different plants of one plate. To verify that these two replicates were similar enough to be pooled for analysis, nuclei extract of two randomly picked timepoints (02:00 and 04:00) of both biological replicates (A and B) were used for immunostaining for H3K27me3 (Figure 14). No significant difference could be found, which led to the conclusion that the replicates A and B were very similar and could be pooled to have a higher number of observations.
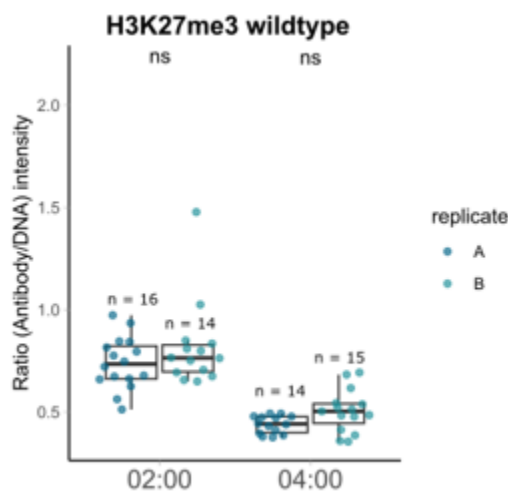

Figure 14 Comparison of biological replicates A and B from experiment 1 (Figure 9) showed no significant differences. Ratio of H3K27me3/ DNA (PI staining) intensity in biological replicates A and B were measured for two timepoints 02:00 and 04:00. n = 14-16.

3.1.6 Comparing ImageJ measurement methods

Next, two different approaches for measuring relative signal in immunostaining experiments were compared. H3K27me3 immunostained slides were quantified in Fiji. In the first approach, regions of interest (ROIs) consisting of the whole nucleus were manually drawn and data were exported for each image one after the other (method referred to as "Manual"). In the second approach, a montage of x-y nuclei was created (Material and Methods 2.4.3, Appendix 8.2.3), and the data were exported at once for multiple ROIs capturing each nucleus of the montage (method referred to as "Montage"). To ensure that the process of creating a montage would not change the

quantification results due to possible change picture size or saturation levels, the measurements were compared. As shown in Figure 15 there was no significant difference. Small variations between values for the same nuclei could be explained by natural discrepancies when manually redrawing nuclei.
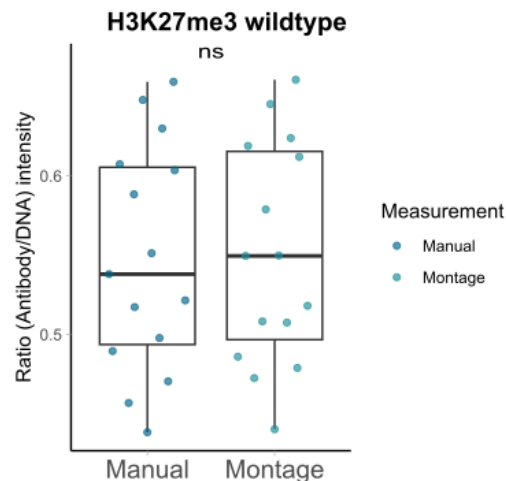
Figure 15 Montage measuring approach does not significantly differ from manual measuring approach in ImageJ. The ratio of H3K27me3/DNA (PI staining) intensity is shown. n = 15. Montage approach: Material and Methods 2.4.3, Appendix 8.2.3

3.1.7 Semi-automated measurements using *Nucl.eye.D*

For the segmentation of nuclei and of chromocenters (CCs) enabling measuring the relative heterochromatin fraction (RHF), a new deep learning-based tool called *Nucl.eye.D* was developed (Johann to Berens *et al.*, 2022). Before using this tool for the real experiments some trial runs were conducted to familiarize with and understand the programme. Some problems were encountered and tried to be solved which are summarized in Table 2. In general, *Nucl.eye.D* is a very powerful tool for analysing big datasets in a fast way. However, some bugs could be improved for a higher user-friendliness and detection accuracy.

Figure reference	Problem encountered	Implemented solution
Figure 16A, B	Z-stacks of DAPI stained nuclei were used to create max projections, which turned out to be very blurry because of diffracted light from the top and bottom of the nucleus. The program had troubles in segmenting the correct outline of the nucleus. (Figure 16A)	Stacks were trimmed to ~five planes in the middle of the nucleus and again a max projection was created. Now, the nuclei borders were correctly detected. (Figure 16B)
Figure 16C, D	In trimmed z-stacks of DAPI stained nuclei not all CCs were correctly detected. (Figure 16C, red arrows)	Single plane PI-stained nuclei for sharper CCs and clear boarders → reliable detection. (Figure 16D)
	Trial run with ~200 nuclei led to abrupt stop of the code without indication of which image caused errors.	Code was modified by the developers to output the batch containing three images of which one caused an error.
Figure 16E, F	Although knowing images of a batch that caused an error, there was no indication which single image was incorrect. Encountering an erroneous image was followed by mislabelling the segmentation mask, which then mismatched completely to according nuclei. (Figure 16E)	Trial and error approaches led to the realization that always the 3rd image of a batch was erroneous. This meant running the whole dataset, then deleting all erroneous images from the dataset, and re-run it again. Segmentation masks were now correctly assigned. (Figure 16F)
Figure 16G	Especially in *3h1* the tool failed to correctly detect CCs in different cases: - areas with a contrast in pixels not visible to our eye were detected - several neighbouring CCs were detected as one single CC instead of detecting them individually - additional nuclei were detected outside the real one, although it was only debris	Remains to be optimized by e.g.: - filter out images with small CC area - filter out several mutually detected CCs by max. CC area - only consider biggest nucleus of an image by filter nucleus size
Figure 16H	Examples of defective files causing an error in *Nucl.eye.D*	Remains to be optimized, possibilities are: - avoid debris outside of nucleus - leave enough space around nuclei boarder while imaging - only image single nuclei

Table 2 Overview of encountered problems working with *Nucl.eye.D* and implemented or suggested solutions. Orange: pre-version used. Blue: *Nucl.eye.D* (Johann to Berens et al., 2022) used.
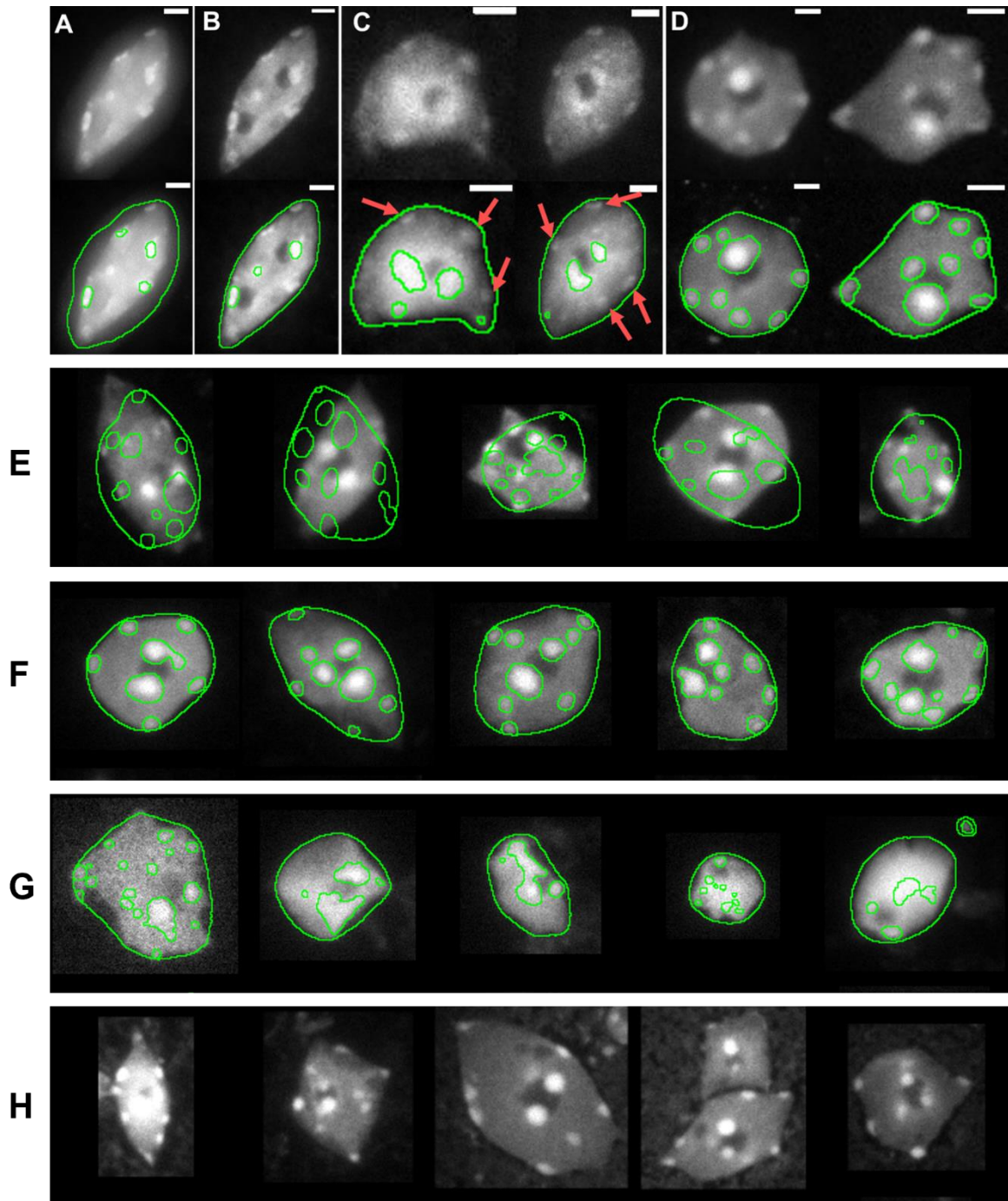
Figure 16 Example images of different problem encounters and implemented solutions using *Nucl.eye.D*. **(A)** Maximum projection of a z-stack nucleus stained with DAPI and the segmentation of the pre-version of *Nucl.eye.D* **(B)** Maximum projection of trimmed z-stack (5 planes) nucleus stained with DAPI and the segmentation of the pre-version of *Nucl.eye.D* **(C)** Maximum projection of trimmed z-stack (~5 planes) nuclei stained with DAPI and the segmentation of the pre-version of *Nucl.eye.D*, RED arrows show missed CCs **(D)** Single plane image of nucleus stained with PI and the segmentation of the published version of *Nucl.eye.D*. **(E)** Mismatched segmentation mask and nuclei caused by erroneous images. **(F)** Correct naming and assignment of masks to nuclei. **(G)** Examples of nuclei that were wrongly segmented (mostly *3h1* nuclei) **(H)** Examples of nuclei causing errors in *Nucl.eye.D*. Scalebar = 2µm

3.2 Immunostaining patterns of H3K27me3, H3K4me3 and RNA Pol II S2P

For the analysis we chose DNA staining to reveal the heterochromatin fraction (CC), specific antibodies for H3K27me3, H3K4me3 and RNA Pol II (ser2P) to mark the facultative heterochromatin, permissive chromatin regions (not necessarily actively transcribed) and actively transcribed regions, respectively. Representative patterns are shown in Figure 17. CCs were widely distributed in the WT, whereas mostly only two CCs associated with nucleolus were found in *3h1* nuclei. In WT nuclei H3K27me3 was found as speckles all over the nucleus except in CCs and the nucleolus. The mutant showed a similar speckly pattern and distribution but compared to the WT nuclei the
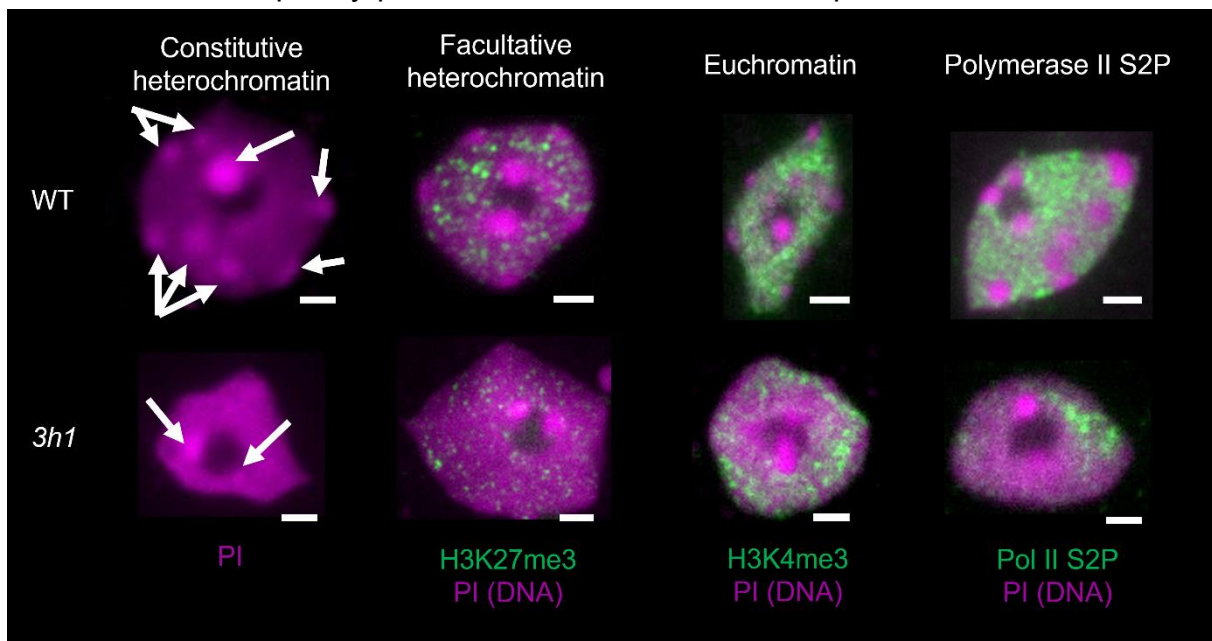

Figure 17 Different immunostaining patterns of WT and *3h1* nuclei marked for H3K27me3, H3K4me3, Pol II S2P and counterstained with PI. The patterns correspond to expected euchromatin and heterochromatin distributions of the WT and mutant *3h1*. White arrows point to chromocenters (CCs) which is constitutive heterochromatin. Imaging was done with the DM6000. Scalebars = 2µm.

single patches of more intense regions (dots) were much smaller. In WT nuclei stained for H3K4me3, the density of the signal was higher as H3K27me3 but still visible as speckles and could be found everywhere in the nucleus except for the CCs and the nucleolus. In *3h1* nuclei distributions were uneven, with different patches of high density dotted pattern next to low density euchromatic areas. For Pol II S2P stained nuclei a dense dotty pattern was stained in euchromatic regions, leaving out CCs and the nucleolus, similar to H3K4me3 staining. The staining in *3h1* nuclei was weaker and

unevenly distributed. In general, we found the markers at locations in the nuclei where we expected them to occur.

3.3 Global analysis of different morphological features shows subtle changes along diurnal rhythm

At germination, light leads to an increase in nuclear size. To investigate whether the nuclei also undergo morphological changes during the diurnal rhythm, we used several shape descriptors (area, circularity, roundness, aspect ratio) and DNA signal descriptors (intensity mean, and standard deviation) in a PCA. In the WT, the PCA revealed changes with dynamics differing between day and night times (Figure 18A). During the day changes are mostly explained by PC1 (46.1%), which was mostly influenced by area, roundness, aspect ratio and DNA standard deviation. During the night morphological features were also influenced by PC2, impacted by circularity and solidity. When comparing WT to *3h1* nuclei we see a clear shift in the features along the x-axis (PC1, 78.6%) which explains most of the variation, which was influenced by DNA mean and standard deviation, roundness, and aspect ratio (Figure 18B). The heatmap with medians shows differences between timepoints and genotypes (Figure 18C). Between *3h1* and WT plants major differences are detected in all timepoints especially in the shape (including roundness, circularity, and solidity), consistent with the reported nuclear phenotypes of *3h1* mutants. In conclusion, the PCA gave us an overview about how morphological features and DNA staining change along the diurnal rhythm, which showed subtle changes due to the combination of several features.
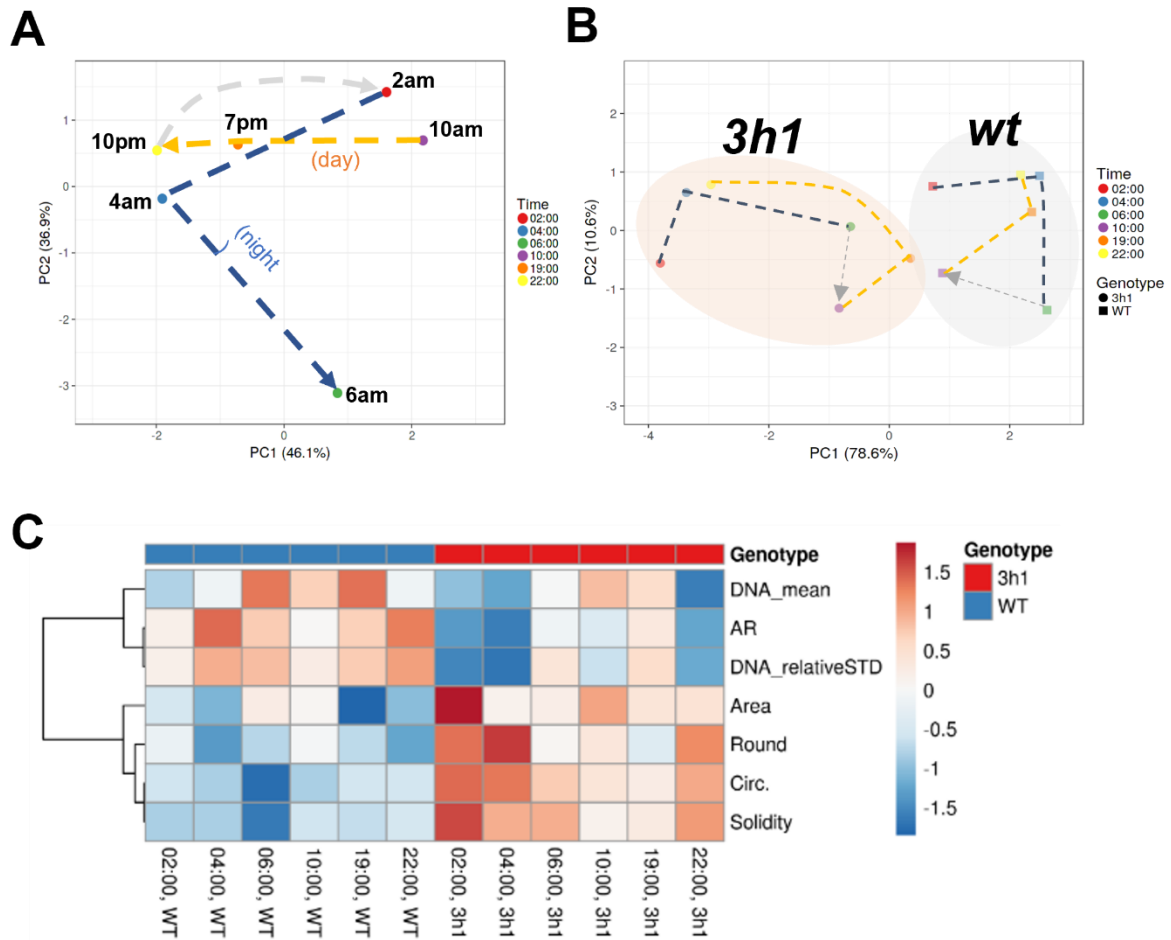
Figure 18 Principal component analysis revealed interesting changes of nuclei morphological features along the diurnal rhythm and between genotypes. **(A)** PCA of WT nuclei morphology. Columns with similar annotations are collapsed by taking median inside each group. Unit variance scaling is applied to rows; SVD with imputation is used to calculate principal components. X and Y axis show principal component 1 and principal component 2 that explain 46.1% and 36.9% of the total variance, respectively. N = ~350 data points **(B)** PCA of WT versus *3h1* nuclei. N = ~760 data points **(C)** Median of nuclei features along 6 timepoints and between WT and *3h1*. Columns with similar annotations are collapsed by taking median inside each group. Rows are centred; unit variance scaling is applied to rows. Rows are clustered using correlation distance and average linkage. Blue: less than median, red: more than median, 0: median). Measured features are described in more details in (Material and Methods 2.4.2). Data was collected and pooled form H3K27me3, H3K4me3 and Pol II S2P immunostaining experiments. PCA were created by C. Baroux with data collected by L. Perseus, unpublished).

3.4 Chromatin organization in WT plants is dynamic along diurnal rhythm

3.4.1 Heterochromatic features are largely stable along the diurnal rhythm

Changes in relative heterochromatin fraction (RHF, dividing the sum of CC signal intensities by the mean nucleus signal intensity) and CCs have been observed in developmental transitions like flowering initiation or seed germination (Tessadori, Schulkes, *et al.*, 2007; Bourbousse *et al.*, 2015). As these transitions depend on light-signalling pathways, we were wondering how heterochromatic features behave along the diurnal rhythm. To investigate this, we analysed the RHF and the abundance of chromocenters (CCs) at the six chosen different timepoints. For this purpose images corresponding to the DNA staining, from the dataset of images generated in an immunostaining experiment (using the anti-H3K27me3 antibody) were used and analysed with *Nucl.eye.D*. As visible in Figure 19A the mean RHF is similar at all timepoints and was ~0.25-0.3, meaning that heterochromatin represents 25-30% of the whole genome. This value is higher as previously observed RHF values of leaf nuclei which was around 0.05 (Rutowicz *et al.*, 2019). Using an ANOVA test, no
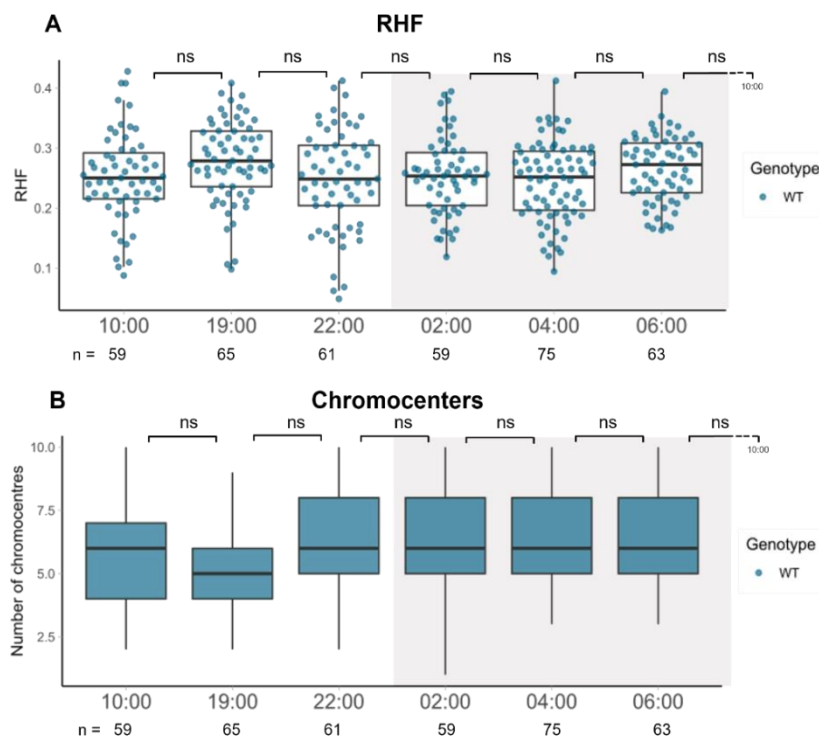

Figure 19 Heterochromatic features remain constant in the diurnal cycle. **(A)** the relative heterochromatin fraction (RHF, [%]) of WT nuclei. **(B)** the number of CCs of WT nuclei. Nuclei were stained with H3K27me3 and PI, but only PI channel was used for analysis with *Nucl.eye.D*. n = number of observed nuclei. Grey area represents the night (light off from 22:00 until 06:00).

significant differences were detected between timepoints. Yet, visual inspection of the graph suggests that the RHF is slightly changing from 10:00 to 19:00 and from 19:00 to 22:00. Doing a Mann–Whitney U test between timepoints 19:00 and 22:00 revealed a moderate significant difference (p = 0.04). The number of CCs shows moderate but not significant changes at 10:00, 19:00 and 22:00. The mean number of CCs ranged from 5-7 (Figure 19B). Thus, the heterochromatin fraction is largely stable along the diurnal rhythm in WT plants. Yet, a repetition of the experiment with new slides would be helpful to see if the RHF in our leaf nuclei remains higher than previously observed results and if dynamics remain constant. Furthermore, a comparison of manual analysis of the RHF compared to the outcome with *Nucl.eye.D* analysed nuclei would be helpful to exclude technical problems.

3.4.2 Histone modification abundance change during the day and night

Transcriptomic analysis revealed a reciprocal relationship between circadian clock genes and histone modifications, which lead to rhythmic changes of H3K4me3 levels in target genes (Song *et al.*, 2019). We wanted to investigate if we could confirm diurnal changes in H3K4me3 abundance and additionally if changes also occur in H3K27me3. For this purpose, immunostainings for H3K4me3 and H3K27me3 at the six timepoints we conducted and mean intensities analysed (normalized by DNA content). H3K27me3 showed significant differences between 19:00 and 22:00 where the ratio increased by two-fold (Figure 20A). After light was turned off there was no immediate change until 02:00. Another reorganization event happened between 02:00 and 04:00, where the ratio dropped by a two-fold. Although there was no significant difference it still seemed that also between the timepoints moderate changes took place. Interestingly, for the timepoints 22:00 and 02:00 the variation was quite big, and the ratio was grouped into nuclei with lower and nuclei with higher ratios (red circles in Figure 20A). In H3K4me3 stained nuclei, most significant changes occurred during the night, from 02:00 to 04:00 and from 04:00 to 06:00 (Figure 20B). Also, after light was turned on there were significant changes from 06:00 to 10:00 and from 10:00 to 19:00. Compared to H3K27me3 there was no significant difference between 19:00 and 22:00 shortly before light was turned off again. At the timepoint 04:00, the measurements revealed again an outsider group with large values (red circles in Figure 20B). Taken together, we observed dynamic changes in both histone modification abundances indicating that there is a diurnal regulation leading to a chromatin re-organization.

Interestingly, the biggest changes happened prior light turning on or off which could speak for an entrainment to prepare for the different light condition in advance.
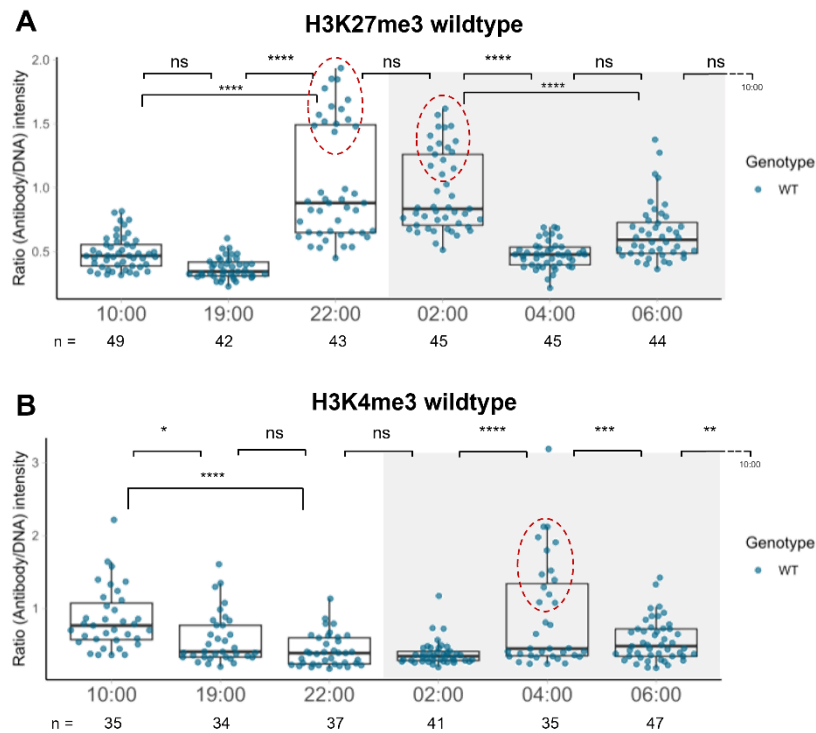

Figure 20 Histone modifications show significant distribution changes along the diurnal rhythm. **(A)** Boxplots of analysed nuclei with H3K27me3/DNA ratio **(B)** Boxplots of analysed nuclei with H3K4me3/DNA ratio. Nuclei were analysed at 6 timepoints in wildtype plants, counterstained with PI and manually segmented with Fiji. n = number of observed nuclei. Grey area represents the night (light off from 22:00 until 06:00). Statistical test: ANOVA with Tukey HSD (Appendix 8.3.3, * = P<0.05, ** = P<0.01, *** = P<0.001, **** = P<0.0001). Red circles show groups of nuclei with high variation.

3.4.3 Pol II S2P moderately changes along diurnal rhythm in WT

Several recent findings based on transcriptomic experiments suggest rhythmic expressions in plants along the diurnal rhythm (Le Martelot *et al.*, 2012; Deng *et al.*, 2022). To assess these results on the cytological level, we decided to investigate the active RNA Polymerase II S2P (Pol II S2P) transcription machinery by immunostaining. Different immunostaining patterns of Pol II S2P in WT and *3h1* nuclei were observed, which we grouped in three different classes: strong signal, homogenous distribution (Class I), strong signal, uneven distribution (Class II), and weak signal (Class III) (Figure 21A). These classes were confirmed in an independent way using the live reporter system *RPS5aSer2P-Mintbody-H2bmRuby* in leaves (Figure 21B). In addition

to the classes, to assess whether the patterns may be linked to nuclei shapes, we scored separately round, 'eye-shaped', elongated nuclei and nuclei with none of these
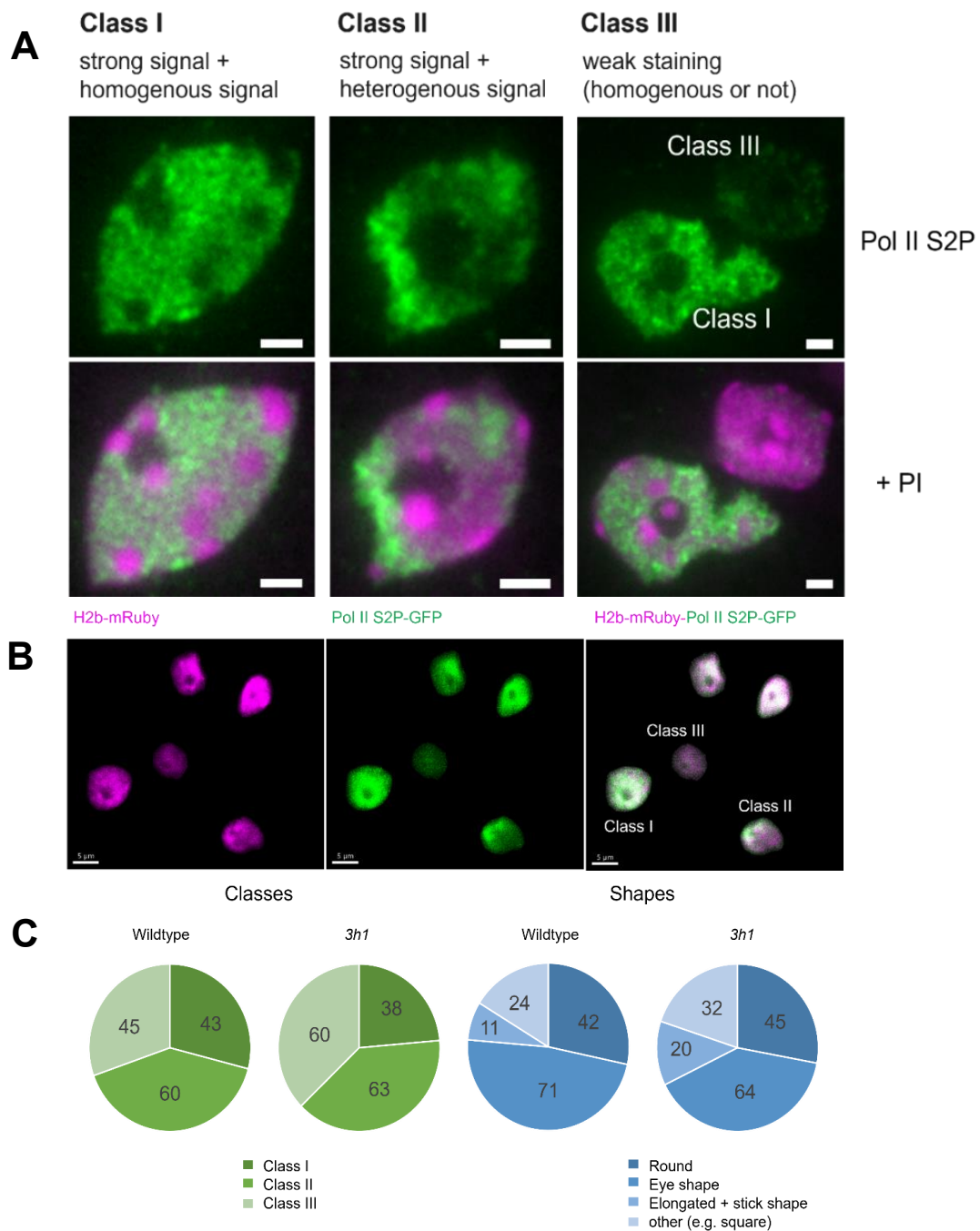
Figure 21 Division into classes and scoring of classes and shapes. **(A)** Nuclei were divided into three classes according to their staining pattern. In green Pol II S2P antibody and in magenta the DNA (PI) staining is visible. Class I nuclei show strong antibody signal and homogenous distributions, class II nuclei show strong signals, but uneven distributions and class III nuclei show a weak signal regardless of the distribution. Scalebar = 2µm **(B)** Live-cell imaging of RPS5aSer2P-Mintbody-H2bmRuby shows same RNA Pol II S2P nuclei classes as observed in immunostaining experiments. Live-cell imaging with SP8. PolIIS2P signal (green) and H2B signal (magenta). Image on the right both shows channels overlayed. **(C)** Scoring of the three classes and of different shapes in WT and *3h1*. n(WT) = 148, n(*3h1*) = 161. Detailed scoring can be found in the Appendix 8.3.2.

defined shapes (Figure 21C, Appendix 8.3.2). Class II nuclei most frequently occurred in WT and *3h1* plants, followed by class III and class I nuclei. In general, the distributions were quite similar, and all staining patterns often occurred, and there was no sign that the weak or uneven staining was due to immunostaining problems. Regarding shape, we saw a higher abundance of eye shaped nuclei in WT and *3h1* plants followed by round nuclei. Elongated and stick shaped nuclei occurred least. A direct association between shape and staining class could not be found. Since all classes and shapes were almost equally abundant, we decided to include all nuclei into our quantification analysis. We quantified the relative abundance of RNA Poll II S2P along the diurnal rhythm as before (Figure 22A). Between 04:00 and 06:00 there was a significant decrease and between 06:00 and 10:00 a significant increase of the ratio. Furthermore, a significant decrease by three-fold between 10:00 to 22:00 and an increase of two-fold between 22:00 to 04:00 was found. This collectively suggests that RNA Pol II S2P activity varies along the diurnal rhythm with small but steady changes.
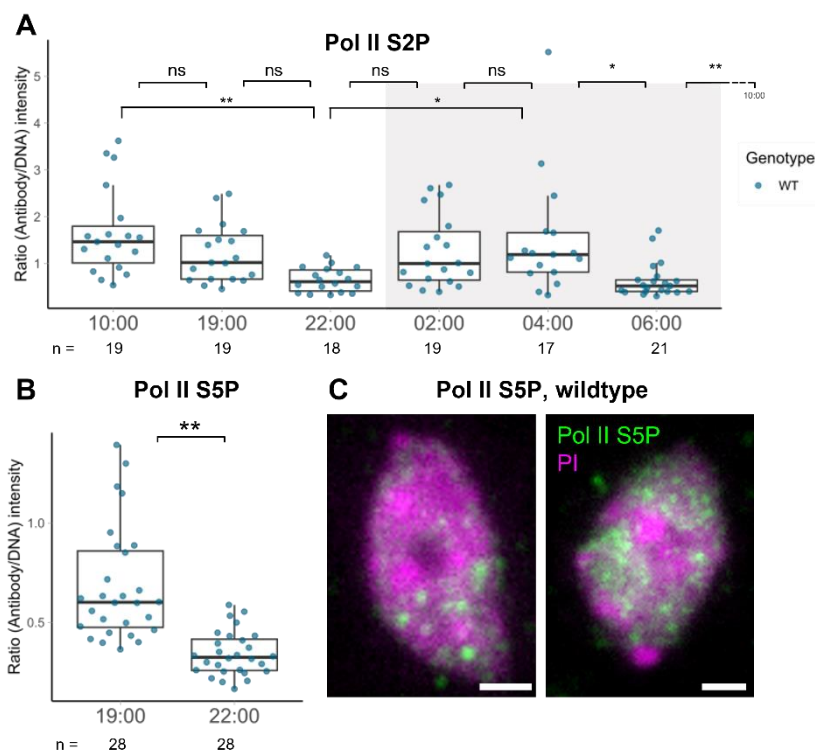
Figure 22 Polymerases II S2P and S5P undergo a modulation of their protein level along the diurnal rhythm. **(A)** Boxplots of analysed nuclei with Pol II S2P/DNA ratio at 6 different timepoints **(B)** Boxplots of analysed nuclei with Pol IIS5P/DNA ratio at two timepoints. **(c)** two WT nuclei stained for Pol II S5P (green) and PI (magenta). Nuclei were counterstained with PI and manually segmented with Fiji. Scalebar = 2µm n = number of observed nuclei. Grey area represents the night (light off from 22:00 until 06:00). Statistical test: ANOVA with Tukey HSD (Appendix 8.3.3, * = P<0.05, ** = P<0.01, *** = P<0.001, **** = P<0.0001).

Two mechanisms can contribute to changes in Pol II S2P levels: a) protein abundance regulated by synthesis and degradation, b) change in PTM signatures, where active (Ser2P) state changes to inactive state (Ser5P). It is possible that these mechanisms co-occur. To test these possibilities, we stained RNA Pol II Ser5P, which marks preferentially inactive Polymerase complexes [Reviewed in (Hsin and Manley, 2012)]. Two timepoints, 19:00 and 22:00, were selected based on major changes found previously in H3K27me3 and H3K4me3. A significant decrease was observed in Pol II S5P (Figure 22B). Like Pol II S2P, Pol II S5P showed a specky staining pattern with various distributions (Figure 22C). In conclusion, Pol IIS2P and Pol II S5P protein levels were both decreasing before light was turned off, which suggests that Pol II S2P is not only deactivated, but a degradation of Pol II proteins happens.

3.5 Chromatin dynamics of *3h1* plants differ to wildtype

3.5.1 Heterochromatic features remain largely stable upon H1 depletion

As H1 plays an important role in the regulation of chromatin organization and is known to de-compact heterochromatin upon depletion (Rutowicz *et al.*, 2019), we were interested to see how *3h1* behaves along the diurnal rhythm and compare it to WT chromatin. As before, the RHF and abundance of CCs were measured with a dataset of H3K27me3 nuclei and segmented with *Nucl.eye.D*. For the RHF only between 02:00 and 06:00 a significant difference was found (Figure 23A). In general, the RHF was ~0.2. However, some outliers with a value of 0.4 or higher were measured. The number of CCs was constant and remained on a level of 2-4 along all timepoints (Figure 23B). Compared to previous findings, where the RHF was ~0.5 and mean number of CC was two (Rutowicz *et al.*, 2019), our results were slightly higher. Looking at segmented nuclei with really high RHF levels (~0.4) it became clear, that detection of CCs was the cause, and many images were wrongly segmented (Figure 16). Therefore, these results should be carefully analysed and need manual filtering of outliers and wrongly detected nuclei. Next, WT and *3h1* nuclei were directly compared to each other. At all six timepoints significant differences were found in RHF and number of CCs. The *3h1* mutant showed lower levels of RHF (~0.5-fold) and CCs (~two-fold) compared to the WT plants (Figure 24A and B). To better see dynamic changes the mean RHF and mean number of CCs were plotted in Figure 24C and D. Dynamic changes were visible in both WT and *3h1* nuclei, however looking at means could be misleading which was influenced by outliers. Therefore, a more representative plot with local regression line
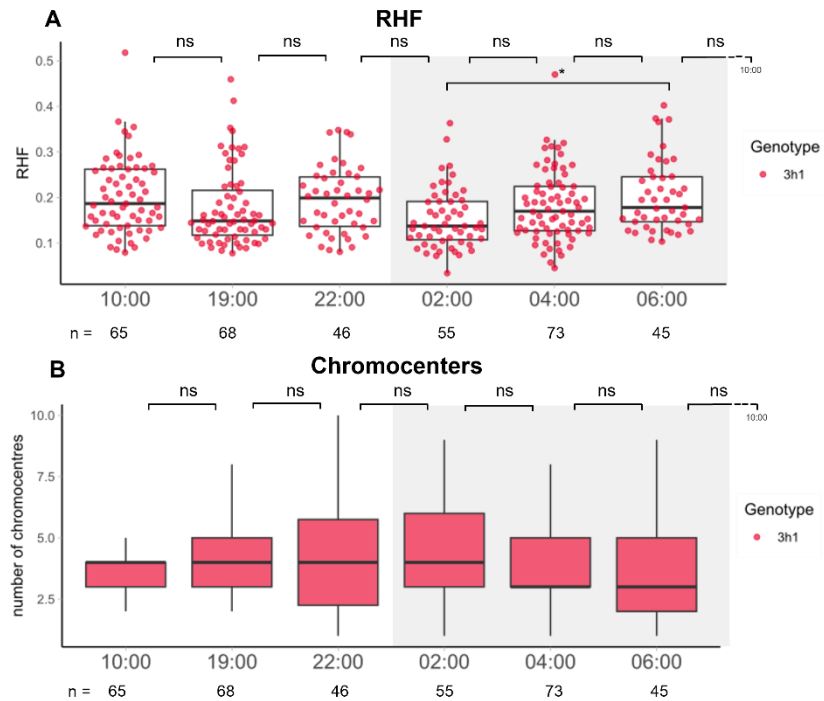
Figure 23 Main heterochromatic features remain constant also in *3h1* nuclei during the diurnal cycle. **(A)** the relative heterochromatin fraction (RHF) of WT nuclei. **(B)** the number of chromocenters (CCs) of *3h1* nuclei. *3h1* nuclei were stained with H3K27me3 and PI, but only PI channel was used for analysis with *Nucl.eye.D*. They were analysed at 6 timepoints. n = number of observed nuclei. Grey area represents the night (light off from 22:00 until 06:00). Statistical test: ANOVA with Tukey HSD (Appendix 8.3.3, * = P<0.05, ** = P<0.01, *** = P<0.001, **** = P<0.0001).

and confidence intervals (CI, α= 0.05) was done, which better reflected the true dynamics. Levels of both RHF (Figure 24E) and number of CCs (Figure 24F) remained mostly stable and RHF had higher values in WT than *3h1* plants. In conclusion this means that we confirm observations of lower RHF and CCs levels upon H1 depletion (Rutowicz *et al.*, 2019), and we show that this state is continuous throughout day and night. Our observed values however are higher compared to previous studies, which could be due to segmentation differences of CCs. In general, the segmentation of *3h1* nuclei needs to be repeated or wrongly detected nuclei have to be filtered.
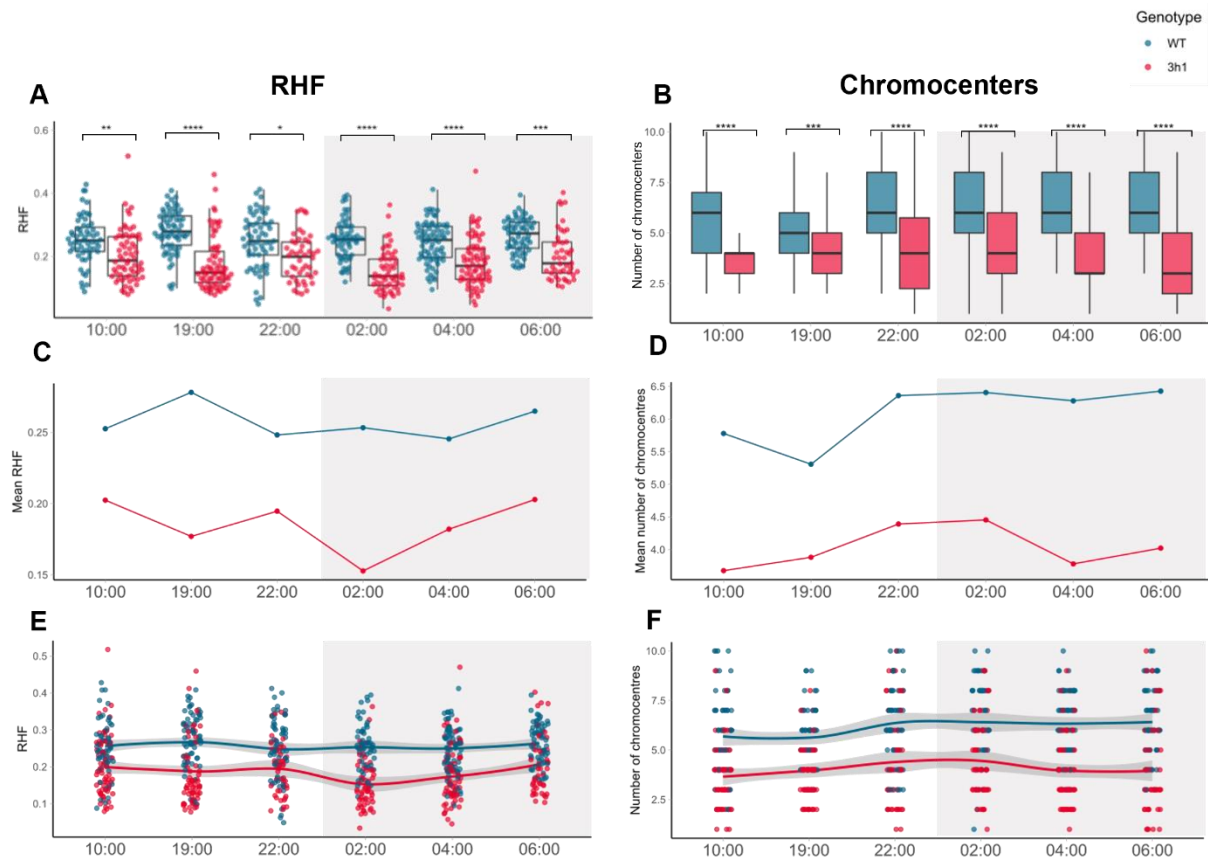
Figure 24 *3h1* nuclei have a lower level of relative heterochromatin factor (RHF) and a reduced chromocenters (CC) number when compared to WT nuclei. **(A)** Boxplot comparing WT and *3h1* RHF values. **(B)** Boxplot comparing WT and *3h1* number of CCs. **(c)** Mean of ratio of RHF, WT versus *3h1* nuclei. **(D)** Mean number of CCs, WT versus *3h1* nuclei **(E)** Local regression line (with locally estimated scatter plot smoothing, LOESS) of the RHF, in grey the CI (α= 0.05) is shown. Single dots represent nuclei. **(F)** Local regression line (with locally estimated scatter plot smoothing, LOESS) of the number of CCs, in grey the CI (α= 0.05) is shown. Single dots represent nuclei. n(WT) =same as in Figure 19, n(*3h1*) = same as in Figure 23. Images from H3K27me3 and PI stained nuclei, analysed with *Nucl.eye.D*. Grey area represents the night (light off from 22:00 until 06:00). Statistical test: ANOVA with Tukey HSD (Appendix 8.3.3, * = P<0.05, ** = P<0.01, *** = P<0.001, **** = P<0.0001).

3.5.2 H1 depletion leads to weaker changes in H3K27me3 and H3K4me3

It has been shown that H1 depletion changes the abundance of H3K27me3 and H3K4me3 (Rutowicz *et al.*, 2019). We observed fluctuations of these two markers along the diurnal rhythm and were interested to see if H1 contributes its regulations. Therefore, immunostaining analysis were done as before.

H3K27me3 showed a significant increase in the intensity ratio during the day and a significant decrease during the night. Especially several hours before turning light on and off major changes were found (19:00-22:00 and 04:00-06:00) (Figure 25A). The level of H3K4me3 remained constant along the diurnal rhythm and no significant differences were found (Figure 25B). In both H3K27me3 and H3K4me3 there are groups of nuclei that show higher ratios (up to two-fold) and are separated from the rest of nuclei (red circles, Figure A, B), similar to observations in WT. Comparing obtained results of *3h1* to WT nuclei revealed significant differences of H3K27me3 levels at 19:00 and 04:00 (Figure 26A). The other timepoints were not significantly different, and *3h1* reached similar values as WT plants. In H3K4me3 nuclei at 10:00
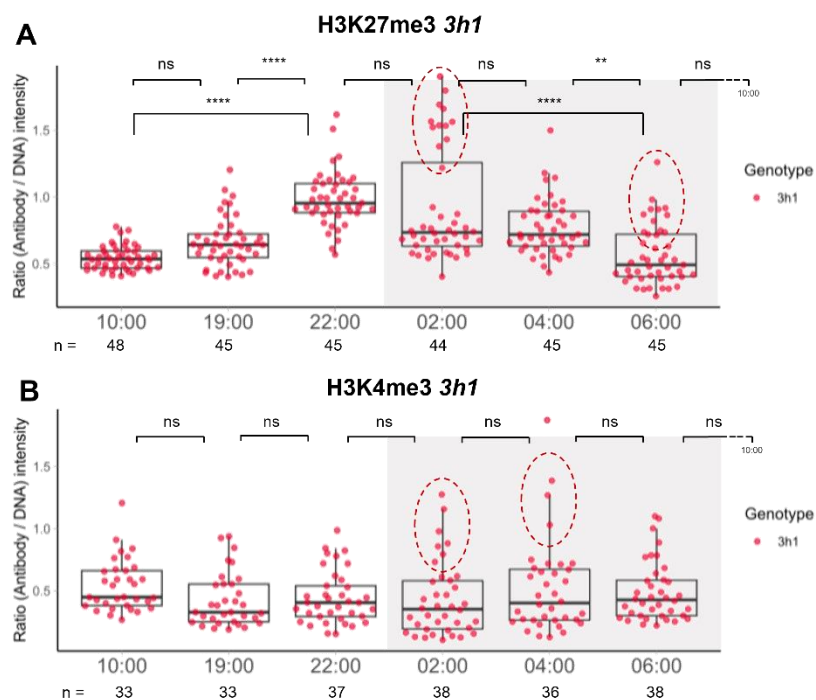
Figure 25 Histone modifications H3K27me3 and H3K4me3 were analysed at 6 timepoints in *3h1* plants. Nuclei were counterstained with PI and manually segmented with Fiji. **(A)** Boxplots of analysed nuclei with H3K27me3/DNA ratio **(B)** Boxplots of analysed nuclei with H3K4me3/DNA ratio. n = number of observed nuclei. Grey area represents the night (light off from 22:00 until 06:00). Statistical test: ANOVA with Tukey HSD (Appendix 8.3.3, * = P<0.05, ** = P<0.01, *** = P<0.001, **** = P<0.0001).

and 04:00 a significant difference between *3h1* and WT nuclei were found (Figure 16B). Looking at the mean ratios it seems that transitions are rougher and flatter in *3h1* compared to WT nuclei (Figure 26C, D). As the mean is influenced by outliers also local linear regression plots with CI (α = 0.05) are shown. In H3K27me3 dynamics remain similar to WT, with equal top and bottom ratios, but transitions between these levels are less pronounced (Figure 26E). In H3K4me3 the dynamic changes found in WT are almost totally lost in *3h1* plants (Figure 26F). Compared to previous findings where histone modification abundances differed by ~two-fold in H3K27me3 and ~five-
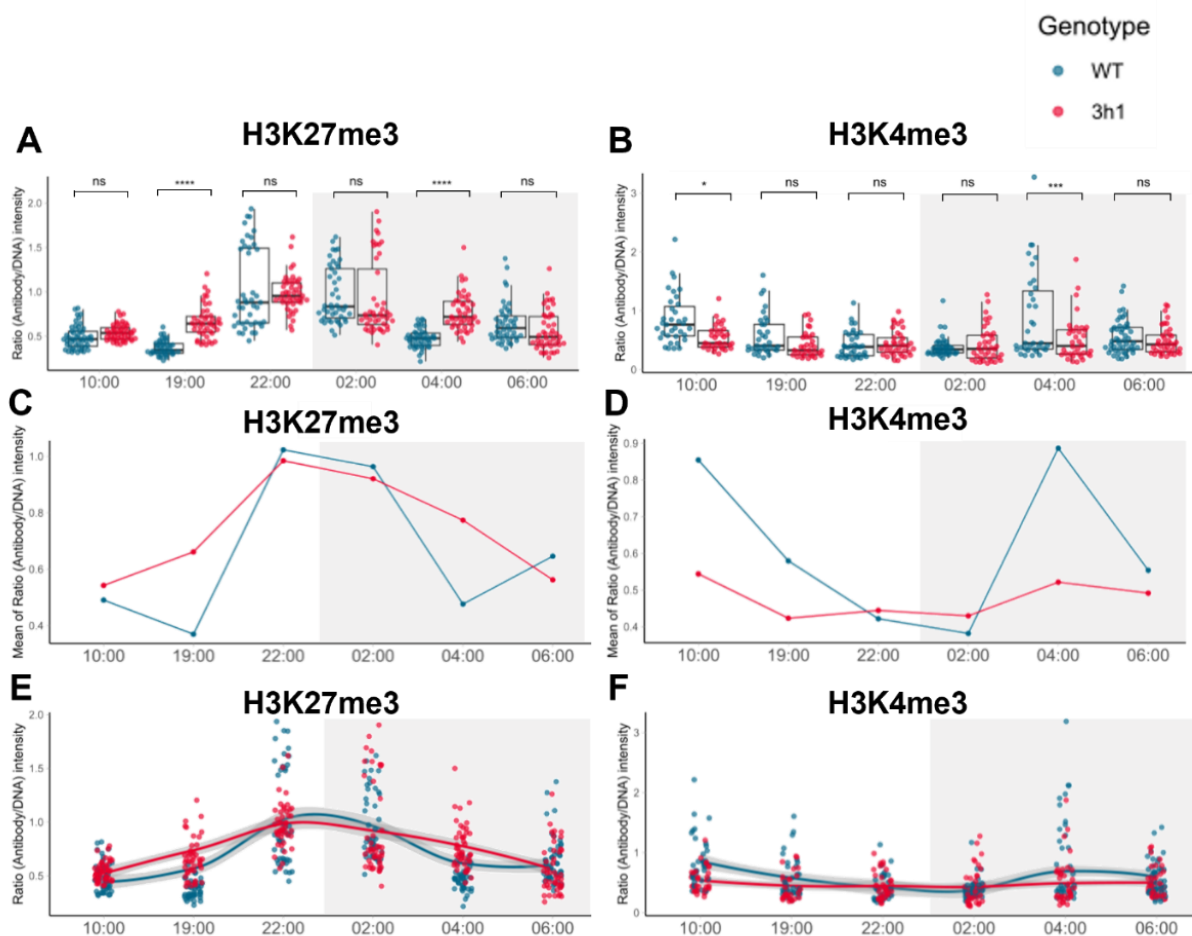
Figure 26 Direct comparison of *3h1* to WT nuclei showed different dynamics upon H1 depletion. n(WT) = same as in Figure 20, n(*3h1*) = same as in Figure 25. **(A)** Boxplot comparing WT and *3h1* nuclei H3K27me3 values. Normalized by DNA (PI) levels **(B)** Boxplot comparing WT and *3h1* nuclei H3K4me3 values. Normalized by DNA (PI) levels **(C)** Mean of ratio of H3K27me3/DNA, WT versus *3h1* nuclei. **(D)** Mean H3K4me3/DNA, WT versus *3h1* nuclei **(E)** Local regression line (with locally estimated scatter plot smoothing, LOESS) of the H3K27me3/DNA ratio, in grey the CI (α= 0.05) is shown. Single dots represent nuclei. **(F)** Local regression line (with locally estimated scatter plot smoothing, LOESS) of the H3K4me3/DNA ratio, in grey the CI (α=0.05) is shown. Single dots represent nuclei. n = number of observed nuclei. Grey area represents the night (light off from 22:00 until 06:00). Statistical test: ANOVA with Tukey HSD (Appendix 8.3.3, * = P<0.05, ** = P<0.01, *** = P<0.001, **** = P<0.0001).

fold in H3K4me3 in WT to *3h1* nuclei (Rutowicz *et al.*, 2019), our results show as well lower levels of *3h1* mutants at certain timepoints but generally not in this extend. It seems that H1 plays a role in regulation of H3K4me3 and might impact also H3K27me3 abundance along diurnal rhythms.

3.5.3 *3h1* have similar Pol II S2P dynamics as WT plants

When comparing different timepoints that were stained for Pol II S2P in *3h1* nuclei there was a significant change found during the day (from 10:00 to 19:00), where the ratio decreased by almost 2-fold (Figure 27A). There was a moderate increase again after the light was turned off at 22:00, until 04:00 in the night. Other timepoints didn't show significant differences, however the levels appeared to fluctuate more, as with H3K4me3. As we already observed how inactive RNA Pol II S5P behaved during changes in WT nuclei, we picked again the same timepoints 19:00 and 22:00 and no significant difference could be found (Figure 27B). The levels were slightly increasing in Pol II S5P compared to Pol II S2P, which would speak for keeping the same
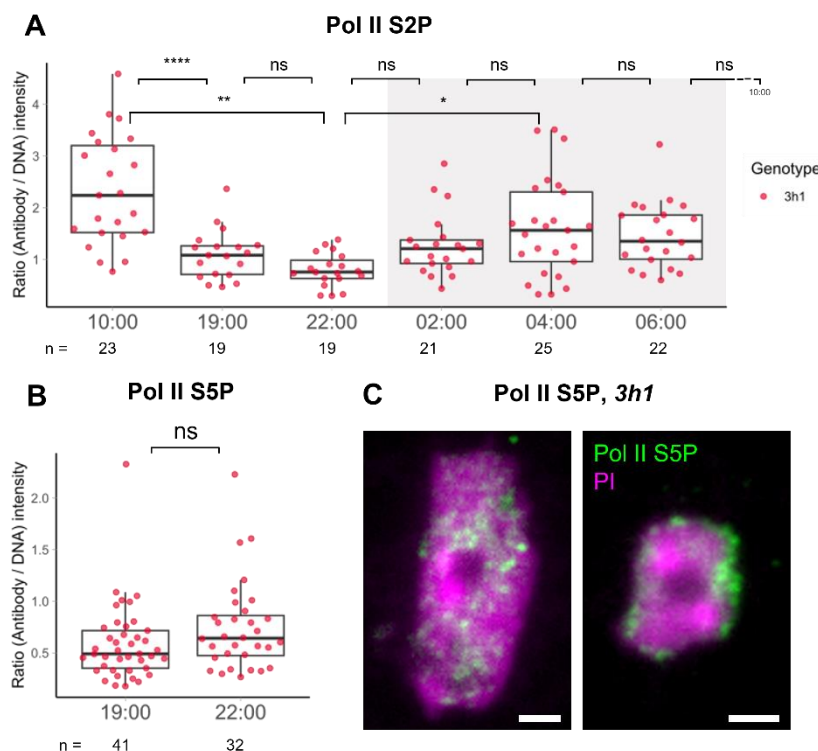
Figure 27 Polymerases II S2P and S5P undergo a modulation of their protein level along the diurnal rhythm in *3h1* plants. **(A)** Boxplots of analysed nuclei with Pol II S2P/DNA ratio at 6 different timepoints **(B)** Boxplots of analysed nuclei with Pol IIS5P/DNA ratio at two timepoints. **(C)** two *3h1* nuclei stained for Pol II S5P (green) and PI (magenta). Scalebar = 2µm. Nuclei were counterstained with PI and manually segmented with Fiji. n = number of observed nuclei. Grey area represents the night (light off from 22:00 until 06:00). Statistical test: ANOVA with Tukey HSD (Appendix 8.3.3, * = P<0.05, ** = P<0.01, *** = P<0.001, **** = P<0.0001).

abundance of RNA Pol II in the nucleus and rather a change from active to passive state. Immunostaining patterns of *3h1* nuclei showed similar variation as observed in WT seedlings (Figure 27C). Interestingly, no major differences in the relative Pol II S2P signal between *3h1* to WT nuclei at different timepoints were found, except at 06:00 (Figure 28A). In the plot showing mean of ratios, bigger differences between WT and *3h1* plants were visible indicating a rhythmic change along the diurnal rhythm, which however must be interpreted with caution. The mean is influenced by outliers and the number of observations was not very high, so more replicates are needed (Figure 28B). This was even better visualized in Figure 28C, where the local regression line with confidence intervals (α= 0.05) are showed. Since the levels of *3h1* and WT nuclei were so similar, it suggested that H1 is not impacting RNA Pol II S2P in a direct way.
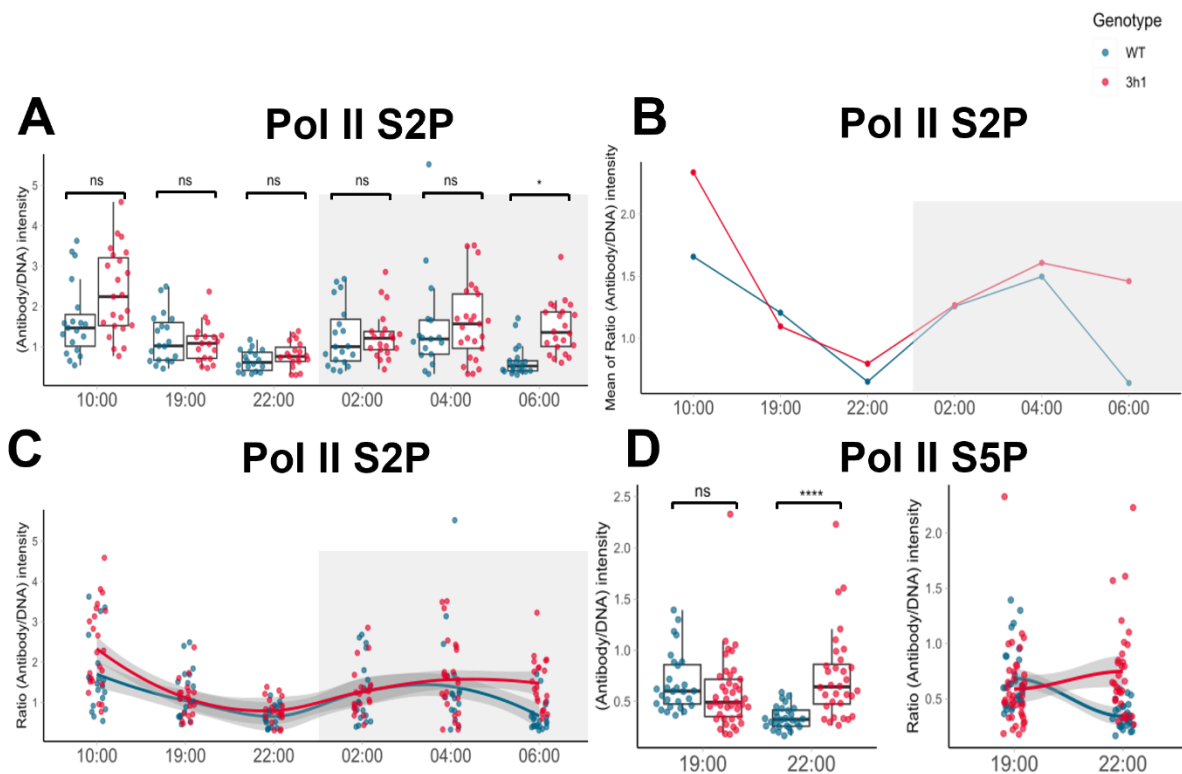
Figure 28 Direct comparison of WT and *3h1* data for RNA Pol II S2P and Pol II S5P. n(WT) = same as in Figure 22, n(*3h1*) = same as in Figure 27. **(A)** Boxplot comparing WT and *3h1* nuclei of Pol II S2P values. Normalized by DNA (PI) levels. **(B)** Local regression line (with locally estimated scatter plot smoothing, LOESS) of the Pol II S2P/DNA ratio, in grey the CI (α = 0.05) is shown. Single dots represent nuclei. **(C)** Mean of ratio of Pol II S2P/DNA, WT versus *3h1* nuclei. **(D)** Boxplots comparing WT and *3h1* nuclei of Pol II S5P/DNA (PI intensity), and local regression line, with CI (grey, a = 0.05). Single dots represent nuclei. n = number of observed nuclei. Grey area represents the night (light off from 22:00 until 06:00). Statistical test: ANOVA with Tukey HSD (Appendix 8.3.3, * = P<0.05, ** = P<0.01, *** = P<0.001, **** = P<0.0001).

When comparing the two selected timepoints 19:00 and 22:00 for RNA Pol II S5P between WT and *3h1* plants, a change in dynamic was observed. At 22:00 a major difference was detected between the two genotypes. In WT nuclei the relative Pol II S2P signal decreased between the timepoints 19.00 and 22:00, while it remained stable in *3h1* mutants.

3.6 Nanoscale analysis indicates dynamic re-distribution of H3K27me3 and Pol II S2P

Our previous results revealed significant changes in the global abundance of chromatin markers (H3K27me3 and H3K4me3) and polymerase proteins (Pol II S2P, Pol II S5P) along the diurnal rhythm. To further investigate such re-organizational events, we wanted to assess 3D chromatin organization and distribution pattern on a nanoscale, using super resolution microscope stimulated emission depletion (STED). Due to time limitations only two timepoints were selected, based on the finding that H3K27me3 levels significantly changed between 19:00 and 22:00. Nuclei were extracted and embedded in acryl-amide pads using a method developed in our lab (Randall *et al.*, 2022). After imaging and deconvolution, the nuclei were manually segmented in Imaris and the antibody intensity was normalized by the DNA intensity to create a ratio over every voxel. This was used for spatial distribution analyses, plotting the voxel distribution relative to the nucleus periphery as a function of their (relative) intensity. Due to time limitations only two timepoints were selected, based on the finding that H3K27me3 levels significantly changed between 19:00 and 22:00. In total 5 nuclei were imaged for H3K27me3 and Pol II S2P, of which three are displayed. In H3K27me3 a speckled pattern was observed all over euchromatin, with some single big clusters (Figure 29A). From this pilot analysis, H3K27me3 seemed to accumulate more towards the nuclear periphery, which was visible when looking at the (Figure 29A, 3rd column) ratio of H3K27me3 divided by DNA. This could be observed as well in the quantification, where the relative amount of H3K27me3 (measured by the mean intensity of the channel ratio) increased towards the periphery of the nucleus. Moreover, H3K27me3 levels were lower at 19:00 than at 22:00 (Figure 29B) consistent with our previous findings. In Pol II S2P stained nuclei the antibody signal was widely distributed in euchromatin and nicely omitted chromocenters (Figure 29C). In these nuclei Pol II S2P showed a speckled but mostly homogenous pattern. Visualising the ratio of RNA PolI S2P relative to DNA (Figure 29C, 3rd column) shows clear, local

clusters of Pol II S2P. Looking at the quantification it is visible that the timepoint of 19:00 started on a higher level and decreased towards the periphery, whereas timepoint 22:00 increased from a very low level (Figure 29D). This could be explained by the presence of a big nucleolus in the centre of the nucleus. The ratio at 19:00 is higher than at 22:00, which confirms previously observed results. However, these outcomes must be interpreted with caution as the number of nuclei is very low, and more replicates are needed for trustworthy results. This pilot experiment suggests a possible dynamic in the redistribution of H3K27me3 and Pol II S2P between 19:00 and 22:00 but requires further investigations for validation.
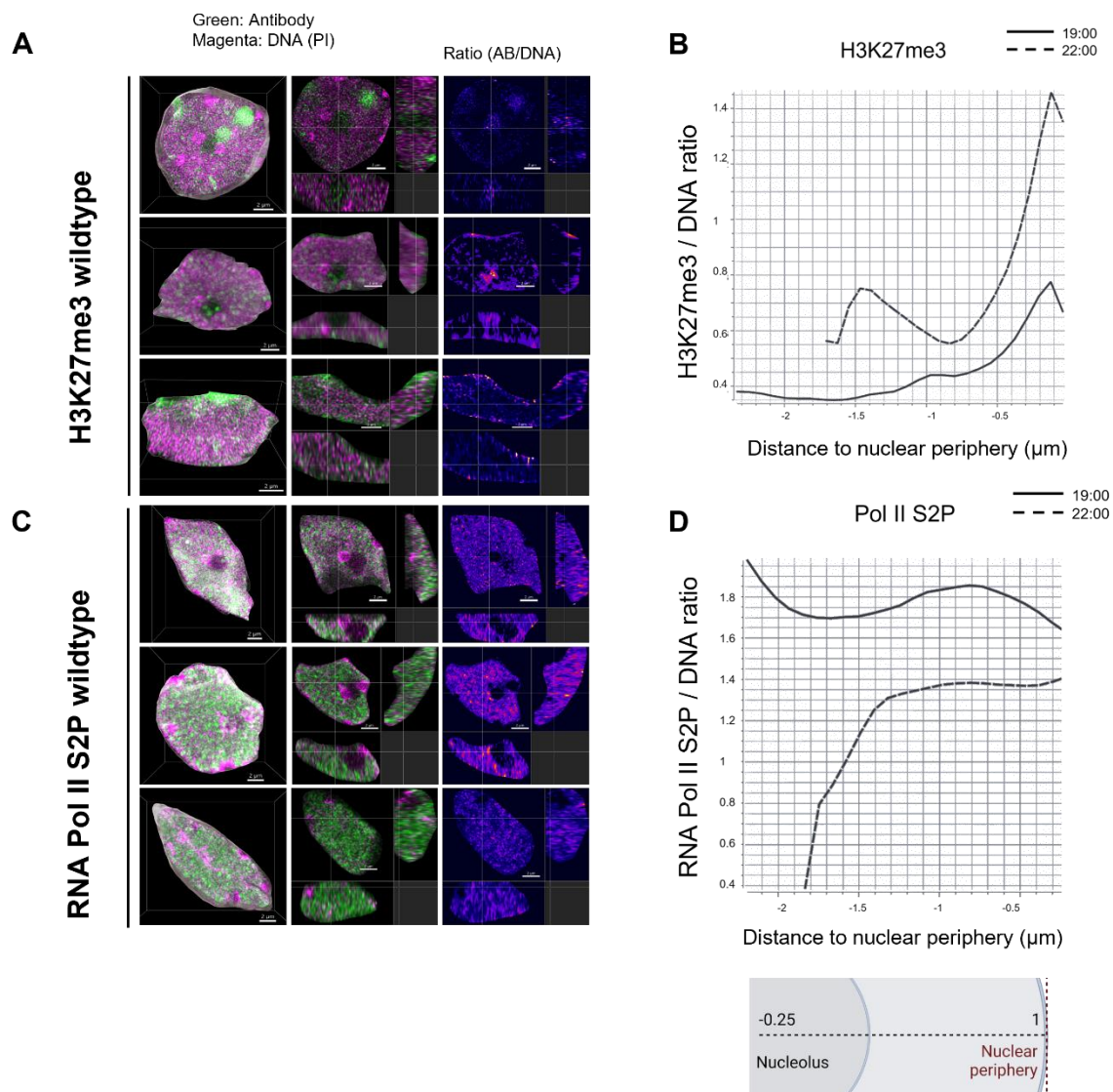
Figure 29 Super-resolution microscopy allows to investigate nano-scale domains and 3D chromatin organization. Images acquired with stimulated depletion emission microscope (STED) and analysed with Imaris. **(A)** Green: H3K27me3 antibody intensity, Magenta: DNA (Live560) intensity, 1st column shows the whole segmented 3D nucleus, 2nd column shows a cross-section of nucleus with antibody and DNA staining, 3rd column displays the ratio (=H3K27me3/DNA). **(B)** Quantification of two timepoints 19:00 and 22:00 shows distance to periphery of the ratio intensity of every voxel. **(C)** Green: Pol II S2P antibody intensity, Magenta: DNA (Live560) intensity, 1st column shows the whole segmented 3D nucleus, 2nd column shows a cross-section of nucleus with antibody and DNA staining, 3rd column displays the ratio (=Pol II S2P/DNA). **(D)** Quantification of two timepoints 19:00 and 22:00 shows distance to periphery of the ratio intensity of every voxel. Scalebar = 2um, n = 5.

52

4 Discussion

Light is not only an essential source of energy, but also delivers important information from the environment. The impact of light on chromatin organization is still not fully uncovered. Coordinated expression of genes during the diurnal rhythm influences various physiological processes, which is partially controlled by changes in 3D chromatin organization and epigenetic modifications. The linker histone H1 is a key regulator of genome packing and plant development is impaired under different light regimes when H1 is depleted. This project aimed to investigate diurnal effects on chromatin organization, and if the presence of H1 impacts this. Our global analysis of abundance and distributions of chromatin features like heterochromatin, histone modifications (H3K27me3, H3K4me3) and Pol II provided quantitative insights in light-dependent chromatin organization.

4.1 Daily remodelling of the epigenetic landscape

Coordinated changes in gene expression is believed to contribute to daily adaptation of physiological processes in plants (Panter *et al.*, 2019). However, the role of diurnal chromatin organization and the potential impact on rhythmic gene expression is not fully understood. One key feature of chromatin organisation is the relative heterochromatin fraction (RHF) measured cytologically. Indeed, heterochromatin was found to be highly dynamic under different developmental and physiological transitions like at flowering, at germination, under de-differentiation (Tessadori, Chupeau, *et al.*, 2007; Tessadori, Schulkes, *et al.*, 2007; Bourbousse *et al.*, 2015). Our observations showed that in WT plants the RHF, and the number of chromocenters (CCs) remain on relative steady level along the day and night with some moderate changes. As CCs mainly contain centromeric repeats, pericentromeric repeats, transposons and rDNA (Fransz *et al.*, 2002; Tessadori, Chupeau, *et al.*, 2007), it seems sensible to keep these sequences silent independent from daylight cycles. However, de-condensation is not necessarily connected to a de-repression of genes, but rather associated to looser chromatin structures that can be more easily re-arranged (Di Stefano *et al.*, 2021). Furthermore, a large-scale rearrangement of heterochromatin would involve many modifications that can be very energy consuming. Next, we investigated histone modifications, which have been shown to occur in distinct phases at their target genes in plants and mammals (Koike *et al.*, 2012; Song *et al.*, 2019), which indicates their

involvement in rhythmic gene expression. Our results showed that H3K27me3 follows a diurnal rhythm with an increasing abundance during the day and a decreasing abundance during the night. H3K4me3 showed a higher peak in mornings, which decreased towards the evening. ChIP-seq analysis revealed that H3K4me3 peaks in morning phases to express morning-phased genes (Song *et al.*, 2019), which underlines our observation. However, we found again an increase during the night, which was probably due to high variability in nuclei (Discussion 4.4). Interestingly, in both histone markers the changes occurred before light was turned on and off, and not immediately after. This aligns with findings of transcript levels of different genes, which strongly change at dawn and dusk in plants grown in short day condition. Furthermore, these changes were associated with histone modifications H3K9ac and H3K27ac (Baerenfaller *et al.*, 2012), demonstrating the involvement of PTMs in rhythmic gene expression.

Also, certain histone demethylases are involved in regulating circadian rhythms. The Jumonji C (JmjC)-containing eraser demethylases are important to modify H3K27me3 signatures (Yamaguchi, 2021). JUMONJI DOMAIN-CONTAINING PROTEIN32 (JMJ32) and JUMONJI DOMAIN-CONTAINING PROTEIN30 (JMJ30) are associated to circadian clock genes *TOC1, CCA1 and LHY* (Jones *et al.*, 2010; Lu *et al.*, 2011), which are regulated by different histone modifications (Hemmes *et al.*, 2012; Malapeira, Khaitova and Mas, 2012; Song and Noh, 2012). Transcriptomic analysis showed that JMJ30 undergoes a steep increase during the day and drops during the night (Rutowicz, unpublished). This was surprising, as we expected an opposite dynamic between the H3K27me3 and demethylase levels. It could be that demethylase activity is regulated by import and export in and out the nucleus, which is not monitored by transcript levels. Diurnal transcriptomic analysis further revealed that *CCA1* and *LHY* decrease during the day and increase during the night, while *TOC1* follows the same rhythm but with opposing dynamics (Rutowicz, unpublished). *CCA1* and *LHY* upregulate the writer SDG2 and repress the demethylase gene JMJ14 in a rhythmic way. This results in diurnal changes in H3K4me3 levels of certain target genes (Song *et al.*, 2019). H3K4me3 is necessary for correct expression of oscillator genes and works as antagonist of binding of clock repressors (Hemmes *et al.*, 2012; Malapeira, Khaitova and Mas, 2012).

Many metabolic processes are associated with the circadian clock. One component of the PRC2 complex, FERTILIZATION-INDEPENDENT ENDOSPERM (FIE), is targeted by TOR, which gets activated by glucose. This induces its translocation to the nucleus (Ye *et al.*, 2022). TOR regulation of H3K37me3 target genes were also activated by environmental cues like vernalization (Ye *et al.*, 2022) or upon stress (Dong *et al.*, 2021). Another example is the sensitivity of the histone mark H3K9me3 to changes in the metabolites SAM and/or SAH of the methionine pathway (Zhou *et al.*, 2013; Inagaki *et al.*, 2017). It was found that reduced levels of SAM and SAH affect H3K4me3 in humans (Mentch *et al.*, 2015). Yet, still many questions remain open on how primary metabolism can impact the chromatin structure and how chromatin changes impact specific metabolic pathways [Reviewed in (Lindermayr *et al.*, 2020)]. As future experiment one could test the impact of sucrose in MS media compared to plants grown without sucrose.

Looking at RNA Pol II S2P, which marks actively transcribing genes, we saw a decrease during the day, increase until mid-night and a decrease again towards the morning. RNA Pol II precedes the mRNA transcripts by around 2-3 hours (Le Martelot *et al.*, 2012; Deng *et al.*, 2022). Connected with histone modification changes, it is feasible that this helps the plant to prepare for adapting the gene expression in time to be ready for the changing light condition and could speak for circadian entrainment. The rhythm of RNA Pol II S2P correlated with H3K4me3 levels and H3K4me3 is known to help in recruitment of RNA Polymerase II machineries to target genes (Chen *et al.*, 2011). Decreasing Pol II S2P levels in the evening prompted us to investigate whether there was a shift from active to inactive polymerase complexes, or if entire complexes were being degraded during this period. Analysis of Pol II S5P showed a decline in Pol II S5P, which speaks for degradation. For future experiments it would be interesting to look at more timepoints with Pol II S5P to see if this is the case along the whole diurnal rhythm or just at certain phases. Furthermore, a marker that tags Polymerase II independently of the transcriptional state (e.g., Pol II β1 subunit) could be used to confirm that general levels are changing according to our findings.

To conclude, heterochromatin remained stable along the diurnal rhythm, but histone modifications (H3K27me3, H3K4me3) showed rhythmic pattern in their abundance, with significant changes a few hours before light was turned on and off. This indicates their association to regulating circadian rhythms, where also metabolic alterations

influence chromatin-modifying enzymes. Our plants were grown in plant incubator with direct light changes from on to off and *vice versa*, meaning that there is no dusk or dawn. This suggests that we see circadian entrainment. To disentangle the observed re-organization from the circadian rhythm it would be interesting to investigate how our selected markers behave in plant backgrounds of clock mutants. Another possibility would be to compare plants grown in diurnal versus continuous light regimes and test what impact sucrose availability or absence in plant growth media has.

4.2 Speckled immunostaining pattern indicate the formation of nuclear bodies

Plant chromatin is tightly organized in a non-random way to orchestrate quick biochemical reactions. When looking at immunostaining pattern of different chromatin marks, we found variable distributions. In H3K27me3 staining we observed speckled pattern all over the nucleus, which could be explained by liquid-liquid phase separation (LLPS). LLPS concentrates different cellular condensates that show distinct biochemical properties in a membraneless manner [Reviewed in (Kim *et al.*, 2021)]. It is dynamic and reversible which allows rapid response to stimuli via fast and precise chromatin reorganizations and gene expression [Reviewed in (Kim *et al.*, 2021)]. The formation of these nuclear bodies is based on chemical forces such as electrostatic interactions, hydrophobic interactions and hydrogen bonds (Murthy *et al.*, 2019). Amino acid residues of PTMs can influence such interactions and therefore they may also lead to the aggregation of similar macromolecules (Bah and Forman-Kay, 2016). A study has shown, that the PRC2 complex forms nuclear bodies where the H3K27me3 mark is established (Zhang *et al.*, 2020). This underlines well our observations and would indicate that heterochromatin organization is at least partially modified by LLPS. This has not yet been shown for H3K4me3, however similar mechanisms could cause the speckles we observed in immunostainings of this mark. Also, for Pol II it is suggested that spatial clusters are formed to coordinate expression of rhythmically expressed genes (Deng *et al.*, 2022). We found variable patterns of Pol II distributions and different nuclei shapes, which are most likely due to biological reasons and were confirmed in an independent approach using live-cell imaging of a reporter line. Different shapes have been described to be specific to different plant tissues (Pavlova *et al.*, 2022). The non-homogeneous distribution pattern of RNA Pol

II S2P could be due to extracting nuclei of different cell types which showed different patterns of specialized gene-expression.

The global changes observed in histone modifications raised new questions such as how these re-organization events are organised on nanoscale-levels. Due to time limitations only a pilot experiment using the stimulated depletion emission microscope (STED) was dedicated to investigating this for H3K27me3 and Pol II S2P at two timepoints in the evening. In both cases we confirmed our results from the cytological experiments, where H3K27me3 levels increased and Pol II S2P levels decreased. The ratio drop at the nuclear periphery was most likely because of inaccurate segmentation at the boarders, which lead to an artefact in the signal intensity. The number of images was very low, so more replicates are needed to draw reliable conclusions. As the antibody signal was bleaching towards the end of z-stacks, acquisition settings need further improvement by e.g. adapting gating time, MOTCOR and delay time (Dumbović *et al.*, 2021). Additionally, the antibody signal could be enhanced by longer incubation time or higher concentrations. Segmenting single antibody clusters would allow to explore the distributions of tethered nuclear bodies.

In conclusion, our observations of speckled pattern suggest that this was due the formation of nuclear bodies, where chromatin with similar states are tethered, to facilitate coordinated expression or silencing mechanisms.

4.3 H1 depletion has moderate effects on epigenetic landscape

The linker histone H1 is a key player in regulating the epigenetic landscape [Reviewed in (Fyodorov *et al.*, 2018)]. Comparing our results of WT to *3h1* plants allowed us to investigate the role of H1 in light-dependent chromatin reorganization. We confirmed that the number of CCs and the RHF are reduced in *3h1* compared to WT nuclei as previously reported by (Rutowicz *et al.*, 2019). This decondensation could also explain observation of morphological features where we found alterations in size and shape of nuclei lacking H1. Similar observations have been made previously (Rutowicz *et al.*, 2019) and were also found in mouse lymphocytes (Willcockson *et al.*, 2021). As in WT plants, there was no change in heterochromatin along the diurnal rhythm. However, due to segmentation difficulties using the semi-automatic segmentation tool *Nucl.eye.d* (Johann to Berens *et al.*, 2022) especially in *3h1* nuclei, only cautious conclusions can

be drawn and reliable results require re-analysis of heterochromatin features. Looking at the histone modifications H3K27me3 and H3K4me3 discrepancies between WT and *3h1* nuclei were found. Facultative heterochromatin reached the same top and bottom levels of the intensity ratio but the transition in between seemed to be less pronounced. At these timepoints the ratio of H3K27me3 was lower in *3h1* compared to WT nuclei, as seen in previous studies (Rutowicz *et al.*, 2019). This could indicate that fine-tuning is lost, and transitions are not as smooth anymore when H1 is lacking, which would support our model of H1 helping to ensure stable epigenetic states. The moderate changes in H3K4me3 levels in WT plants were totally lost in *3h1* seedlings and remained constant throughout the diurnal rhythm. This aligns with previous findings that levels of H3K4me3 are lowered upon H1 depletion (Rutowicz *et al.*, 2019). It seemed that H3K4me3 methylation is stronger influenced by H1 than H3K27me3, as the *3h1* mutant showed stronger discrepancies to the WT.

It is worth mentioning that the linker histone H1 did not greatly impact the expression of any investigated histone demethylases (*JMJ13, JMJ12, JMJ11, JMJ32, JMJ30*) or clock genes (*CCA1, LHY, TOC1*) in transcriptomic experiments. Only *MEA* showed a reduced level of expression in *3h1* compared to WT plants, while the expression of other PRC2 components (*CLF* and *SWN*) remained equal (Rutowicz, unpublished). It was suggested that the reduction of H3K27me3 does not cause an upregulation of genes in *3h1* seedlings (Rutowicz *et al.*, 2019).

When looking at transcription machineries we did not observe major effects in the abundance of Pol II S2P. Minor differences were found between certain timepoints where Pol II S2P levels were increased compared to WT. A possibility is that decondensation of heterochromatin in *3h1* mutants facilitates the access of transcription machineries to a greater number of genes. Surprisingly, when looking at inactive Pol II S5P between timepoints 19:00 and 22:00 the levels increased in contrast to what was observed in WT plants. This indicates a deactivation of Pol II S2P. As the number of observations was quite low, more replicates are needed, and it would be interesting to also investigate other timepoints.

In conclusion, H3K27me3 and H3K4me3 levels were impacted by H1 depletion, which indicates that rough re-organizations still happen, but fine-tuning is lost. This would support the model suggested by our group, however further investigation is needed.

4.4 Variations in measurements can have various reasons

In our nuclei histone modification analyses we observed batches with higher ratios compared to the rest. A high ratio means that the antibody intensity was much stronger than the DNA intensity. This could be explained by different aspects. The quality of nuclei extract could have varied and influenced subsequent steps such as the immunostainings. Clearing steps with Xylene, an organic solvent, could have caused slight DNA alteration (Aquino *et al.*, 2016), which decrease antibody recognition and detection. Furthermore, a bias in choosing nuclei during the imaging sessions could have impacted end results. However, to reduce variation caused by technical origins and bias, all genotypes, timepoints and replicates of the same marker were processed in parallel, and nuclei were selected based on DNA and not antibody staining. Variations might also be explained by plants growing at different places in the incubator which can have slightly altered light conditions or by nuclei coming from different cell types and with different functions (Pavlova *et al.*, 2022). We found many different shapes when scoring in Pol II-stained nuclei and in our live-cell reporter line. Therefore, we could expect that also their chromatin organization is adapted to specific gene expression needed in those cell types.

Surprisingly, when analysing the RHF and number of CCs there were hardly any nuclei with more than 10 CCs. Due to endoreduplication we would expect nuclei with 4C-32C or even higher [Reviewed in (Sugimoto-Shirasu and Roberts, 2003)]. In our case it seems that all nuclei were only 2C and thus maximum 5 chromosomes or 10 CCs were detected. As endoreduplication leads to an increase in genome content in epidermis cells of *A. thaliana*, also the nucleus gets bigger [Reviewed in (Sugimoto-Shirasu and Roberts, 2003)]. A possible explanation for only finding 2C nuclei is, that bigger nuclei were filtered out in the extraction step. To avoid endoreduplication bias the immunostaining experiments we always normalized antibody with DNA intensities.

In conclusion, it is difficult to determine if the observed observations are caused by technical or biological origins or both. Technical variations were tried to be reduced to a minimum, so for future experiments if would be interesting to investigate the role of nuclei size, shape, and cell tissue specific functions on variation.

4.5 *Nucl.eye.D* as a powerful high-throughput segmentation tool

Advancements in microscopic cytological approaches enable detailed analysis of nuclear organization. With rising amount of data, it is crucial to have reliable qualitative and quantitative methods to detect such nuclear structures. The recently developed semi-automated segmentation tool *Nucl.eye.D* (Johann to Berens *et al.*, 2022), has been used and tested in this study for analysis purpose. A great advantage of *Nucl.eye.D* is that a huge amount of data (in our case >800 nuclei) can be analysed at once, therefore, it proved to be a powerful tool for high-throughput quantification. However, it took some time to get familiar with the segmentation process and the different macros. Aspects, such as printing out defective images or even automatically exclude them, would provide a higher user-friendliness. Until now it remained unclear what caused images to be erroneous. In some cases, it was possible that the nucleus was too close to the image boarder, or it is possible that there was debris in the background which was misleading. Maybe images were somehow corrupted in the metadata, which would have prevented the computer from correctly reading the information. The usability of images could be optimized by improving staining quality for which we suggest using PI instead of DAPI counterstain. After segmentation a manual curation is needed to filter out wrongly detected nuclei. One possibility to do so, would be looking at the average CC area and set a threshold. Then all masks that were wrongly detecting too big CC areas (e.g., by segmenting two CCs as one big CC, Figure 16) could be filtered out. If these small adjustments can be made, the program will ease the workload, save time and be a powerful tool for high-throughput segmentation.

4.6 Conclusion and outlook

Our cytological analysis of abundance and distributions of chromatin features like heterochromatin fraction, histone modifications (H3K27me3, H3K4me3) and Pol II provided quantitative insights in diurnal changes of chromatin architecture. Constitutive heterochromatin remained largely unaffected during the diurnal rhythm, indicating that big rearrangements only happen during major developmental transitional phases. H3K27me3 and H3K4me3 abundance changed rhythmically during the day and bigger rearrangements usually occurred shortly before light is turned on and off. This indicates an entrainment of recruitment mechanism in a circadian way. However

further analysis with e.g. clock mutants are needed to confirm this hypothesis. Furthermore, H3K27me3 and H3K4me3 nuclei immunostainings showed speckled patterns indicating the formation of nuclear bodies that could be associated with the LLPS model. The formation of such bodies would help regulating genes in a coordinated manner. H3K4me3 rhythmic abundance correlated well with the RNA Pol II S2P abundance. Pol II S2P distribution also changed in a diurnal manner, confirming results observed from transcriptomic analysis in other plant species. Also, changes in Pol II S2P levels were observed ahead of turning on and off the light, and as Pol II precedes mRNA transcripts by a few hours, it is possible that the plant prepares "in advance" for the changing light condition. We found that H1 impacts the regulation of histone modifications H3K27me3 and H3K4me3 along the diurnal rhythm, which supports our model that fine-tuning regulations are lost. H3K4me3 completely lost its diurnal rhythm. Surprisingly, the transcription machinery Pol II was not heavily affected by H1 depletion and levels showed similar dynamics as WT plants.

As follow up experiments it is sensible to repeat experiment independently under same conditions to see if our observations can be confirmed with replicates. Furthermore, it would be also interesting to compare results from experiment 1 (A and B replicates) to those of experiment 2 (C and D), to see if temperature impacts chromatin organization. For future nuclei extraction it is advisable fix leaves of night timepoints using a green lamp, to not trigger light-dependent rearrangements of chromatin. Other molecular methods could be used to independently underline our findings, for example with western blots of demethylases at the same timepoints. This would also allow to see if changes of histone modifications are active or passive processes. Furthermore, would be interesting to investigate time spans before light is on and off a bit closer and take additional timepoints into account. Investigating changes on a nano-scale level and with a higher number of replicates and improved image acquisition settings would allow to investigate the shape and positioning of nanodomains relative to each other and to nuclear periphery. Other interesting testing would be comparing different light conditions with variations in intensity, quality, and wavelengths to further explore the impact of light on chromatin. Many questions concerning the dynamic reorganization along the diurnal rhythm remain unclear and require further analysis.

5 Acknowledgement

6 References

Alberts, B. (2015) *Molecular biology of the cell*. Sixth edition. New York, NY: Garland Science, Taylor and Francis Group.

Aquino, T.D. *et al.* (2016) 'DNA damage and cytotoxicity in pathology laboratory technicians exposed to organic solvents', *Anais da Academia Brasileira de Ciências*, 88(1), pp. 227–236. Available at: https://doi.org/10.1590/0001-3765201620150194.

Baerenfaller, K. *et al.* (2012) 'Systems-based analysis of Arabidopsis leaf growth reveals adaptation to water deficit', *Molecular Systems Biology*, 8(1), p. 606. Available at: https://doi.org/10.1038/msb.2012.39.

Baerenfaller, K. *et al.* (2016) 'Diurnal changes in the histone H3 signature H3K9ac|H3K27ac|H3S28p are associated with diurnal gene expression in *Arabidopsis*: Diurnal chromatin modification signature', *Plant, Cell & Environment*, 39(11), pp. 2557–2569. Available at: https://doi.org/10.1111/pce.12811.

Bah, A. and Forman-Kay, J.D. (2016) 'Modulation of Intrinsically Disordered Protein Function by Post-translational Modifications', *Journal of Biological Chemistry*, 291(13), pp. 6696–6705. Available at: https://doi.org/10.1074/jbc.R115.695056.

Berger, F. (2019) 'Emil Heitz, a true epigenetics pioneer', *Nature Reviews Molecular Cell Biology*, 20(10), pp. 572–572. Available at: https://doi.org/10.1038/s41580-019-0161-z.

Bourbousse, C. *et al.* (2015) 'Light signaling controls nuclear architecture reorganization during seedling establishment', *Proceedings of the National Academy of Sciences*, 112(21). Available at: https://doi.org/10.1073/pnas.1503512112.

Bourbousse, C., Barneche, F. and Laloi, C. (2020) 'Plant Chromatin Catches the Sun', *Frontiers in Plant Science*, 10, p. 1728. Available at: https://doi.org/10.3389/fpls.2019.01728.

Brown, S.W. (1966) 'Heterochromatin: Heterochromatin provides a visible guide to suppression of gene action during development and evolution.', *Science*, 151(3709), pp. 417–425. Available at: https://doi.org/10.1126/science.151.3709.417.

Chen, Y. *et al.* (2011) 'Prediction of RNA Polymerase II recruitment, elongation and stalling from histone modification data', *BMC Genomics*, 12(1), p. 544. Available at: https://doi.org/10.1186/1471-2164-12-544.

Chen, Z.J. and Mas, P. (2019) 'Interactive roles of chromatin regulation and circadian clock function in plants', *Genome Biology*, 20(1), p. 62. Available at: https://doi.org/10.1186/s13059-019-1672-9.

Cookson, S.J., Radziejwoski, A. and Granier, C. (2006) 'Cell and leaf size plasticity in Arabidopsis: what is the role of endoreduplication?', *Plant, Cell and Environment*, 29(7), pp. 1273–1283. Available at: https://doi.org/10.1111/j.1365-3040.2006.01506.x.

Deng, L. *et al.* (2022) 'Diurnal RNAPII-tethered chromatin interactions are associated with rhythmic gene expression in rice', *Genome Biology*, 23(1), p. 7. Available at: https://doi.org/10.1186/s13059-021-02594-7.

Di Stefano, M. *et al.* (2021) 'Polymer modelling unveils the roles of heterochromatin and nucleolar organizing regions in shaping 3D genome organization in *Arabidopsis thaliana*', *Nucleic Acids Research*, 49(4), pp. 1840–1858. Available at: https://doi.org/10.1093/nar/gkaa1275.

Dong, Y. *et al.* (2021) *TOR represses stress responses through global regulation of H3K27 trimethylation in plants*. preprint. Plant Biology. Available at: https://doi.org/10.1101/2021.03.28.437410.

Dumbović, G. *et al.* (2021) 'Stimulated emission depletion (STED) super resolution imaging of RNA- and protein-containing domains in fixed cells', *Methods*, 187, pp. 68–76. Available at: https://doi.org/10.1016/j.ymeth.2020.04.009.

Fransz, P. *et al.* (2002) 'Interphase chromosomes in *Arabidopsis* are organized as well defined chromocenters from which euchromatin loops emanate', *Proceedings of the National Academy of Sciences*, 99(22), pp. 14584–14589. Available at: https://doi.org/10.1073/pnas.212325299.

Fyodorov, D.V. *et al.* (2018) 'Emerging roles of linker histones in regulating chromatin structure and function', *Nature Reviews Molecular Cell Biology*, 19(3), pp. 192–206. Available at: https://doi.org/10.1038/nrm.2017.94.

Gendreau, E. *et al.* (1997) 'Cellular Basis of Hypocotyl Growth in Arabidopsis thaliana', *Plant Physiology*, 114(1), pp. 295–305. Available at: https://doi.org/10.1104/pp.114.1.295.

Hemmes, H. *et al.* (2012) 'Circadian Clock Regulates Dynamic Chromatin Modifications Associated with Arabidopsis CCA1/LHY and TOC1 Transcriptional Rhythms', *Plant and Cell Physiology*, 53(12), pp. 2016–2029. Available at: https://doi.org/10.1093/pcp/pcs148.

Henry, K.W. *et al.* (2003) 'Transcriptional activation via sequential histone H2B ubiquitylation and deubiquitylation, mediated by SAGA-associated Ubp8', *Genes & Development*, 17(21), pp. 2648–2663. Available at: https://doi.org/10.1101/gad.1144003.

Hsin, J.-P. and Manley, J.L. (2012) 'The RNA polymerase II CTD coordinates transcription and RNA processing', *Genes & Development*, 26(19), pp. 2119–2137. Available at: https://doi.org/10.1101/gad.200303.112.

Inagaki, S. *et al.* (2017) 'Gene-body chromatin modification dynamics mediate epigenome differentiation in *Arabidopsis*', *The EMBO Journal*, 36(8), pp. 970–980. Available at: https://doi.org/10.15252/embj.201694983.

Izzo, A. and Schneider, R. (2016) 'The role of linker histone H1 modifications in the regulation of gene expression and chromatin dynamics', *Biochimica et Biophysica Acta (BBA) - Gene Regulatory Mechanisms*, 1859(3), pp. 486–495. Available at: https://doi.org/10.1016/j.bbagrm.2015.09.003.

Jerzmanowski, A. (2004) 'The linker histones', in *New Comprehensive Biochemistry*. Elsevier, pp. 75–102. Available at: https://doi.org/10.1016/S0167-7306(03)39004-0.

Jing, Y. *et al.* (2013) '*Arabidopsis* Chromatin Remodeling Factor PICKLE Interacts with Transcription Factor HY5 to Regulate Hypocotyl Cell Elongation', *The Plant Cell*, 25(1), pp. 242–256. Available at: https://doi.org/10.1105/tpc.112.105742.

Johann to Berens, P. *et al.* (2022) 'Advanced Image Analysis Methods for Automated Segmentation of Subnuclear Chromatin Domains', *Epigenomes*, 6(4), p. 34. Available at: https://doi.org/10.3390/epigenomes6040034.

Jones, M.A. *et al.* (2010) 'Jumonji domain protein JMJD5 functions in both the plant and human circadian systems', *Proceedings of the National Academy of Sciences*, 107(50), pp. 21623–21628. Available at: https://doi.org/10.1073/pnas.1014204108.

Jovtchev, G. *et al.* (2006) 'Nuclear DNA content and nuclear and cell volume are positively correlated in angiosperms', *Cytogenetic and Genome Research*, 114(1), pp. 77–82. Available at: https://doi.org/10.1159/000091932.

Kasinsky, H.E. *et al.* (2001) 'Origin of H1 linker histones', *The FASEB Journal*, 15(1), pp. 34–42. Available at: https://doi.org/10.1096/fj.00-0237rev.

Kim, J. *et al.* (2017) 'The Importance of the Circadian Clock in Regulating Plant Metabolism', *International Journal of Molecular Sciences*, 18(12), p. 2680. Available at: https://doi.org/10.3390/ijms18122680.

Kim, J. *et al.* (2021) 'Get closer and make hotspots: liquid–liquid phase separation in plants', *EMBO reports*, 22(5). Available at: https://doi.org/10.15252/embr.202051656.

Kinoshita, I., Sanbe, A. and Yokomura, E. (2008) 'Difference in light-induced increase in ploidy level and cell size between adaxial and abaxial epidermal pavement cells of Phaseolus vulgaris primary leaves', *Journal of Experimental Botany*, 59(6), pp. 1419–1430. Available at: https://doi.org/10.1093/jxb/ern055.

Koike, N. *et al.* (2012) 'Transcriptional Architecture and Chromatin Landscape of the Core Circadian Clock in Mammals', *Science*, 338(6105), pp. 349–354. Available at: https://doi.org/10.1126/science.1226339.

Larkins, B.A. *et al.* (2001) 'Investigating the hows and whys of DNA endoreduplication', *Journal of Experimental Botany*, 52(355), pp. 183–192. Available at: https://doi.org/10.1093/jexbot/52.355.183.

Le Martelot, G. *et al.* (2012) 'Genome-Wide RNA Polymerase II Profiles and RNA Accumulation Reveal Kinetics of Transcription and Associated Epigenetic Changes During Diurnal Cycles', *PLoS Biology*. Edited by A. Kramer, 10(11), p. e1001442. Available at: https://doi.org/10.1371/journal.pbio.1001442.

Li, Y. *et al.* (2021) 'Diurnal transcriptomics analysis reveals the regulatory role of the circadian rhythm in super-hybrid rice LY2186', *Genomics*, 113(3), pp. 1281–1290. Available at: https://doi.org/10.1016/j.ygeno.2020.12.046.

Lindermayr, C. *et al.* (2020) 'Interactions between metabolism and chromatin in plant models', *Molecular Metabolism*, 38, p. 100951. Available at: https://doi.org/10.1016/j.molmet.2020.01.015.

Lloyd, J.P.B. and Lister, R. (2022) 'Epigenome plasticity in plants', *Nature Reviews Genetics*, 23(1), pp. 55–68. Available at: https://doi.org/10.1038/s41576-021-00407-y.

López-Juez, E. *et al.* (2008) 'Distinct Light-Initiated Gene Expression and Cell Cycle Programs in the Shoot Apex and Cotyledons of *Arabidopsis*', *The Plant Cell*, 20(4), pp. 947–968. Available at: https://doi.org/10.1105/tpc.107.057075.

Lu, S.X. *et al.* (2011) 'The Jumonji C Domain-Containing Protein JMJ30 Regulates Period Length in the Arabidopsis Circadian Clock', *Plant Physiology*, 155(2), pp. 906–915. Available at: https://doi.org/10.1104/pp.110.167015.

Malapeira, J., Khaitova, L.C. and Mas, P. (2012) 'Ordered changes in histone modifications at the core of the Arabidopsis circadian clock', *Proceedings of the National Academy of Sciences*, 109(52), pp. 21540–21545. Available at: https://doi.org/10.1073/pnas.1217022110.

Martire, S. and Banaszynski, L.A. (2020) 'The roles of histone variants in fine-tuning chromatin organization and function', *Nature Reviews Molecular Cell Biology*, 21(9), pp. 522–541. Available at: https://doi.org/10.1038/s41580-020-0262-8.

Mentch, S.J. *et al.* (2015) 'Histone Methylation Dynamics and Gene Regulation Occur through the Sensing of One-Carbon Metabolism', *Cell Metabolism*, 22(5), pp. 861–873. Available at: https://doi.org/10.1016/j.cmet.2015.08.024.

Metsalu, T. and Vilo, J. (2015) 'ClustVis: a web tool for visualizing clustering of multivariate data using Principal Component Analysis and heatmap', *Nucleic Acids Research*, 43(W1), pp. W566–W570. Available at: https://doi.org/10.1093/nar/gkv468.

Millán-Zambrano, G. *et al.* (2022) 'Histone post-translational modifications — cause and consequence of genome function', *Nature Reviews Genetics*, 23(9), pp. 563–580. Available at: https://doi.org/10.1038/s41576-022-00468-7.

Murthy, A.C. *et al.* (2019) 'Molecular interactions underlying liquid−liquid phase separation of the FUS low-complexity domain', *Nature Structural & Molecular Biology*, 26(7), pp. 637–648. Available at: https://doi.org/10.1038/s41594-019-0250-x.

Nassrallah, A. *et al.* (2018) 'DET1-mediated degradation of a SAGA-like deubiquitination module controls H2Bub homeostasis', *eLife*, 7, p. e37892. Available at: https://doi.org/10.7554/eLife.37892.

Olins, D.E. and Olins, A.L. (2003) 'Chromatin history: our view from the bridge', *Nature Reviews Molecular Cell Biology*, 4(10), pp. 809–814. Available at: https://doi.org/10.1038/nrm1225.

Paik, I. and Huq, E. (2019) 'Plant photoreceptors: Multi-functional sensory proteins and their signaling networks', *Seminars in Cell & Developmental Biology*, 92, pp. 114–121. Available at: https://doi.org/10.1016/j.semcdb.2019.03.007.

Panter, P.E. *et al.* (2019) 'Circadian Regulation of the Plant Transcriptome Under Natural Conditions', *Frontiers in Genetics*, 10, p. 1239. Available at: https://doi.org/10.3389/fgene.2019.01239.

Patitaki, E. *et al.* (2022) 'Light, chromatin, action: nuclear events regulating light signaling in Arabidopsis', *New Phytologist*, 236(2), pp. 333–349. Available at: https://doi.org/10.1111/nph.18424.

Pavlova, P. *et al.* (2022) '2D morphometric analysis of Arabidopsis thaliana nuclei reveals characteristic profiles of different cell types and accessions', *Chromosome Research*, 30(1), pp. 5–24. Available at: https://doi.org/10.1007/s10577-021-09673-2.

Perrella, G. and Kaiserli, E. (2016) 'Light behind the curtain: photoregulation of nuclear architecture and chromatin dynamics in plants', *New Phytologist*, 212(4), pp. 908–919. Available at: https://doi.org/10.1111/nph.14269.

Protacio, R.U. *et al.* (2000) 'Effects of Histone Tail Domains on the Rate of Transcriptional Elongation through a Nucleosome', *Molecular and Cellular Biology*, 20(23), pp. 8866–8878. Available at: https://doi.org/10.1128/MCB.20.23.8866-8878.2000.

Rajan, S.T. (2014) 'Health Hazards of Xylene: A Literature Review', *JOURNAL OF CLINICAL AND DIAGNOSTIC RESEARCH* [Preprint]. Available at: https://doi.org/10.7860/JCDR/2014/7544.4079.

Randall, R.S. *et al.* (2022) 'Image analysis workflows to reveal the spatial organization of cell nuclei and chromosomes', *Nucleus*, 13(1), pp. 277–299. Available at: https://doi.org/10.1080/19491034.2022.2144013.

Rosa, S. and Shaw, P. (2013) 'Insights into Chromatin Structure and Dynamics in Plants', *Biology*, 2(4), pp. 1378–1410. Available at: https://doi.org/10.3390/biology2041378.

Rutowicz, K. *et al.* (2015) 'A specialized histone H1 variant is required for adaptive responses to complex abiotic stress and related DNA methylation in Arabidopsis', *Plant Physiology*, p. pp.00493.2015. Available at: https://doi.org/10.1104/pp.15.00493.

Rutowicz, K. *et al.* (2019) 'Linker histones are fine-scale chromatin architects modulating developmental decisions in Arabidopsis', *Genome Biology*, 20(1), p. 157. Available at: https://doi.org/10.1186/s13059-019-1767-3.

Schindelin, J. *et al.* (2012) 'Fiji: an open-source platform for biological-image analysis', *Nature Methods*, 9(7), pp. 676–682. Available at: https://doi.org/10.1038/nmeth.2019.

Sequeira-Mendes, J. *et al.* (2014) 'The Functional Topography of the *Arabidopsis* Genome Is Organized in a Reduced Number of Linear Motifs of Chromatin States', *The Plant Cell*, 26(6), pp. 2351–2366. Available at: https://doi.org/10.1105/tpc.114.124578.
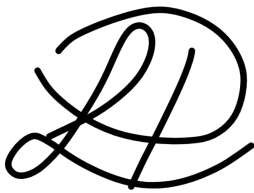
Shibuta, M.K. *et al.* (2021) 'A live imaging system to analyze spatiotemporal dynamics of RNA polymerase II modification in Arabidopsis thaliana', *Communications Biology*, 4(1), p. 580. Available at: https://doi.org/10.1038/s42003-021-02106-0.

Song, H.-R. and Noh, Y.-S. (2012) 'Rhythmic oscillation of histone acetylation and methylation at the Arabidopsis central clock loci', *Molecules and Cells*, 34(3), pp. 279–287. Available at: https://doi.org/10.1007/s10059-012-0103-5.

Song, Q. *et al.* (2019) 'Diurnal regulation of SDG2 and JMJ14 by circadian clock oscillators orchestrates histone modification rhythms in Arabidopsis', *Genome Biology*, 20(1), p. 170. Available at: https://doi.org/10.1186/s13059-019-1777-1.

Tessadori, F., Chupeau, M.-C., *et al.* (2007) 'Large-scale dissociation and sequential reassembly of pericentric heterochromatin in dedifferentiated *Arabidopsis* cells', *Journal of Cell Science*, 120(7), pp. 1200–1208. Available at: https://doi.org/10.1242/jcs.000026.

Tessadori, F., Schulkes, R.K., *et al.* (2007) 'Light-regulated large-scale reorganization of chromatin during the floral transition in Arabidopsis: Chromatin reorganization during floral transition', *The Plant Journal*, 50(5), pp. 848–857. Available at: https://doi.org/10.1111/j.1365-313X.2007.03093.x.

Van Buskirk, E.K., Decker, P.V. and Chen, M. (2012) 'Photobodies in Light Signaling', *Plant Physiology*, 158(1), pp. 52–60. Available at: https://doi.org/10.1104/pp.111.186411.

Vanrobays, E., Thomas, M. and Tatout, C. (2017) 'Heterochromatin Positioning and Nuclear Architecture', in J.A. Roberts (ed.) *Annual Plant Reviews online*. Chichester, UK: John Wiley & Sons, Ltd, pp. 157–190. Available at: https://doi.org/10.1002/9781119312994.apr0502.

Willcockson, M.A. *et al.* (2021) 'H1 histones control the epigenetic landscape by local chromatin compaction', *Nature*, 589(7841), pp. 293–298. Available at: https://doi.org/10.1038/s41586-020-3032-z.

Yamaguchi, N. (2021) 'Removal of H3K27me3 by JMJ Proteins Controls Plant Development and Environmental Responses in Arabidopsis', *Frontiers in Plant Science*, 12, p. 687416. Available at: https://doi.org/10.3389/fpls.2021.687416.

Ye, R. *et al.* (2022) 'Glucose-driven TOR–FIE–PRC2 signalling controls plant development', *Nature*, 609(7929), pp. 986–993. Available at: https://doi.org/10.1038/s41586-022-05171-5.

Zhang, D. *et al.* (2014) 'The Chromatin-Remodeling Factor PICKLE Integrates Brassinosteroid and Gibberellin Signaling during Skotomorphogenic Growth in *Arabidopsis*', *The Plant Cell*, 26(6), pp. 2472–2485. Available at: https://doi.org/10.1105/tpc.113.121848.

Zhang, Y. *et al.* (2020) 'Phase separation of Arabidopsis EMB1579 controls transcription, mRNA splicing, and development', *PLOS Biology*. Edited by X. Chen, 18(7), p. e3000782. Available at: https://doi.org/10.1371/journal.pbio.3000782.

Zhou, H.-R. *et al.* (2013) 'Folate Polyglutamylation Is Involved in Chromatin Silencing by Maintaining Global DNA Methylation and Histone H3K9 Dimethylation in Arabidopsis', *The Plant Cell*, 25(7), pp. 2545–2559. Available at: https://doi.org/10.1105/tpc.113.114678.

7 Statement of authorship

I declare that I have used no other sources and aids other than those indicated. All passages quoted from publications or paraphrased from these sources are indicated as such, i.e. cited and/or attributed. This thesis was not submitted in any form for another degree or diploma at any university or other institution of tertiary education.

Zürich, 28.03.2023

Lena Perseus

8   Appendix

8.1   Protocols

8.1.1   Protocol: Making MS Plates

Components	(1% agar full MS):	(1/2 MS)

- MS Salt   2.15 g   1.075 g
- Agar   5 g   5g
- MilliQ water   500 mL   500mL
- Empty plastic petri dishes (around 20-25)
- pH should be 5.7

1. Measure out MS and agar and add directly to a bottle and add milliQ water.
2. Autoclave bottle and leave in 60°C incubator until ready for use.
3. In the fume hood lay out lower halves of petri dishes and pour in agar solution to fill up to half of the dish (maximum).
4. Allow to dry under the flow hood, replace the lids on the dishes and store the dishes in autoclave bags, seal the bag with tape and store at 4°C.

8.1.2   Protocol: Seed Sterilization

Required Solutions und Preparation:

- Sterile 1 mL tips, 1 mL pipette
- Bottle of sterile water
- 70% EtOH
    - 100% EtOH (glass bottle): 70 mL
    - ddH2O: 30 mL
    - Prepare in Schott bottle and store @ RT (bench)
- Solid waste beaker, Liquid waste bottle
- Seeds in Eppendorf tubes (always label the tubes!)
- Permanent marker
- Timer
- Toothpicks and filter paper (per seed type one piece)

Procedure:

1. Clean the bench of the laminar-hood with 70% EtOH (technical) always from back to front
2. Place the water, waste bottle/beaker, tips, pipette and seed aliquots inside the hood
3. Repeat the washing step for 3 times (total 4 washes)
4. Add 70% EtOH to each tube with seeds. Mix the seeds and the solution by inverting the tubes and wait for 1-4 min.
5. Remove the solution with a sterile tip (possible to leave some solution) in all the aliquots.
6. Add 1 mL sterile water with a clean tip und mix by inverting the tubes and allow the seeds to settle down.
7. Repeat the washing step for 3 times (total 4 washes)
8. Add 500 µL- 1 mL sterile water to the seeds.
9. Pipette the seed in water with a 1 mL filter tip and transfer them to the filter paper.
10. With toothpicks place seeds as wanted on the MS plates.
11. Let seeds dry for 10-15 min under the hood, seal with 3M tape.
12. Place for 3 days @ 4°C in the dark for stratification.

8.1.3 Protocol: Nuclei isolation

Protocol from Ashenafi and Baroux, Methods Mol Biol, 2018. Modified by Ricardo Randall/Elizabeth Kracik-Dyer/Lena Perseus

Materials:

- Plant material (~15 small leaves from 20 dag plate grown seedlings is sufficient)
- Razor blades, 9mm Petri dishes, Partec Filter 30 µm (the green one), microscope slides (Superfrost), 18x18mm coverslips, 2mL Dounce homogenizer, moist chamber
- 10X PBS (1 L)
  - 80 g NaCl
  - 2 g KCl

- 26.8 g Na2HPO4•7H2O
- 2.4 g KH2PO4
- 800 mL ddH2O, adjust pH with HCl to 7.5 and make up to 1L.

- 4% formaldehyde in 1x PBS + 0.1% Triton-X100 (10 mL)
  - 1.08 mL of 37% Formaldehyde
  - 100 uL of 10% Triton-X100
  - 8.82 mL of 1x PBS

- NIB (nuclei isolation buffer: 50 mL)
  - 214.2 mg of MgCl2 (45 mM)
  - 209.3 mg of MOPS (20 mM¬)
  - 387 mg of sodium citrate (30 mM)
  - 151.5 ul of 10% Triton X-100 (0.3%)
  - Adjust pH to 7 with HCl

Procedure:

1. Work under fume hood: Add **2 mL ice cold formaldehyde solution** in a multi-well plate (keep on ice). Cut of leaves from seedlings and immediately submerse in formaldehyde solution. **Apply vacuum for 2 × 15 min**, release and stir sample between vacuum steps (keep samples on ice during vacuum infiltration if possible).

2. Work under fume hood: Aspirate away the formaldehyde solution. Wash the sample in **ice-cold 1× PBS, 3x for 10 min** (enough to cover tissue). Aspirate and dispose of PBS between washes. Re-suspend sample after washes in 2 mL 1x PBS.

3. Move fixed tissue to glass petri dish and **chop with a razor blade** in a small drop of NIB until very fine (should take around 1 minute: ensure razor blade is new and sharp for best results).

4. Collect chopped sample at the edge of the petri dish with the razor and pipet sample using **600 μL of NIB** and put into the 2mL douncer, **homogenize a few times** then strain through 30μm Partec filter into an Eppendorf tube.

5. **Centrifuge for 10min at 800g (rcf)** at room temperature and the **lowest ramp** (important for removing chloroplasts).

6. Remove the supernatant and re-suspend pellet in 150uL of NIB.

7. Sonicate for **6 cycles (5s ON / 10s OFF)** on **low power** (using Bioruptor UCD-200) in ice cold water.

8. Nuclei can be checked by putting 5 uL of the nuclei extraction solution on a slide, allowing the spot to dry (approx. 30 min) and adding 20 uL DAPI in Vectashield, and checking using a widefield or confocal microscope (shape, size, quality, number). Can also be checked quickly without drying.

9. Spot 5 uL of nuclei extract per slide and air dry protected from light. Always spot in the center and/or mark the area with a carbon/diamond pen on the back side.

8.1.4 Protocol: Acrylamide Pad Embedding

Materials:

- Fresh nuclei extract (not older than 24hrs, kept in fridge in PBS)
- Microscopy slides (superfrost) and confocal coverslip 0.17 (Hecht Assistant)
- 1x PBS and blocking buffer (see protocol of Immunostaining)
- Polymerization Stock solution: (fridge)
    - 30% acrylamide
    - 3.3% bisacrylamide
    - In 1x PBS pH 7.5
- 20% NaS in ddH2O (aliquot of 20mg NaS from -20°C, add 100uL sterile ddH20)
- 20% APS in ddH2O (aliquot of 20mg APS from -20°C, add 100uL sterile ddH20)
- DNA counterstain and Twinseal
- Glycerol (80% glycerol, 5% Propylgallate): always prepare freshly!
    - **200µl** of ddH$_2$O
    - **0.05g** of Propyl gallate
    - **800µl** of Glycerol (very viscous, so take up slowly)
    - → Mix very well by vortexing (can take up to 10min until fully dissolved)

Procedure: Work fast! (It is recommended to train first with a blank sample (no nuclei) for polymerisation)

1. Mix **80uL** of nuclei suspension with **12uL** of Polymerization buffer. Mix by pipetting then add **4uL** of 20% NaS and **4uL** of 20% APS, and mix by pipetting.

2. Pipette **15uL** per Superfrost slide and cover with a regular 22x22mm coverslip. Let polymerize for **~30min**. For preparing several slides, use a volume dispenser (pipette 150uL and spot 10 slides).

3. Remove the coverslip (if necessary gently use forceps and dip in 1xPBS) and add **50uL** of Blocking buffer, cover with a coverslip and incubate for **45min** at room temperature.

4. Remove the coverslip, rinse with 1xPBS and add **50uL** of primary antibodies in Immunostaining buffer. Cover with a coverslip and incubate in humidity chamber **overnight at 4°C** (or 30min at 37°C).

5. Remove the coverslip, rinse with 1xPBS. Go back to step 4 for secondary antibodies.

6. Check one preparation: counterstain with DNA marker, mount with **20µl of Glycerol per slide** and then seal with Twinseal

8.1.5 Protocol: Clearing steps

Materials:

- Microscopy slides with nuclei extract (labelled with pencil, not pen!), coplin jar
- 100% Ethanol
- Xylene (Xylol)
- 100% Methanol
- 1xPBS (see protocol for Nuclei extraction)

Procedure:

1. Wash 5min in 100% Ethanol: Xylene (1:1 solution)
2. Wash 5min in 100% Methanol
3. Wash 5min in 100% Methanol: 1xPBS (1:1 solution)
4. Wash 10min in 1xPBS

8.1.6 Protocol: Immunostaining

Materials:

- Nuclei on slide (embedded in acrylamide or air-dried)
- Moist Chamber, Coplin-Jar, incubator @ 37°C, 20x20 coverslips, 18x18mm confocal coverslip 0.17 (Hecht Assistant)
- Blocking buffer (**for 10mL**)
  - 1x PBS pH 7.5 (**1mL** of 10x stock solution)
  - 143mM NaCl (**286uL** of 5M stock solution)
  - 4% BSA (**0.4g**)
  - ddH2O **up to 10mL**
  - filter sterilize, keep at 4°C
- Immunostaining buffer, ISB (**for 10mL**)
  - 1x PBS pH 7.5 (**1mL** of 10x stock solution)
  - 143mM NaCl (**286uL** of 5M stock solution)
  - 1% BSA (**0.1g**)
  - 0.05% Tween20 (**5uL** of 10% stock solution)
  - ddH2O **up to 10mL**
  - filter sterilize, keep at 4°C
- Antibodies (example) → always prepare fresh and mix well before use!
  - 10-3 RαH3K27me3 (1:1000 dilutions to make 1 ug/ml) in ISB
  - 157-1 GαR-OregonGreen (1:1000 dilution to make 2ug/ml) in ISB
- 2 ug/mL Propidium Iodide in 1x PBS
  - 10 ml 1x PBS
  - 1 mg Propidium Iodide
- 100 ug/ml PI in 1x PBS
  - Dilute the 2ug/mL solution 1:50 in 1x PBS
- RNAse A: Roche, 100 µg/mL in 1xPBS
- DNA counterstaining (either one of them)
  - VECTASHIELD® Antifade Mounting Medium with Propidium Iodide (PI) H-1300
  - VECTASHIELD® Antifade Mounting Medium with DAPI H-1100

Procedure:

1. **Blocking:** Remove the coverslip by rinsing in PBS (if embedded nuclei prep); Add **50uL** of Blocking buffer, cover with a coverslip and incubate for **45min** at room temperature in **moist chamber**.

2. **Wash:** Remove the coverslip (without force, usually falls off when dipped in the solution in Coplin-Jar, do not try to pull off with tweezers), rinse in Coplin-Jar filled with PBS (**10min at RT** and with **mild shaking**)

3. **Primary antibody:** take out the slides, drain the excess of liquid by holding vertically on a paper towel and dry the back side carefully, add **50uL** of the primary antibody in Immunostaining buffer. Cover with a coverslip and incubate in moist chamber for **30min @ 37C.**

4. **Wash:** Remove the coverslip as before, rinse in Coplin-Jar filled with PBS (**10min at RT** with **mild shaking**).

5. **Secondary antibody:** as for step 3.

6. **Wash:** as for step 4

7. **RNAse treatment** (only if using PI as counterstain): add **100uL of 100ug/mL** DNAse-free **RNAse**, **30min at 37°C**, rinse **10min in 1xPBS**, mild shaking

8. **Counterstain:** Drain the excess of liquid, wipe the back of the slide, add with DNA marker (DAPI, PI, Hoechst580CP)
   - **DAPI or PI in Vectashield:** add 2uL if nuclei directly on slide, 20uL if embedded nuclei
   - **DAPI or PI in PBS** (2ug/mL): add 10uL, cover with coverslip, incubate 10min, wash quickly in PBS (30sec)
   - **Hoechst580CP/Live560:** add 50uL of 2uM Hoechst580P in 1x PBS, cover with a coverslip and incubate in moist chamber for 1h at 37°C.

9. **Mount and seal**, then keep the slide at **4°C**
   - **Vectashield:** add 20uL, cover with a coverslip, avoid bubbles, seal with Twinseal or nail polish (note: nail polish gives autofluorescence, avoid for super resolution microscopy)

8.2 ImageJ/Fij Macros and guides

8.2.1 Colour composition macro

```
1  //To quickly colour the AB channel (first) green and the DNA channel (second) in magenta
2  //for efficient use, install shortcut on your computer linked to this macro
3  run("Make Composite", "display=Color");
4  Stack.setChannel(1);
5  Stack.setChannel(1);
6  run("Green");
7  Stack.setChannel(2);
8  run("Magenta");
9  Stack.setDisplayMode("composite");
10
```

### 8.2.2 Creating maximum projections and saving files automatically

```
1  macro {
2
3  {run("Bio-Formats Macro Extensions");
4
5
6  dir1 = getDirectory("Choose folder with lif files ");
7  list = getFileList(dir1);
8
9  print ("Selected folder: " + dir1);
10
11
12 setBatchMode(true);
13
14 // create folders for the tifs
15 dir1parent = File.getParent(dir1);
16 dir1name = File.getName(dir1);
17 dir2 = dir1parent+File.separator+dir1name+"--Tiff_MaxProjection";
18 if (File.exists(dir2)==false) {
19         File.makeDirectory(dir2); // new directory for tiff
20     }
21
22 for (i=0; i<list.length; i++) {
23     showProgress(i+1, list.length);
24     print("\nprocessing ... "+i+1+"/"+list.length+"\n"+list[i]);
25     path=dir1+list[i];
26
27     //how many series in this lif file?
28     Ext.setId(path);//-- Initializes the given path (filename).
29     Ext.getSeriesCount(seriesCount); //-- Gets the number of image series in the active dataset.
30
31 print ("Total of " + seriesCount + " files to process:");
32     for (j=1; j<=seriesCount; j++) {
33         run("Bio-Formats", "open=path autoscale color_mode=Grayscale view=Hyperstack stack_order=XYCZT series_"+j);
34         name=File.nameWithoutExtension;
35
36     //retrieve name of the series from metadata
37         text=getMetadata("Info");
38         n1=indexOf(text,"Image name = ")+13;// 13 Zeichen
39         n2=indexOf(text,"Position = ");
40 // It was "Location" on the original script
41         //seriesname=substring(text, n1, n2-1); // Its supposed to take the image name from metadata?
42         // this is not being used, as it gets a huge string (looks like metadata is different now)
43             close("C2-*");
44     //project and save
45
46         if (nSlices>1) {
47             run("Z Project...", "projection=[Max Intensity]");
48             save_path = dir2+File.separator+name+"_Image"+j;
49             print (save_path);
50             saveAs("TIFF", save_path);
51         }
52         else {
53             save_path = dir2+File.separator+name+"_Image"+j;
54             print (save_path);
55             saveAs("TIFF", save_path);
56             run("Close All");
57         }
58
59     }
60
61 }
62 showMessage(" -- finished --");
63 run("Close All");
64 setBatchMode(false);
65
66 } // macro
67
```

8.2.3 Creating a montage to measure nuclei in ImageJ – Quick Guide

1. Open project/image with nuclei from one slide
2. Image > Color > Split channels (repeat this with every single nuclei-images)
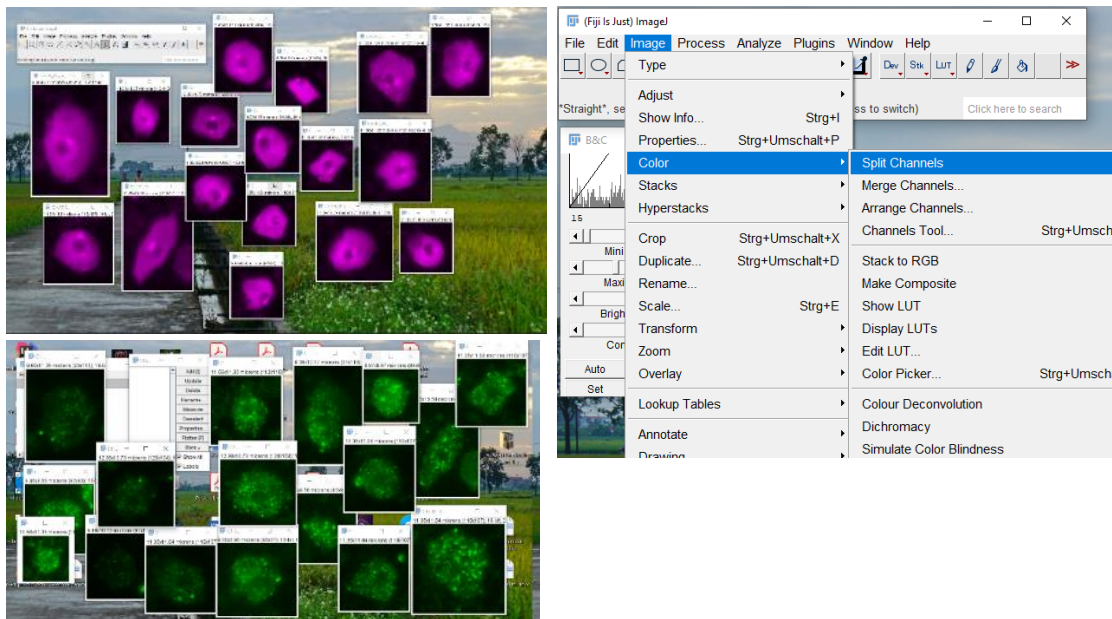
3. Image > stacks > images to stack (all separated images are put together to one stack) → tick "Copy (Center)" and "Use Title as Labels".
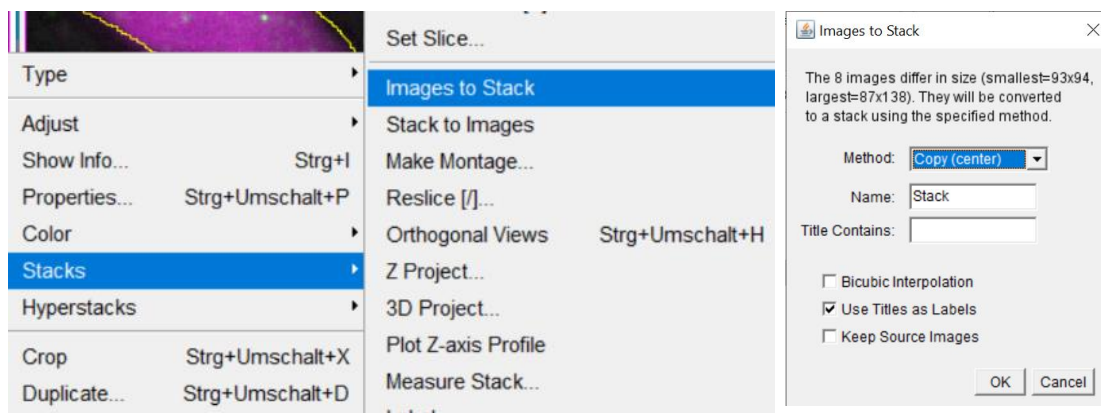
4. Image > stacks > make montage.
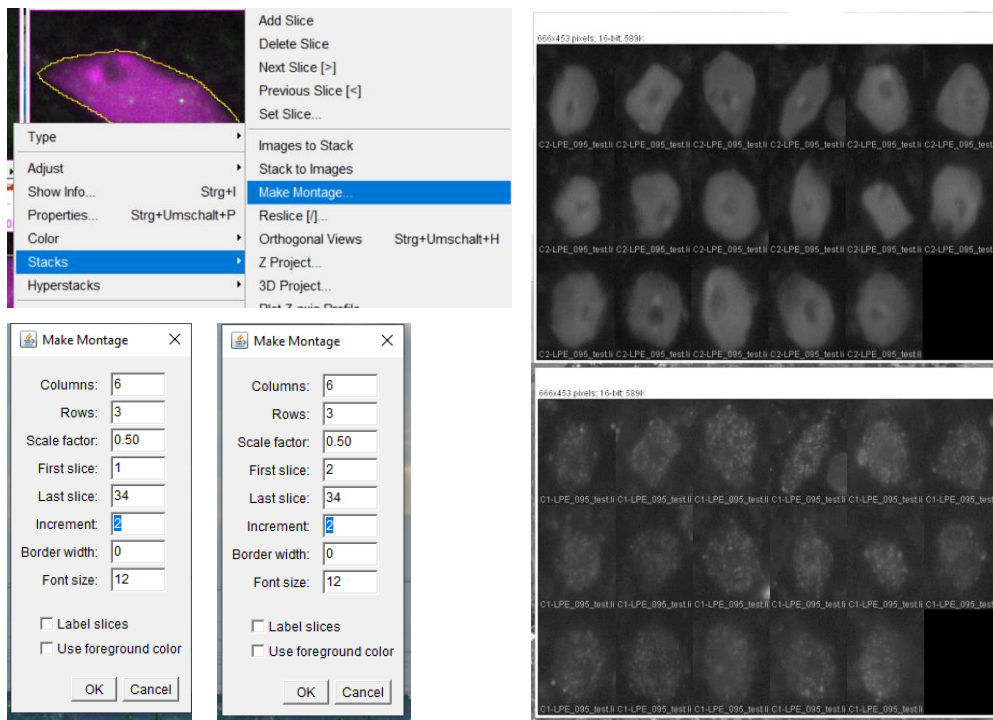
➔ Do this twice to create two montages:
- one for DNA images, second for AB images
- Change the "first slide" from 1 to 2 (after creating the first montage)
- Increment: set to two 2

5. Then start marking the nuclei (open ROI manager and use "add" to save every roi selection) in one channel. ➔ when finished, click on the second montage and select "show all".
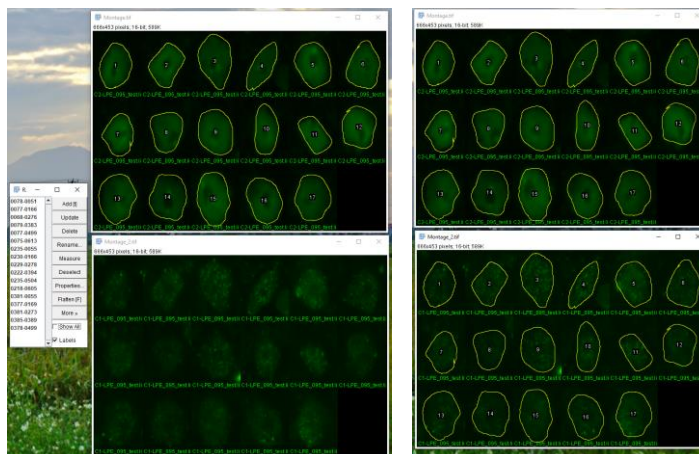
➔ Now you can use "measure" in the ROI selection to measure all nuclei.

8.2.4 Draw, measure, save and open ROIs:

Draw and save ROI:

1. Open image/ project
2. Analyse > tools > ROI manager → open this window
3. Draw the ROI with the **freehand selection tool**
4. Press [t] or "add" in ROI manager
   a. Several nuclei ROI can be added → add all nuclei in a montage
5. Save ROI in ROI Manager

Open ROI:

1. Open image/project
2. Open Roi manager → more > open... > select the ROI zip file
3. Click on "show all"

Measure ROI:

1. Either directly draw the ROI and press "Ctrl + m"
2. If you want to measure several ROIs (regions of interest) in one image at once (e.g., in montage): open ROI manager (and select "show all") → press "measure".
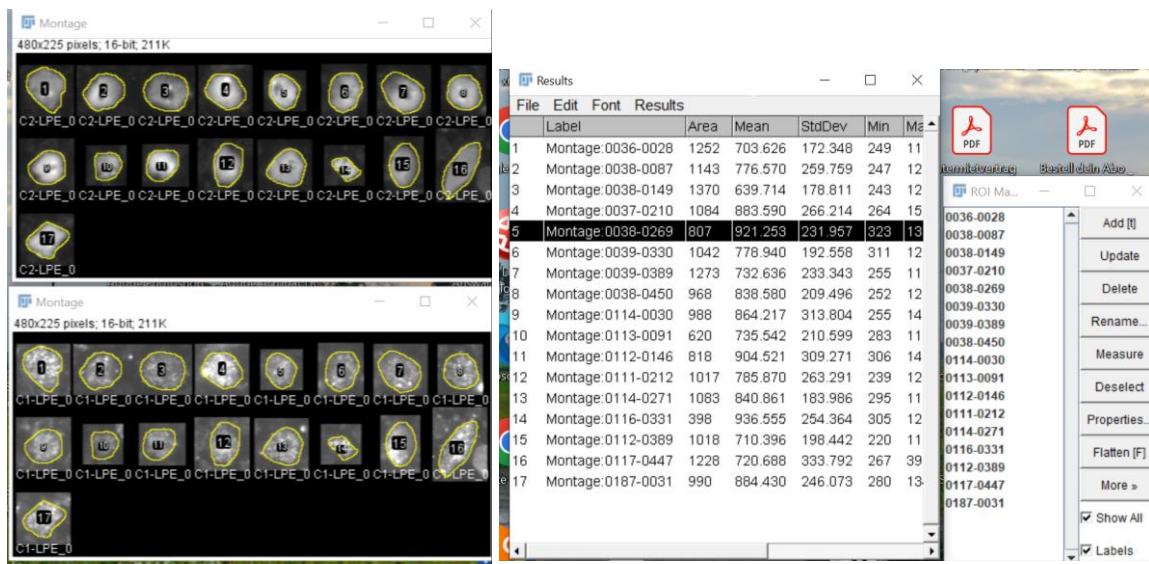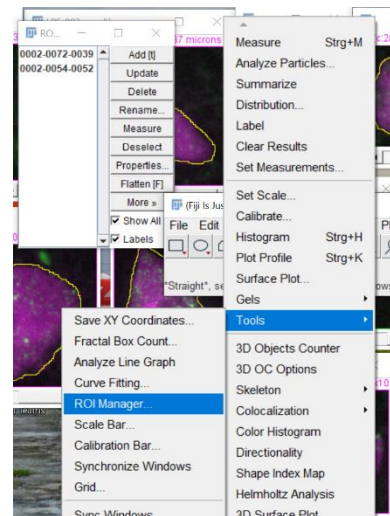
8.3 Statistical analysis and scorings

8.3.1 R code

```r
#Written by Edouard Tourdot, edited by Lena Perseus

#--------------------------------------------------------
#Installs and loads a list of R packages.
#Prompts the user to select a folder containing an Excel file, and another
folder to save results. Reads the Excel file and performs some data cleanin
g. Creates a list of comparison groups for a statistical test.Performs an A
NOVA (analysis of variance) test on the data and applies the Tukey HSD (hon
estly significant difference) post-hoc test. Filters the results of the Tuk
ey HSD test to focus on the interactions between the "Genotype" and "Timepo
int" variables.Plots the data using ggplot2 and displays statistical signif
icance on the plot.
#--------------------------------------------------------

# Install and load packages
package_list <- c("dplyr",
                  "stats",
                  "readxl",
                  "gplots",
                  "reshape2",
                  "ggpubr",
                  "tidyverse",
                  "stringr",
                  "rstatix",
                  "ggbeeswarm",
                  "viridis")
for (pkg in package_list) {
  if (pkg %in% rownames(installed.packages()) == FALSE)
  {install.packages(pkg)}
  if (pkg %in% rownames(.packages()) == FALSE)
  {library(pkg, character.only = TRUE)}
}

# Prompt user to select folders for data and saving results
#folder <- choose.dir(caption = "Where are your datas ?")
#save.data <- choose.dir(caption = "Where to save results ?")

# Read Excel file and perform data cleaning
dt <- read_excel("Zwischenspeicher_R_plots/H3K27me3_R_data.xlsx")
#View(dt)

dt <- dt[is.na(dt$Timepoint)==F,]
subdt <- dt%>% select(c("Genotype",
                        "Timepoint",
                        "DNA_mean",
                        "AB_mean"))
subdt

timepoints <- c("10:00",
                "19:00",
                "22:00",
                "02:00",
```

```r
                 "04:00",
                 "06:00")
subdt$Timepoint <- as.factor(subdt$Timepoint)
subdt$Timepoint.simp <- factor(str_extract(subdt$Timepoint,
                                   pattern = "[0-9]{1,}"),
                        levels = c("5","14","17","21","23","1"))
levels(subdt$Timepoint.simp)<- timepoints

#compute intensity ratio between AB and DNA
subdt <- subdt %>% mutate(ratio=AB_mean/DNA_mean)
subdt$Genotype <- factor(subdt$Genotype,
                    levels = c("WT","3h1"))
subdt$ratio

#filter WT or 3h1
subdt_WT <- filter(subdt, Genotype == "WT")
subdt_3h1 <- filter(subdt, Genotype == "3h1")

#calculate the mean of ratio of each timepoint and genotype and add them to
the lists
mean_ratio <- subdt %>% group_by(Timepoint.simp,Genotype) %>% summarise (Me
an = mean(ratio))

# Create list of comparison groups for statistical test
comparisons_WTvs3h1 <- list()
for (i in 1:length(levels(subdt$Timepoint.simp))) {
  timepoint <- levels(subdt$Timepoint.simp)[i]
  comparisons_WTvs3h1[[i]] <- c(paste0("WT:",timepoint),
                        paste0("3h1:",timepoint))
}
comparisons_WTvs3h1
#View(subdt_WT)


#Create list for comparing timepoints
comparisons_WT <- list(c("10:00", "19:00"), c("19:00", "22:00"), c("22:00",
"02:00"), c("02:00", "04:00"), c("04:00", "06:00"), c("06:00", "10:00"))
comparisons_WT

# Perform one way ANOVA and Tukey HSD test
stat.temp <- aov(data = subdt,
                formula = ratio~Genotype * Timepoint.simp)
stat.t.temp <- tukey_hsd(stat.temp)
print(stat.t.temp)

# Perform one way ANOVA and Tukey HSD test for WT
stat.temp_WT <- aov(data = subdt_WT, formula = ratio~Timepoint.simp)
stat.t.temp_WT <- tukey_hsd(stat.temp_WT)
#print(stat.t.temp_WT)

# Perform one way ANOVA and Tukey HSD test for WT
stat.temp_3h1 <- aov(data = subdt_3h1, formula = ratio~Timepoint.simp)
stat.t.temp_3h1 <- tukey_hsd(stat.temp_3h1)
#print(stat.t.temp_3h1)
```

```r
# Filter results to focus on interactions between "Genotype" and "Timepoint"
f_stat.t.temp_time <- stat.t.temp %>% filter(term == "Genotype:Timepoint.simp")
Pattern  <- "[0-9]{2}:[0-9]{2}"
f_stat.t.temp_time$group1.t <- str_extract(f_stat.t.temp_time$group1, pattern = Pattern)
f_stat.t.temp_time$group2.t <- str_extract(f_stat.t.temp_time$group2, pattern = Pattern)
f_stat.t.temp_time$group1 <- str_remove(f_stat.t.temp_time$group1, pattern = Pattern)
f_stat.t.temp_time$group2 <- str_remove(f_stat.t.temp_time$group2, pattern = Pattern)
stat <- f_stat.t.temp_time %>% filter(group1!=group2 & group1.t==group2.t)


#colours
colors_Palette <- c("#006587","#e9002c")


# Plot data using ggplot2 and display statistical significance

#Boxplot WT vs 3h1 grouped
p1 <- ggplot(subdt, aes(x = Timepoint.simp,
                        y = ratio))+
  geom_boxplot(aes(group = interaction(Genotype,
                                       Timepoint.simp)),
               outlier.shape = NA)+
  geom_quasirandom(aes(color = Genotype),
                   alpha=0.65,
                   dodge.width = 1)+
  stat_pvalue_manual(data = stat,
                     label = "p.adj.signif",
                     xmin = "group2.t",
                     xmax = NULL,
                     y.position = 2.5)+
  scale_color_manual(values = colors_Palette)+
  xlab("")+
  ylab("(Antibody/DNA) intensity")+
  ggtitle("Title")+
  theme_light() +
  theme(panel.border = element_blank(),
        panel.grid.major = element_blank(),
        panel.grid.minor = element_blank(),
        axis.line = element_line(colour = "black"),
        axis.text.x = element_text(size = 14),
        panel.background = element_blank(),
        plot.title = element_text(size = 14, face = "bold", hjust = 0.5))
p1

# Save plot
# ggsave(filename = paste0(save.data,"/nameyourplothere_Boxplot.svg"),
#        plot = p1,
#        device = "svg",
#        width = 200,
```

```r
#         height = 80,
#         units = "mm",
#         limitsize = F
# )


#smoothed graph WT vs 3h1 grouped ((compare means))showing CI)
p2 <- ggplot(subdt, aes(x = Timepoint.simp, y = ratio, color = Genotype, gr
oup = Genotype))+
  geom_smooth()+
  geom_point(position = position_jitter(w = 0.1, h = 0),  alpha = 0.65)+
  xlab("")+
  ylab("Ratio (Antibody/DNA) intensity")+
  ggtitle("title")+
  scale_color_manual(values = colors_Palette)+
  theme_light() +
  theme(panel.border = element_blank(),
        panel.grid.major = element_blank(),
        panel.grid.minor = element_blank(),
        axis.line = element_line(colour = "black"),
        axis.text.x = element_text(size = 14),
        panel.background = element_blank(),
        plot.title = element_text(size = 14, face = "bold", hjust = 0.5))
p2

## `geom_smooth()` using method = 'loess' and formula = 'y ~ x'

# Save plot
# ggsave(filename = paste0(save.data,"/nameyourplothere_SmoothGraph.svg"),
#         plot = p2,
#         device = "svg",
#         width = 200,
#         height = 80,
#         units = "mm",
#         limitsize = F
# )


p3 <- ggplot(mean_ratio, aes(x = Timepoint.simp, y = Mean, color = Genotype
, group = Genotype))+
  geom_line()+
  geom_point()+
  xlab("")+
  ylab("Mean of Ratio (Antibody/DNA) intensity")+
  ggtitle("Title")+
  scale_color_manual(values = colors_Palette)+
  theme_light() +
  theme(panel.border = element_blank(),
        panel.grid.major = element_blank(),
        panel.grid.minor = element_blank(),
        axis.line = element_line(colour = "black"),
        axis.text.x = element_text(size = 14),
        panel.background = element_blank(),
```

```
        plot.title = element_text(size = 14, face = "bold", hjust = 0.5))
p3

# Save plot
# ggsave(filename = paste0(save.data,"/nameyourplothere_LineGraph.svg"),
#        plot = p3,
#        device = "svg",
#        width = 200,
#        height = 80,
#        units = "mm",
#        limitsize = F
# )

#Boxplot WT only

p4 <- ggplot(subdt_WT, aes(x = Timepoint.simp, y = ratio, group = Timepoint
.simp))+
  geom_boxplot(outlier.shape = NA)+
  scale_color_manual(values = colors_Palette[1])+
  geom_quasirandom(aes(color = Genotype),
                   alpha=0.65,
                   dodge.width = 1)+
  geom_smooth()+
  xlab("")+
  ylab("Ratio (Antibody/DNA) intensity")+
  theme_light() +
    theme(panel.border = element_blank(),
        panel.grid.major = element_blank(),
        panel.grid.minor = element_blank(),
        axis.line = element_line(colour = "black"),
        axis.text.x = element_text(size = 14),
        panel.background = element_blank(),
        plot.title = element_text(size = 14, face = "bold", hjust = 0.5))
p4

## `geom_smooth()` using method = 'loess' and formula = 'y ~ x'

# Save plot
# ggsave(filename = paste0(save.data,"/nameyourplothere_Boxplot_WT.svg"),
#        plot = p4,
#        device = "svg",
#        width = 200,
#        height = 80,
#        units = "mm",
#        limitsize = F
# )

#Boxplot 3h1 only

p5 <- ggplot(subdt_3h1, aes(x = Timepoint.simp, y = ratio, group = Timepoin
t.simp))+
  geom_boxplot(outlier.shape = NA)+
  scale_color_manual(values = colors_Palette[2])+
  geom_quasirandom(aes(color = Genotype),
                   alpha=0.65,
```

```
                  dodge.width = 1)+
  xlab("")+
  ylab("Ratio (Antibody / DNA) intensity")+
  theme_light() +
  ggtitle("Title")+
  theme(panel.border = element_blank(),
        panel.grid.major = element_blank(),
        panel.grid.minor = element_blank(),
        axis.line = element_line(colour = "black"),
        axis.text.x = element_text(size = 14),
        panel.background = element_blank(),
        plot.title = element_text(size = 14, face = "bold", hjust = 0.5))
p5

# Save plot
#ggsave(filename = paste0(save.data,"/nameyourplothere_Boxplot_3h1.svg"),
#       plot = p5,
#       device = "svg",
#       width = 200,
#       height = 80,
#       units = "mm",
#       limitsize = F
# )
```

8.3.2 Scoring of classes and shapes for Pol II S2P

Total WT	Class I	Class II	Class III		
Round	17	8	17	42	
Eye shape	22	27	22	71	
Elongated + stick shape	1	6	4	11	
other shape (e.g. more square)	3	19	2	24	
	43	60	45	**148**	(total nuclei)
Total 3h1	Class I	Class II	Class III		
Round	12	19	14	45	
Eye shape	17	21	26	64	
Elongated + stick shape	3	10	7	20	
other shape (e.g. more square)	6	13	13	32	
	38	63	60	**161**	(total nuclei)

8.3.3 Statistical tests

group1	group2	estimate	conf.low	conf.high	p.adj	p.adj.signif
Dilution experiments: H3K27me3 only (Chapter 3.1.4)						
WT:1/500	3h1:1/500	-109.1427	-221.45433	3.168933	6.14E-02	ns
WT:1/500	WT:1/1000	-148.1028	-260.41443	-35.791167	3.52E-03	**
WT:1/500	3h1:1/1000	-284.8492	-397.16083	-172.53757	9.66E-09	****
WT:1/500	WT:1/2000	-184.3118	-296.62343	-72.000167	1.53E-04	***
WT:1/500	3h1:1/2000	-287.377	-399.68863	-175.06537	7.54E-09	****
3h1:1/500	WT:1/1000	-38.9601	-151.27173	73.351533	9.08E-01	ns
3h1:1/500	3h1:1/1000	-175.7065	-288.01813	-63.394867	3.33E-04	***
3h1:1/500	WT:1/2000	-75.1691	-187.48073	37.142533	3.68E-01	ns
3h1:1/500	3h1:1/2000	-178.2343	-290.54593	-65.922667	2.66E-04	***
WT:1/1000	3h1:1/1000	-136.7464	-249.05803	-24.434767	8.67E-03	**
WT:1/1000	WT:1/2000	-36.209	-148.52063	76.102633	9.31E-01	ns
WT:1/1000	3h1:1/2000	-139.2742	-251.58583	-26.962567	7.13E-03	**
3h1:1/1000	WT:1/2000	100.5374	-11.77423	212.849033	1.04E-01	ns
3h1:1/1000	3h1:1/2000	-2.5278	-114.83943	109.783833	1.00E+00	ns
WT:1/2000	3h1:1/2000	-103.0652	-215.37683	9.246433	8.95E-02	ns
Dilution experiments: H3K4me3 only (Chapter 3.1.4)						
WT:1/500	3h1:1/500	119.5773	3.32873	235.82587	0.0404	*
WT:1/500	WT:1/1000	11.6632	-104.58537	127.91177	1	ns
WT:1/500	3h1:1/1000	-43.4578	-159.70637	72.79077	0.877	ns
WT:1/500	WT:1/2000	-85.7617	-202.01027	30.48687	0.264	ns
WT:1/500	3h1:1/2000	-104.89206	-224.32611	14.541997	0.116	ns
3h1:1/500	WT:1/1000	-107.9141	-224.16267	8.33447	0.0832	ns
3h1:1/500	3h1:1/1000	-163.0351	-279.28367	-46.78653	0.00163	**
3h1:1/500	WT:1/2000	-205.339	-321.58757	-89.09043	0.0000431	****
3h1:1/500	3h1:1/2000	-224.46936	-343.90341	-105.0353	0.0000131	****
WT:1/1000	3h1:1/1000	-55.121	-171.36957	61.12757	0.726	ns
WT:1/1000	WT:1/2000	-97.4249	-213.67347	18.82367	0.149	ns
WT:1/1000	3h1:1/2000	-116.55526	-235.98931	2.878797	0.0596	ns
3h1:1/1000	WT:1/2000	-42.3039	-158.55247	73.94467	0.889	ns
3h1:1/1000	3h1:1/2000	-61.43426	-180.86831	57.999797	0.653	ns
WT:1/2000	3h1:1/2000	-19.13036	-138.56441	100.303697	0.997	ns
Dilution experiments: Pol II S2P/DNA (Chapter 3.1.4)						
WT:1/500	3h1:1/500	0.23731538	0.06295395	0.41167681	1.85E-03	**
WT:1/500	WT:1/1000	-0.0208324	-0.1994997	0.15783488	9.99E-01	ns
WT:1/500	3h1:1/1000	0.3275878	0.15322638	0.50194923	4.11E-06	****
WT:1/500	WT:1/2000	-0.1677309	-0.3420923	0.00663053	6.67E-02	ns
WT:1/500	3h1:1/2000	-0.0072321	-0.1858994	0.17143521	1.00E+00	ns
3h1:1/500	WT:1/1000	-0.2581478	-0.4368151	-0.0794805	7.59E-04	***
3h1:1/500	3h1:1/1000	0.09027242	-0.084089	0.26463385	6.65E-01	ns
3h1:1/500	WT:1/2000	-0.4050463	-0.5794077	-0.2306849	8.93E-09	****
3h1:1/500	3h1:1/2000	-0.2445475	-0.4232148	-0.0658802	1.71E-03	**
WT:1/1000	3h1:1/1000	0.34842021	0.16975292	0.52708751	1.61E-06	****
WT:1/1000	WT:1/2000	-0.1468985	-0.3255658	0.03176881	1.71E-01	ns

WT:1/1000	3h1:1/2000	0.01360033	-0.1692715	0.19647214	1.00E+00	ns
3h1:1/1000	WT:1/2000	-0.4953187	-0.6696801	-0.3209573	3.78E-12	****
3h1:1/1000	3h1:1/2000	-0.3348199	-0.5134872	-0.1561526	4.38E-06	****
WT:1/2000	3h1:1/2000	0.16049882	-0.0181685	0.33916611	1.05E-01	ns
A vs B replicate of H3K27me3 (Chapter 3.1.5)						
A:02:00	B:02:00	0.07908682	-0.052206	0.2103797	3.89E-01	ns
A:02:00	A:04:00	-0.299993	-0.4312858	-0.1687001	7.80E-07	****
A:02:00	B:04:00	-0.2345075	-0.3634451	-0.1055698	6.82E-05	****
B:02:00	A:04:00	-0.3790798	-0.5146785	-0.2434811	4.86E-09	****
B:02:00	B:04:00	-0.3135943	-0.4469139	-0.1802747	4.02E-07	****
A:04:00	B:04:00	0.0654855	-0.0678341	0.1988051	5.66E-01	ns
RHF (Chapter 3.4.1 and 3.5.1)						
WT:10:00	WT:19:00	0.02556465	-0.0175254	0.06865468	7.30E-01	ns
WT:10:00	3h1:19:00	-0.0755643	-0.1181996	-0.0329289	6.05E-07	****
WT:10:00	WT:22:00	-0.0043641	-0.0481212	0.03939298	1.00E+00	ns
WT:10:00	3h1:22:00	-0.0578467	-0.1049812	-0.0107123	3.63E-03	**
WT:10:00	WT:02:00	0.00073196	-0.0433883	0.04485217	1.00E+00	ns
WT:10:00	3h1:02:00	-0.0997972	-0.1447125	-0.054882	0.00E+00	****
WT:10:00	WT:04:00	-0.0071342	-0.048835	0.03456658	1.00E+00	ns
WT:10:00	3h1:04:00	-0.0704721	-0.1124237	-0.0285206	3.29E-06	****
WT:10:00	WT:06:00	0.01231913	-0.0310951	0.05573338	9.99E-01	ns
WT:10:00	3h1:06:00	-0.0496802	-0.0971081	-0.0022524	3.06E-02	*
3h1:10:00	WT:19:00	0.0757099	0.03367529	0.1177445	3.51E-07	****
3h1:10:00	3h1:19:00	-0.025419	-0.0669874	0.01614938	6.90E-01	ns
3h1:10:00	WT:22:00	0.04578115	0.00306301	0.08849928	2.36E-02	*
3h1:10:00	3h1:22:00	-0.0077015	-0.0538731	0.03847006	1.00E+00	ns
3h1:10:00	WT:02:00	0.05087721	0.00778718	0.09396724	6.57E-03	**
3h1:10:00	3h1:02:00	-0.049652	-0.0935557	-0.0057483	1.20E-02	*
3h1:10:00	WT:04:00	0.04301103	0.00240175	0.08362031	2.70E-02	*
3h1:10:00	3h1:04:00	-0.0203269	-0.0611936	0.02053987	8.97E-01	ns
3h1:10:00	WT:06:00	0.06246438	0.02009749	0.10483128	1.03E-04	***
3h1:10:00	3h1:06:00	0.000465	-0.046006	0.046936	1.00E+00	ns
WT:19:00	3h1:19:00	-0.1011289	-0.1426973	-0.0595605	0.00E+00	****
WT:19:00	WT:22:00	-0.0299288	-0.0726469	0.01278939	4.80E-01	ns
WT:19:00	3h1:22:00	-0.0834114	-0.1295829	-0.0372398	3.16E-07	****
WT:19:00	WT:02:00	-0.0248327	-0.0679227	0.01825734	7.66E-01	ns
WT:19:00	3h1:02:00	-0.1253619	-0.1692656	-0.0814582	0.00E+00	****
WT:19:00	WT:04:00	-0.0326989	-0.0733082	0.00791042	2.59E-01	ns
WT:19:00	3h1:04:00	-0.0960368	-0.1369035	-0.05517	0.00E+00	****
WT:19:00	WT:06:00	-0.0132455	-0.0556124	0.02912138	9.97E-01	ns
WT:19:00	3h1:06:00	-0.0752449	-0.1217159	-0.0287739	9.51E-06	****
3h1:19:00	WT:22:00	0.07120017	0.02894069	0.11345964	3.01E-06	****
3h1:19:00	3h1:22:00	0.01771753	-0.02803	0.06346506	9.83E-01	ns
3h1:19:00	WT:02:00	0.07629623	0.03366086	0.1189316	4.38E-07	****
3h1:19:00	3h1:02:00	-0.024233	-0.0676905	0.01922461	8.02E-01	ns
3h1:19:00	WT:04:00	0.06843005	0.02830352	0.10855657	2.08E-06	****
3h1:19:00	3h1:04:00	0.00509215	-0.0352949	0.04547921	1.00E+00	ns

3h1:19:00	WT:06:00	0.0878834	0.04597901	0.12978779	0.00E+00	****
3h1:19:00	3h1:06:00	0.02588402	-0.0201657	0.07193376	7.94E-01	ns
WT:22:00	3h1:22:00	-0.0534826	-0.1002773	-0.0066879	1.04E-02	*
WT:22:00	WT:02:00	0.00509606	-0.038661	0.04885314	1.00E+00	ns
WT:22:00	3h1:02:00	-0.0954331	-0.1399917	-0.0508745	0.00E+00	****
WT:22:00	WT:04:00	-0.0027701	-0.0440865	0.03854629	1.00E+00	ns
WT:22:00	3h1:04:00	-0.066108	-0.1076775	-0.0245385	1.56E-05	****
WT:22:00	WT:06:00	0.01668324	-0.0263619	0.05972839	9.82E-01	ns
WT:22:00	3h1:06:00	-0.0453161	-0.0924063	0.00177404	7.20E-02	ns
3h1:22:00	WT:02:00	0.0585787	0.01144426	0.10571314	2.97E-03	**
3h1:22:00	3h1:02:00	-0.0419505	-0.0898299	0.00592896	1.53E-01	ns
3h1:22:00	WT:04:00	0.05071252	0.0058347	0.09559034	1.21E-02	*
3h1:22:00	3h1:04:00	-0.0126254	-0.0577363	0.03248555	9.99E-01	ns
3h1:22:00	WT:06:00	0.07016588	0.0236916	0.11664016	5.89E-05	****
3h1:22:00	3h1:06:00	0.0081665	-0.0420775	0.05841049	1.00E+00	ns
WT:02:00	3h1:02:00	-0.1005292	-0.1454444	-0.0556139	0.00E+00	****
WT:02:00	WT:04:00	-0.0078662	-0.049567	0.03383462	1.00E+00	ns
WT:02:00	3h1:04:00	-0.0712041	-0.1131556	-0.0292525	2.40E-06	****
WT:02:00	WT:06:00	0.01158717	-0.0318271	0.05500142	9.99E-01	ns
WT:02:00	3h1:06:00	-0.0504122	-0.09784	-0.0029844	2.59E-02	*
3h1:02:00	WT:04:00	0.092663	0.05012194	0.13520407	0.00E+00	****
3h1:02:00	3h1:04:00	0.0293251	-0.0134618	0.07211201	5.16E-01	ns
3h1:02:00	WT:06:00	0.11211636	0.0678944	0.15633832	0.00E+00	****
3h1:02:00	3h1:06:00	0.05011698	0.00194871	0.09828524	3.30E-02	*
WT:04:00	3h1:04:00	-0.0633379	-0.1027371	-0.0239387	1.16E-05	****
WT:04:00	WT:06:00	0.01945335	-0.0214998	0.0604065	9.23E-01	ns
WT:04:00	3h1:06:00	-0.042546	-0.0877319	0.00263981	8.73E-02	ns
3h1:04:00	WT:06:00	0.08279125	0.0415828	0.12399971	1.74E-09	****
3h1:04:00	3h1:06:00	0.02079187	-0.0246255	0.06620924	9.40E-01	ns
WT:06:00	3h1:06:00	-0.0619994	-0.1087712	-0.0152276	9.57E-04	***
CCs (Chapter 3.4.1 and 3.5.1)						
WT:10:00	3h1:10:00	-2.1027379	-3.202076	-1.0033999	3.65E-08	****
WT:10:00	WT:19:00	-0.4719687	-1.5713068	0.62736935	9.62E-01	ns
WT:10:00	3h1:19:00	-1.8973081	-2.9850466	-0.8095696	1.02E-06	****
WT:10:00	WT:22:00	0.58099472	-0.5353615	1.69735096	8.65E-01	ns
WT:10:00	3h1:22:00	-1.3883567	-2.5908781	-0.1858352	9.05E-03	**
WT:10:00	WT:02:00	0.62711864	-0.4985021	1.75273941	8.03E-01	ns
WT:10:00	3h1:02:00	-1.3251156	-2.4710194	-0.1792117	8.85E-03	**
WT:10:00	WT:04:00	0.50033898	-0.5635563	1.56423422	9.28E-01	ns
WT:10:00	3h1:04:00	-1.9988391	-3.069132	-0.9285462	9.48E-08	****
WT:10:00	WT:06:00	0.64891041	-0.4586993	1.75652008	7.46E-01	ns
WT:10:00	3h1:06:00	-1.7574388	-2.9674448	-0.5474328	1.46E-04	***
3h1:10:00	WT:19:00	1.63076923	0.55835783	2.70318063	4.94E-05	****
3h1:10:00	3h1:19:00	0.20542986	-0.8550875	1.26594724	1.00E+00	ns
3h1:10:00	WT:22:00	2.68373266	1.59388253	3.77358279	0.00E+00	****
3h1:10:00	3h1:22:00	0.71438127	-0.4635745	1.89233708	7.01E-01	ns
3h1:10:00	WT:02:00	2.72985658	1.63051853	3.82919464	0.00E+00	****

3h1:10:00	3h1:02:00	0.77762238	-0.3424748	1.89771956	4.95E-01	ns
3h1:10:00	WT:04:00	2.60307692	1.56702908	3.63912477	0.00E+00	****
3h1:10:00	3h1:04:00	0.10389884	-0.9387175	1.14651521	1.00E+00	ns
3h1:10:00	WT:06:00	2.75164835	1.67075926	3.83253745	0.00E+00	****
3h1:10:00	3h1:06:00	0.34529915	-0.8402963	1.53089456	9.98E-01	ns
WT:19:00	3h1:19:00	-1.4253394	-2.4858567	-0.364822	7.36E-04	***
WT:19:00	WT:22:00	1.05296343	-0.0368867	2.14281356	6.95E-02	ns
WT:19:00	3h1:22:00	-0.916388	-2.0943438	0.26156785	3.10E-01	ns
WT:19:00	WT:02:00	1.09908735	-0.0002507	2.19842541	5.01E-02	ns
WT:19:00	3h1:02:00	-0.8531469	-1.973244	0.26695033	3.43E-01	ns
WT:19:00	WT:04:00	0.97230769	-0.0637402	2.00835554	8.98E-02	ns
WT:19:00	3h1:04:00	-1.5268704	-2.5694868	-0.484254	1.21E-04	***
WT:19:00	WT:06:00	1.12087912	0.03999002	2.20176822	3.42E-02	*
WT:19:00	3h1:06:00	-1.2854701	-2.4710655	-0.0998747	2.05E-02	*
3h1:19:00	WT:22:00	2.4783028	1.40015429	3.5564513	0.00E+00	****
3h1:19:00	3h1:22:00	0.50895141	-0.6581865	1.67608927	9.57E-01	ns
3h1:19:00	WT:02:00	2.52442672	1.43668822	3.61216522	0.00E+00	****
3h1:19:00	3h1:02:00	0.57219251	-0.5365223	1.68090735	8.72E-01	ns
3h1:19:00	WT:04:00	2.39764706	1.37391563	3.42137848	0.00E+00	****
3h1:19:00	3h1:04:00	-0.101531	-1.1319095	0.92884744	1.00E+00	ns
3h1:19:00	WT:06:00	2.54621849	1.47712909	3.61530788	0.00E+00	****
3h1:19:00	3h1:06:00	0.13986928	-1.0349785	1.31471709	1.00E+00	ns
WT:22:00	3h1:22:00	-1.9693514	-3.1632052	-0.7754976	5.61E-06	****
WT:22:00	WT:02:00	0.04612392	-1.0702323	1.16248016	1.00E+00	ns
WT:22:00	3h1:02:00	-1.9061103	-3.0429149	-0.7693057	3.47E-06	****
WT:22:00	WT:04:00	-0.0806557	-1.1347441	0.9734326	1.00E+00	ns
WT:22:00	3h1:04:00	-2.5798338	-3.640379	-1.5192887	0.00E+00	****
WT:22:00	WT:06:00	0.06791569	-1.0302775	1.1661089	1.00E+00	ns
WT:22:00	3h1:06:00	-2.3384335	-3.5398259	-1.1370412	1.66E-08	****
3h1:22:00	WT:02:00	2.01547531	0.81295386	3.21799676	3.52E-06	****
3h1:22:00	3h1:02:00	0.06324111	-1.1582872	1.2847694	1.00E+00	ns
3h1:22:00	WT:04:00	1.88869565	0.74374639	3.03364491	5.61E-06	****
3h1:22:00	3h1:04:00	-0.6104824	-1.7613788	0.54041399	8.49E-01	ns
3h1:22:00	WT:06:00	2.03726708	0.85158799	3.22294617	1.65E-06	****
3h1:22:00	3h1:06:00	-0.3690821	-1.6509363	0.91277206	9.99E-01	ns
WT:02:00	3h1:02:00	-1.9522342	-3.0981381	-0.8063304	2.14E-06	****
WT:02:00	WT:04:00	-0.1267797	-1.1906749	0.93711558	1.00E+00	ns
WT:02:00	3h1:04:00	-2.6259577	-3.6962506	-1.5556649	0.00E+00	****
WT:02:00	WT:06:00	0.02179177	-1.0858179	1.12940144	1.00E+00	ns
WT:02:00	3h1:06:00	-2.3845574	-3.5945634	-1.1745515	8.60E-09	****
3h1:02:00	WT:04:00	1.82545455	0.74012206	2.91078703	3.17E-06	****
3h1:02:00	3h1:04:00	-0.6737235	-1.765328	0.41788095	6.77E-01	ns
3h1:02:00	WT:06:00	1.97402597	0.84580937	3.10224258	9.24E-07	****
3h1:02:00	3h1:06:00	-0.4323232	-1.6612203	0.79657382	9.92E-01	ns
WT:04:00	3h1:04:00	-2.4991781	-3.5043536	-1.4940026	0.00E+00	****
WT:04:00	WT:06:00	0.14857143	-0.8962492	1.19339206	1.00E+00	ns
WT:04:00	3h1:06:00	-2.2577778	-3.4105854	-1.1049702	1.21E-08	****

3h1:04:00	WT:06:00	2.64774951	1.59641516	3.69908386	0.00E+00	****
3h1:04:00	3h1:06:00	0.2414003	-0.9173141	1.40011475	1.00E+00	ns
WT:06:00	3h1:06:00	-2.4063492	-3.5996185	-1.21308	9.14E-10	****
H3K27me3/DNA (Chapter 3.4.2 and 3.5.2)						
WT:10:00	3h1:10:00	0.05188041	-0.113181	0.21694182	9.97E-01	ns
WT:10:00	WT:19:00	-0.1210555	-0.291969	0.04985797	4.60E-01	ns
WT:10:00	3h1:19:00	0.17084721	0.00302943	0.33866499	4.17E-02	*
WT:10:00	WT:22:00	0.53272088	0.36288088	0.70256089	2.89E-10	****
WT:10:00	3h1:22:00	0.49410247	0.32628469	0.66192025	2.89E-10	****
WT:10:00	WT:02:00	0.47303426	0.30521647	0.64085204	2.89E-10	****
WT:10:00	3h1:02:00	0.43024094	0.261432	0.59904989	2.89E-10	****
WT:10:00	WT:04:00	-0.0142645	-0.1820823	0.15355327	1.00E+00	ns
WT:10:00	3h1:04:00	0.28322607	0.11540829	0.45104385	3.10E-06	****
WT:10:00	WT:06:00	0.15557347	-0.0132355	0.32438241	1.04E-01	ns
WT:10:00	3h1:06:00	0.07170557	-0.0961122	0.23952335	9.63E-01	ns
3h1:10:00	WT:19:00	-0.1729359	-0.3446692	-0.0012027	4.66E-02	*
3h1:10:00	3h1:19:00	0.1189668	-0.0496858	0.28761937	4.67E-01	ns
3h1:10:00	WT:22:00	0.48084048	0.31017558	0.65150537	2.89E-10	****
3h1:10:00	3h1:22:00	0.44222206	0.2735695	0.61087463	2.89E-10	****
3h1:10:00	WT:02:00	0.42115385	0.25250129	0.58980642	2.89E-10	****
3h1:10:00	3h1:02:00	0.37836054	0.20872169	0.54799938	3.50E-10	****
3h1:10:00	WT:04:00	-0.0661449	-0.2347975	0.10250764	9.80E-01	ns
3h1:10:00	3h1:04:00	0.23134566	0.0626931	0.39999823	5.06E-04	***
3h1:10:00	WT:06:00	0.10369307	-0.0659458	0.27333191	6.89E-01	ns
3h1:10:00	3h1:06:00	0.01982516	-0.1488274	0.18847773	1.00E+00	ns
WT:19:00	3h1:19:00	0.29190274	0.11751856	0.46628692	3.95E-06	****
WT:19:00	WT:22:00	0.65377641	0.47744531	0.83010752	2.89E-10	****
WT:19:00	3h1:22:00	0.615158	0.44077382	0.78954217	2.89E-10	****
WT:19:00	WT:02:00	0.59408979	0.41970561	0.76847396	2.89E-10	****
WT:19:00	3h1:02:00	0.55129647	0.37595825	0.72663469	2.89E-10	****
WT:19:00	WT:04:00	0.10679102	-0.0675932	0.28117519	6.86E-01	ns
WT:19:00	3h1:04:00	0.4042816	0.22989742	0.57866577	2.97E-10	****
WT:19:00	WT:06:00	0.276629	0.10129078	0.45196722	2.04E-05	****
WT:19:00	3h1:06:00	0.1927611	0.01837692	0.36714527	1.62E-02	*
3h1:19:00	WT:22:00	0.36187368	0.18854149	0.53520586	1.62E-09	****
3h1:19:00	3h1:22:00	0.32325526	0.15190408	0.49460644	7.83E-08	****
3h1:19:00	WT:02:00	0.30218705	0.13083587	0.47353822	7.94E-07	****
3h1:19:00	3h1:02:00	0.25939374	0.08707172	0.43171575	6.63E-05	****
3h1:19:00	WT:04:00	-0.1851117	-0.3564629	-0.0137605	2.15E-02	*
3h1:19:00	3h1:04:00	0.11237886	-0.0589723	0.28373004	5.85E-01	ns
3h1:19:00	WT:06:00	-0.0152737	-0.1875957	0.15704828	1.00E+00	ns
3h1:19:00	3h1:06:00	-0.0991416	-0.2704928	0.07220954	7.59E-01	ns
WT:22:00	3h1:22:00	-0.0386184	-0.2119506	0.13471377	1.00E+00	ns
WT:22:00	WT:02:00	-0.0596866	-0.2330188	0.11364555	9.93E-01	ns
WT:22:00	3h1:02:00	-0.1024799	-0.2767719	0.07181204	7.40E-01	ns
WT:22:00	WT:04:00	-0.5469854	-0.7203176	-0.3736532	2.89E-10	****
WT:22:00	3h1:04:00	-0.2494948	-0.422827	-0.0761626	1.85E-04	***

WT:22:00	WT:06:00	-0.3771474	-0.5514394	-0.2028554	5.50E-10	****
WT:22:00	3h1:06:00	-0.4610153	-0.6343475	-0.2876831	2.89E-10	****
3h1:22:00	WT:02:00	-0.0210682	-0.1924194	0.15028296	1.00E+00	ns
3h1:22:00	3h1:02:00	-0.0638615	-0.2361835	0.10846049	9.88E-01	ns
3h1:22:00	WT:04:00	-0.508367	-0.6797182	-0.3370158	2.89E-10	****
3h1:22:00	3h1:04:00	-0.2108764	-0.3822276	-0.0395252	3.52E-03	**
3h1:22:00	WT:06:00	-0.338529	-0.510851	-0.166207	1.70E-08	****
3h1:22:00	3h1:06:00	-0.4223969	-0.5937481	-0.2510457	2.89E-10	****
WT:02:00	3h1:02:00	-0.0427933	-0.2151153	0.1295287	1.00E+00	ns
WT:02:00	WT:04:00	-0.4872988	-0.6586499	-0.3159476	2.89E-10	****
WT:02:00	3h1:04:00	-0.1898082	-0.3611594	-0.018457	1.58E-02	*
WT:02:00	WT:06:00	-0.3174608	-0.4897828	-0.1451388	1.83E-07	****
WT:02:00	3h1:06:00	-0.4013287	-0.5726799	-0.2299775	2.94E-10	****
3h1:02:00	WT:04:00	-0.4445055	-0.6168275	-0.2721834	2.89E-10	****
3h1:02:00	3h1:04:00	-0.1470149	-0.3193369	0.02530714	1.83E-01	ns
3h1:02:00	WT:06:00	-0.2746675	-0.4479549	-0.1013801	1.81E-05	****
3h1:02:00	3h1:06:00	-0.3585354	-0.5308574	-0.1862134	1.83E-09	****
WT:04:00	3h1:04:00	0.29749058	0.12613941	0.46884176	1.31E-06	****
WT:04:00	WT:06:00	0.16983799	-0.002484	0.34216	5.76E-02	ns
WT:04:00	3h1:06:00	0.08597008	-0.0853811	0.25732126	8.91E-01	ns
3h1:04:00	WT:06:00	-0.1276526	-0.2999746	0.04466942	3.86E-01	ns
3h1:04:00	3h1:06:00	-0.2115205	-0.3828717	-0.0401693	3.36E-03	**
WT:06:00	3h1:06:00	-0.0838679	-0.2561899	0.08845411	9.10E-01	ns
H3K4me3/DNA (Chapter 3.4.2 and 3.5.2)						
WT:10:00	3h1:10:00	-0.3103198	-0.5825145	-0.0381252	1.09E-02	*
WT:10:00	WT:19:00	-0.2748644	-0.5449909	-0.0047379	4.19E-02	*
WT:10:00	3h1:19:00	-0.4311349	-0.7033295	-0.1589402	1.93E-05	****
WT:10:00	WT:22:00	-0.4326091	-0.6971223	-0.1680958	8.15E-06	****
WT:10:00	3h1:22:00	-0.4099588	-0.6744721	-0.1454456	3.38E-05	****
WT:10:00	WT:02:00	-0.4727326	-0.7308973	-0.2145678	2.48E-07	****
WT:10:00	3h1:02:00	-0.4247662	-0.6875821	-0.1619502	1.13E-05	****
WT:10:00	WT:04:00	0.03213568	-0.2360262	0.30029758	1.00E+00	ns
WT:10:00	3h1:04:00	-0.3328932	-0.5991863	-0.0666	2.77E-03	**
WT:10:00	WT:06:00	-0.3004226	-0.5508836	-0.0499616	5.29E-03	**
WT:10:00	3h1:06:00	-0.3628494	-0.6256654	-0.1000335	4.55E-04	***
3h1:10:00	WT:19:00	0.03545547	-0.2386749	0.30958579	1.00E+00	ns
3h1:10:00	3h1:19:00	-0.120815	-0.3969835	0.15535347	9.55E-01	ns
3h1:10:00	WT:22:00	-0.1222892	-0.39089	0.14631157	9.41E-01	ns
3h1:10:00	3h1:22:00	-0.099639	-0.3682398	0.16896182	9.87E-01	ns
3h1:10:00	WT:02:00	-0.1624127	-0.424764	0.09993846	6.70E-01	ns
3h1:10:00	3h1:02:00	-0.1144463	-0.3813758	0.15248312	9.61E-01	ns
3h1:10:00	WT:04:00	0.34245552	0.07026088	0.61465016	2.49E-03	**
3h1:10:00	3h1:04:00	-0.0225733	-0.2929271	0.24778043	1.00E+00	ns
3h1:10:00	WT:06:00	0.00989728	-0.2448768	0.26467133	1.00E+00	ns
3h1:10:00	3h1:06:00	-0.0525296	-0.3194591	0.21439987	1.00E+00	ns
WT:19:00	3h1:19:00	-0.1562705	-0.4304008	0.11785982	7.75E-01	ns
WT:19:00	WT:22:00	-0.1577447	-0.4242494	0.10876006	7.30E-01	ns

WT:19:00	3h1:22:00	-0.1350944	-0.4015992	0.13141031	8.83E-01	ns
WT:19:00	WT:02:00	-0.1978682	-0.458073	0.06233661	3.43E-01	ns
WT:19:00	3h1:02:00	-0.1499018	-0.414722	0.11491838	7.83E-01	ns
WT:19:00	WT:04:00	0.30700005	0.03687357	0.57712653	1.14E-02	*
WT:19:00	3h1:04:00	-0.0580288	-0.3263002	0.21024262	1.00E+00	ns
WT:19:00	WT:06:00	-0.0255582	-0.2781215	0.22700509	1.00E+00	ns
WT:19:00	3h1:06:00	-0.0879851	-0.3528053	0.17683513	9.95E-01	ns
3h1:19:00	WT:22:00	-0.0014742	-0.270075	0.2671266	1.00E+00	ns
3h1:19:00	3h1:22:00	0.02117605	-0.2474247	0.28977685	1.00E+00	ns
3h1:19:00	WT:02:00	-0.0415977	-0.3039489	0.22075349	1.00E+00	ns
3h1:19:00	3h1:02:00	0.00636868	-0.2605608	0.27329814	1.00E+00	ns
3h1:19:00	WT:04:00	0.46327055	0.19107591	0.73546519	2.58E-06	****
3h1:19:00	3h1:04:00	0.09824169	-0.1721121	0.36859546	9.89E-01	ns
3h1:19:00	WT:06:00	0.1307123	-0.1240618	0.38548635	8.74E-01	ns
3h1:19:00	3h1:06:00	0.06828544	-0.198644	0.3352149	1.00E+00	ns
WT:22:00	3h1:22:00	0.02265025	-0.2381634	0.28346385	1.00E+00	ns
WT:22:00	WT:02:00	-0.0401235	-0.2944963	0.21424924	1.00E+00	ns
WT:22:00	3h1:02:00	0.00784288	-0.2512492	0.26693492	1.00E+00	ns
WT:22:00	WT:04:00	0.46474474	0.20023147	0.72925802	9.69E-07	****
WT:22:00	3h1:04:00	0.09971589	-0.1629027	0.36233445	9.85E-01	ns
WT:22:00	WT:06:00	0.1321865	-0.114364	0.37873703	8.38E-01	ns
WT:22:00	3h1:06:00	0.06975964	-0.1893324	0.32885168	9.99E-01	ns
3h1:22:00	WT:02:00	-0.0627738	-0.3171465	0.19159899	1.00E+00	ns
3h1:22:00	3h1:02:00	-0.0148074	-0.2738994	0.24428467	1.00E+00	ns
3h1:22:00	WT:04:00	0.44209449	0.17758122	0.70660777	4.41E-06	****
3h1:22:00	3h1:04:00	0.07706564	-0.1855529	0.3396842	9.98E-01	ns
3h1:22:00	WT:06:00	0.10953625	-0.1370143	0.35608678	9.50E-01	ns
3h1:22:00	3h1:06:00	0.04710939	-0.2119827	0.30620143	1.00E+00	ns
WT:02:00	3h1:02:00	0.0479664	-0.2046409	0.30057372	1.00E+00	ns
WT:02:00	WT:04:00	0.50486827	0.24670352	0.76303302	2.27E-08	****
WT:02:00	3h1:04:00	0.13983941	-0.1163837	0.39606251	8.21E-01	ns
WT:02:00	WT:06:00	0.17231002	-0.0674168	0.41203682	4.34E-01	ns
WT:02:00	3h1:06:00	0.10988316	-0.1427242	0.36249047	9.57E-01	ns
3h1:02:00	WT:04:00	0.45690187	0.19408592	0.71971781	1.35E-06	****
3h1:02:00	3h1:04:00	0.09187301	-0.1690359	0.35278192	9.92E-01	ns
3h1:02:00	WT:06:00	0.12434362	-0.120385	0.36907228	8.81E-01	ns
3h1:02:00	3h1:06:00	0.06191676	-0.1954422	0.31927572	1.00E+00	ns
WT:04:00	3h1:04:00	-0.3650289	-0.631322	-0.0987357	5.25E-04	***
WT:04:00	WT:06:00	-0.3325582	-0.5830192	-0.0820973	9.67E-04	***
WT:04:00	3h1:06:00	-0.3949851	-0.6578011	-0.1321692	7.15E-05	****
3h1:04:00	WT:06:00	0.03247061	-0.2159885	0.28092974	1.00E+00	ns
3h1:04:00	3h1:06:00	-0.0299563	-0.2908652	0.23095266	1.00E+00	ns
WT:06:00	3h1:06:00	-0.0624269	-0.3071555	0.1823018	1.00E+00	ns
Pol II S2P/DNA (Chapter 3.4.3 and 3.5.3)						
WT:10:00	3h1:10:00	0.67882766	-0.0909961	1.44865143	1.44E-01	ns
WT:10:00	WT:19:00	-0.4514624	-1.2571109	0.35418606	7.88E-01	ns
WT:10:00	3h1:19:00	-0.5618539	-1.3675024	0.24379455	4.78E-01	ns

WT:10:00	WT:22:00	-1.0067854	-1.8235468	-0.190024	3.66E-03	**
WT:10:00	3h1:22:00	-0.8618471	-1.6674955	-0.0561986	2.45E-02	*
WT:10:00	WT:02:00	-0.4002542	-1.2059027	0.4053943	8.92E-01	ns
WT:10:00	3h1:02:00	-0.3894568	-1.1756892	0.39677565	8.94E-01	ns
WT:10:00	WT:04:00	-0.1600894	-0.9890948	0.66891607	1.00E+00	ns
WT:10:00	3h1:04:00	-0.0496918	-0.8054571	0.70607344	1.00E+00	ns
WT:10:00	WT:06:00	-1.0171771	-1.8034095	-0.2309446	1.66E-03	**
WT:10:00	3h1:06:00	-0.1979243	-0.9756226	0.57977409	1.00E+00	ns
3h1:10:00	WT:19:00	-1.1302901	-1.9001139	-0.3604663	1.43E-04	***
3h1:10:00	3h1:19:00	-1.2406816	-2.0105054	-0.4708578	1.56E-05	****
3h1:10:00	WT:22:00	-1.6856131	-2.4670594	-0.9041667	8.86E-10	****
3h1:10:00	3h1:22:00	-1.5406747	-2.3104985	-0.7708509	1.76E-08	****
3h1:10:00	WT:02:00	-1.0790818	-1.8489056	-0.3092581	3.77E-04	***
3h1:10:00	3h1:02:00	-1.0682844	-1.8177646	-0.3188042	2.69E-04	***
3h1:10:00	WT:04:00	-0.838917	-1.633152	-0.044682	2.82E-02	*
3h1:10:00	3h1:04:00	-0.7285195	-1.4459735	-0.0110654	4.29E-02	*
3h1:10:00	WT:06:00	-1.6960047	-2.4454849	-0.9465245	1.08E-10	****
3h1:10:00	3h1:06:00	-0.8767519	-1.6172747	-0.1362292	6.67E-03	**
WT:19:00	3h1:19:00	-0.1103915	-0.91604	0.69525697	1.00E+00	ns
WT:19:00	WT:22:00	-0.555323	-1.3720844	0.26143843	5.19E-01	ns
WT:19:00	3h1:22:00	-0.4103846	-1.2160331	0.39526384	8.75E-01	ns
WT:19:00	WT:02:00	0.05120824	-0.7544402	0.85685672	1.00E+00	ns
WT:19:00	3h1:02:00	0.06200567	-0.7242267	0.84823808	1.00E+00	ns
WT:19:00	WT:04:00	0.29137305	-0.5376324	1.1203785	9.91E-01	ns
WT:19:00	3h1:04:00	0.4017706	-0.3539947	1.15753587	8.40E-01	ns
WT:19:00	WT:06:00	-0.5657146	-1.351947	0.22051778	4.27E-01	ns
WT:19:00	3h1:06:00	0.25353815	-0.5241602	1.03123651	9.95E-01	ns
3h1:19:00	WT:22:00	-0.4449315	-1.2616929	0.37182993	8.17E-01	ns
3h1:19:00	3h1:22:00	-0.2999931	-1.1056416	0.50565535	9.86E-01	ns
3h1:19:00	WT:02:00	0.16159975	-0.6440487	0.96724823	1.00E+00	ns
3h1:19:00	3h1:02:00	0.17239717	-0.6138352	0.95862959	1.00E+00	ns
3h1:19:00	WT:04:00	0.40176456	-0.4272409	1.23077001	9.07E-01	ns
3h1:19:00	3h1:04:00	0.51216211	-0.2436032	1.26792738	5.24E-01	ns
3h1:19:00	WT:06:00	-0.4553231	-1.2415555	0.33090929	7.50E-01	ns
3h1:19:00	3h1:06:00	0.36392966	-0.4137687	1.14162802	9.26E-01	ns
WT:22:00	3h1:22:00	0.14493833	-0.6718231	0.96169973	1.00E+00	ns
WT:22:00	WT:02:00	0.60653121	-0.2102302	1.42329261	3.76E-01	ns
WT:22:00	3h1:02:00	0.61732864	-0.1802873	1.41494453	3.11E-01	ns
WT:22:00	WT:04:00	0.84669602	0.00688667	1.68650537	4.61E-02	*
WT:22:00	3h1:04:00	0.95709357	0.18949287	1.72469428	3.06E-03	**
WT:22:00	WT:06:00	-0.0103917	-0.8080075	0.78722424	1.00E+00	ns
WT:22:00	3h1:06:00	0.80886113	0.01965618	1.59806607	3.90E-02	*
3h1:22:00	WT:02:00	0.46159288	-0.3440556	1.26724137	7.63E-01	ns
3h1:22:00	3h1:02:00	0.47239031	-0.3138421	1.25862272	7.04E-01	ns
3h1:22:00	WT:04:00	0.70175769	-0.1272478	1.53076314	1.89E-01	ns
3h1:22:00	3h1:04:00	0.81215524	0.05638998	1.56792051	2.32E-02	*
3h1:22:00	WT:06:00	-0.15533	-0.9415624	0.63090243	1.00E+00	ns

3h1:22:00	3h1:06:00	0.6639228	-0.1137756	1.44162116	1.79E-01	ns
WT:02:00	3h1:02:00	0.01079742	-0.775435	0.79702983	1.00E+00	ns
WT:02:00	WT:04:00	0.24016481	-0.5888406	1.06917025	9.98E-01	ns
WT:02:00	3h1:04:00	0.35056236	-0.4052029	1.10632763	9.30E-01	ns
WT:02:00	WT:06:00	-0.6169229	-1.4031553	0.16930954	2.91E-01	ns
WT:02:00	3h1:06:00	0.20232991	-0.5753684	0.98002827	9.99E-01	ns
3h1:02:00	WT:04:00	0.22936738	-0.580782	1.03951673	9.99E-01	ns
3h1:02:00	3h1:04:00	0.33976494	-0.3952678	1.07479763	9.32E-01	ns
3h1:02:00	WT:06:00	-0.6277203	-1.3940449	0.13860427	2.31E-01	ns
3h1:02:00	3h1:06:00	0.19153249	-0.5660338	0.94909877	1.00E+00	ns
WT:04:00	3h1:04:00	0.11039755	-0.6702187	0.89101378	1.00E+00	ns
WT:04:00	WT:06:00	-0.8570877	-1.667237	-0.0469383	2.77E-02	*
WT:04:00	3h1:06:00	-0.0378349	-0.8397048	0.76403498	1.00E+00	ns
3h1:04:00	WT:06:00	-0.9674852	-1.7025179	-0.2324525	1.23E-03	**
3h1:04:00	3h1:06:00	-0.1482325	-0.8741294	0.57766452	1.00E+00	ns
WT:06:00	3h1:06:00	0.81925278	0.0616865	1.57681906	2.16E-02	*
Pol II S5P (Chapter 3.4.3 and 3.5.3)						
WT:19:00	3h1:19:00	-0.0963831	-0.3091163	0.11635019	6.41E-01	ns
WT:19:00	WT:22:00	-0.3418831	-0.5737921	-0.109974	1.11E-03	**
WT:19:00	3h1:22:00	0.06266072	-0.1618843	0.28720572	8.86E-01	ns
3h1:19:00	WT:22:00	-0.2455	-0.4582333	-0.0327668	1.67E-02	*
3h1:19:00	3h1:22:00	0.15904378	-0.0456366	0.36372419	1.85E-01	ns
WT:22:00	3h1:22:00	0.40454378	0.17999878	0.62908878	4.12E-05	****